

Supporting Information for the manuscript:

A fundamental role of solvent polarity and remote substitution of 2-(4-R-phenyl)-1H-imidazo[4,5-f][1,10]phenanthroline framework in controlling of ground- and excited-state properties of Re(I) chromophores [ReCl(CO)₃(R-C₆H₄-imphen)]

Agata Szłapa-Kula^a, Joanna Palion-Gazda^a, Przemyslaw Ledwon^b, Karol Erfurt^c, Barbara Machura^{a*}

^a*Institute of Chemistry, Faculty of Science and Technology, University of Silesia in Katowice, Szkolna 9, Poland*

^b*Department of Physical Chemistry and Technology of Polymers, Silesian University of Technology, Strzody 9, 44-100 Gliwice, Poland*

^c*Department of Chemical Organic Technology and Petrochemistry, Silesian University of Technology, Krzywoustego 4, 44-100 Gliwice, Poland*

Synthesis and Characterization	
1. Preparation of 1H-imidazo[4,5-f][1,10]phenanthroline derivatives (L ¹ - L ⁵)	
NMR spectra of free ligands (L¹-L⁵)	
2. ¹ H NMR and ¹³ C NMR spectra of free ligands L ¹ - L ⁵	Figures S1-S5
NMR spectra of Rhenium(I) complexes 1-5	
3. ¹ H and ¹³ C NMR, ¹ H - ¹ H COSY, ¹ H - ¹³ C HMQC, ¹ H - ¹³ C HMBC NMR spectra of Re(I) complexes 1-5	Figures S6-S10
IR spectra of Rhenium(I) complexes 1-5	
4. FT-IR spectra of 1-5 (red line) along with FT-IR spectra of the free ligands L ¹ - L ⁵ (blue line).	Figure S11
5. Carbonyl stretching frequencies for complexes 1-5	Table S1
HRMS spectra of Rhenium(I) complexes 1-5	
6. HRMS spectra of complexes 1-5	Figure S12
X-Ray analysis	
7. Crystal data and structure refinement of the complex 4	Table S2
8. Bond lengths [Å] and angles [°] of complex 4	Table S3
9. Short intra- and intermolecular hydrogen bonds for complex 4	Table S4
10. X—Y...Cg(J)(π-ring) interactions for complex 4	Table S5
Thermal studies	
11. TGA thermograms of 1-5 and free ligands L ¹ - L ⁵	Figure S13
12. Thermal stability of the synthesized compounds	Table S6
UV-Vis spectroscopy	
13. Absorption spectra of the complexes 1-5 in CHCl ₃ , THF, DMF, and CH ₃ CN	Figure S14

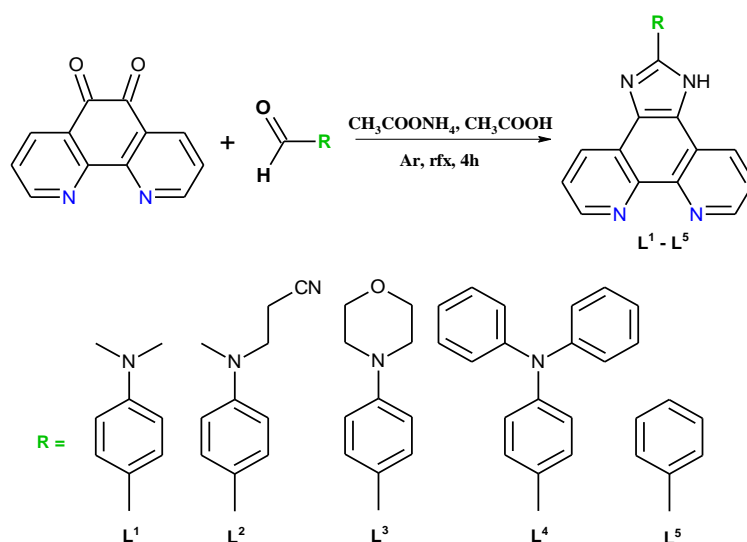
14. Impact of solvent polarity on UV–Vis spectra of complexes 1–5	Figure S15
15. The absorption maxima and molar extinction coefficient for 1–5 in four solvents of different polarity	Table S7
16. Comparison of UV–Vis spectra of complexes 1–5 with free ligands L¹–L⁵	Figure S16
17. UV-Vis spectra of 1–5 in THF recorded once every two hours over 12h at room temperature	Figure S17
18. UV-Vis spectra of 1–5 in THF after sample exposure to light (440 nm)	Figure S18
Photoluminescence	
19. Absorption, excitation and emission steady-state spectra of 1–5 in deaerated chloroform solution along with the corresponding TCSPC decay curves	Figure S19
20. Decay curves of 1–5 in toluene at room temperature	Figure S20
21. Emission spectra for compounds 1–5 in different solvents along with the corresponding TCSPC decay curves	Figure S21
22. Emission spectra of 1–5 in CHCl ₃ /CH ₃ CN mixture with different acetonitrile fraction (f_{CH_3CN})	Figure S22
23. Emission spectra of 1–5 in air-equilibrated, degassed, and oxygenated chloroform solutions, along with decay curves	Figure S23
24. Decay curves of 1–5 in ethanol-methanol rigid-glass matrix (77K)	Figure S24
25. Absorption and emission steady-state spectra of 1–5 in solid state along with the corresponding TCSPC decay curves	Figure S25
26. Normalized emission spectra of 1–5 in CHCl ₃ , along with the emission spectra of free ligands	Figure S26
27. Phosphorescence spectra of 1–5 versus phosphorescence of the appropriate free ligand at 77 K in EtOH:MeOH rigid matrix. The triplet ligand emissions were induced by addition of 10% ethyl iodide	Figure S27
28. Time-resolved emission spectra of 1–5 at 77 K	Figure S28
DFT and TD-DFT calculations	
29. Theoretical bond lengths [Å] and angles [°] for 1–5 , along with the experimental bond lengths [Å] and angles [°] for 4 and [ReCl(CO) ₃ (Br-thiophene-imphen)]	Table S8
30. Selected molecular orbitals of 1–5 and their percentage composition in chloroform. The calculations were performed at DFT/PBE0/def2-TZVPD/def2-TZVP level with the use of the PCM model at polarities corresponding to CHCl ₃	Figure S29
31. Calculated ionization potentials and electron affinities (vertical and adiabatic), energy gap, as well as hole and electrons reorganization energies and extraction potentials for 1–5 . The calculations were performed at DFT/PBE0/def2-TZVPD/def2-TZVP level with the use of the PCM model at polarities corresponding to CHCl ₃	Table S9
32. Experimental (red line) absorption spectra of 1–5 in CHCl ₃ alongside with natural transition orbitals calculated for vertical excitations, which were assigned to the lowest-energy absorption band. The calculations were performed at TD-	Figure S30

DFT/PCM/PBE1PBE/def2-TZVPD/def2-TZVP level with the use of the PCM model at polarities corresponding to CHCl ₃	
33. The energies and characters of the spin-allowed electronic transitions assigned to the lowest wavelength absorption bands of 1–5 computed at TD-DFT/PBE0/def2-TZVPD/def2-TZVP level with the use of the PCM model at polarities corresponding to CHCl ₃	Table S10
34. The energies of theoretical phosphorescence emissions, calculated from the difference between the ground singlet and the triplet state $\Delta E_{T_1-S_0}$, along with the experimental values and the spin density surface plots for 1–5 . Blue and grey colours show regions of excess α spin density and excess β spin density values, respectively	Table S11
Spectroelectrochemistry	
35. UV-VIS of complexes 1–5 and corresponding ligand in the solution CH ₂ Cl ₂ /Bu ₄ NPF ₆ . Spectra recorded for different potentials related to: neutral state, first oxidation state and neutral state after oxidation process.	Figure S31
36. UV-VIS of complexes 1, 2, 4 and corresponding ligand in the solution CH ₂ Cl ₂ /Bu ₄ NPF ₆ . Spectra recorded for compounds at potential related to second oxidation state and potential related to neutral state after oxidation process.	Figure S32
Femtosecond transient absorption spectroscopy	
37. Summary of the global lifetime analysis of 1 (pump wavelength 355 nm; pump power 0.2 μ j per pulse) containing 3d fsTA map, evolution associated spectra, residual map, time traces at several wavelength and transient spectra.	Figure S33
38. Summary of the global lifetime analysis of 5 (pump wavelength 355 nm; pump power 0.26 μ j per pulse) containing 3d fsTA map, evolution associated spectra, residual map, time traces at several wavelength and transient spectra.	Figure S34

SYNTHESIS AND CHARACTERIZATION

Preparation of 1H-imidazo[4,5-f][1,10]phenanthroline derivatives (L¹-L⁵).

1.05g (5 mmol) 1,10-phenanthroline-5,6-dione and 5 mmol appropriate aldehyde, 7.7g (100 mmol) ammonium acetate and 20 ml acetic acid were placed in a round-bottom flask. The resulting mixture was brought to reflux and left under vigorous stirring for 4 hours. The reaction was carried out under an argon atmosphere. After this time, the mixture was cooled to room temperature and then poured into 300 ml of distilled water. 50 ml of ammonia were added dropwise with stirring, then the resulting precipitate was filtered, next rinsed with 50 ml of distilled water and allowed to air dry.



Scheme SX. Synthetic pathway of 1H-imidazo[4,5-f][1,10]phenanthroline derivatives (L¹-L⁵).

2-(4-[N,N-dimethylamino]phenyl)-1H-imidazo[4,5-f][1,10]phenanthroline (L¹): Yield: 74%. ¹H NMR (400 MHz, DMSO) δ 13.39 (s, 1H), 9.04 – 8.98 (m, 2H), 8.91 (d, J = 8.1 Hz, 2H), 8.12 (d, J = 8.5 Hz, 2H), 7.86 – 7.79 (m, 2H), 6.91 (d, J = 8.6 Hz, 2H), 3.02 (s, 6H). ¹³C NMR (100 MHz, DMSO) δ 151.74, 151.07, 147.36, 129.51, 129.47, 127.37, 123.15, 123.09, 117.40, 111.87, 54.92.

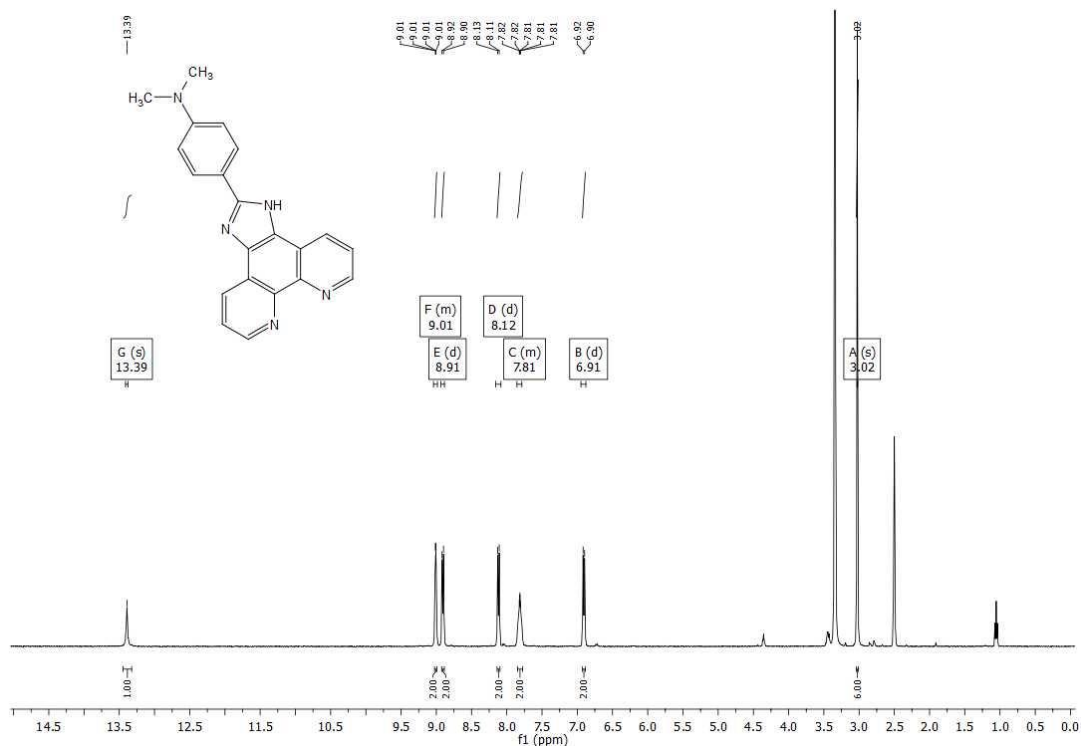
2-(4-[(2-cyanoethyl)methylamino]phenyl)-1H-imidazo[4,5-f][1,10]phenanthroline (L²): Yield: 75%. ¹H NMR (400 MHz, DMSO) δ 13.43 (s, 1H), 9.02 – 9.00 (m, 2H), 8.91 (d, J = 8.0 Hz, 2H), 8.13 (d, J = 8.7 Hz, 2H), 7.87 – 7.77 (m, 2H), 6.99 (d, J = 8.7 Hz, 2H), 3.80 (t, J = 6.6 Hz, 2H), 3.07 (s, 3H), 2.80 (t, J = 6.5 Hz, 2H). ¹³C NMR (100 MHz, DMSO) δ 152.02, 151.36, 147.48, 129.48, 129.40, 127.30, 123.24, 123.17, 119.17, 114.78, 48.50, 25.02, 23.90.

2-(4-morpholinophenyl)-1H-imidazo[4,5-f][1,10]phenanthroline (L³): Yield: 69%. ¹H NMR (400 MHz, DMSO) δ 13.49 (s, 1H), 9.02 (d, *J* = 3.3 Hz, 2H), 8.91 (dd, *J* = 8.1, 1.6 Hz, 2H), 8.15 (d, *J* = 8.8 Hz, 2H), 7.86 – 7.77 (m, 2H), 7.15 (d, *J* = 8.8 Hz, 2H), 3.79 – 3.76 (m, 4H), 3.28 – 3.25 (m, 4H). ¹³C NMR (100 MHz, DMSO) δ 152.22, 151.64, 148.03, 147.91, 129.96, 127.74, 123.71, 123.54, 120.76, 114.94, 66.45, 48.03, 39.99.

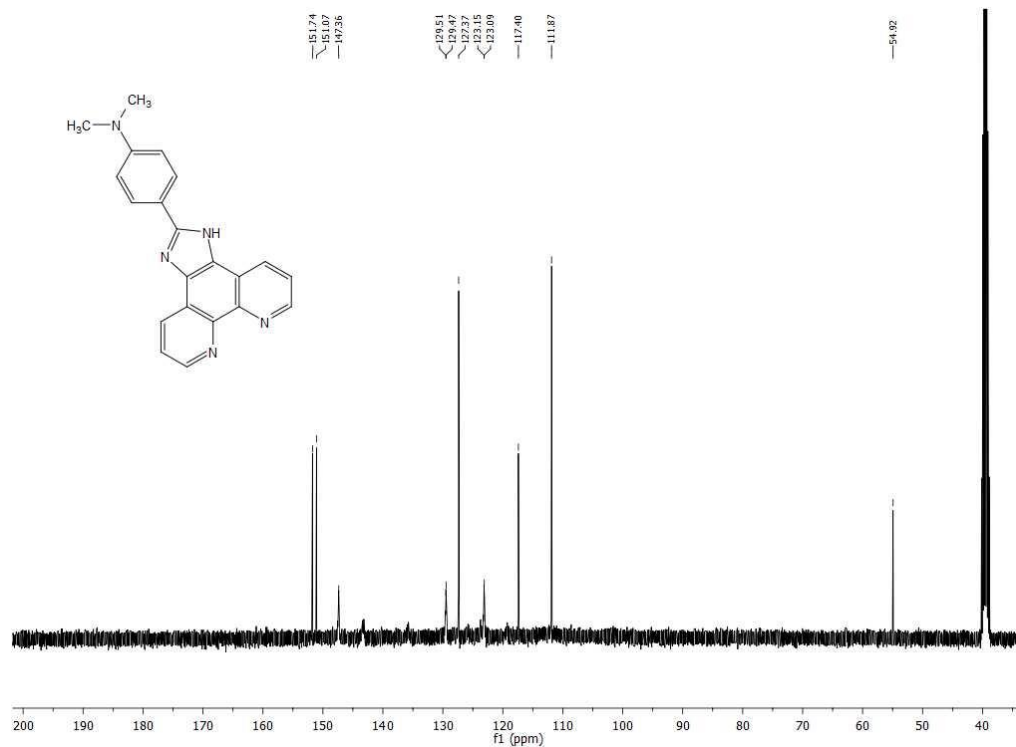
2-(4-[N,N-diphenylamino]phenyl)-1H-imidazo[4,5-f][1,10]phenanthroline (L⁴): Yield: 51%. ¹H NMR (400 MHz, DMSO) δ 13.61 (s, 1H), 9.03 (dd, *J* = 4.2, 1.5 Hz, 2H), 8.93 – 8.88 (m, 2H), 8.16 (d, *J* = 8.7 Hz, 2H), 7.89 – 7.76 (m, 2H), 7.38 (t, *J* = 7.9 Hz, 4H), 7.16 – 7.12 (m, 8H). ¹³C NMR (100 MHz, DMSO) δ 150.62, 148.52, 147.73, 147.63, 146.69, 129.74, 127.49, 126.18, 124.75, 123.85, 123.43, 123.35, 123.09, 122.04.

2-phenyl-1H-imidazo[4,5-f][1,10]phenanthroline (L⁵): Yield: 81%. ¹H NMR (400 MHz, DMSO) δ 13.77 (s, 1H), 9.06 – 9.04 (m, 2H), 8.97 – 8.92 (m, 2H), 8.30 (d, *J* = 7.2 Hz, 2H), 7.90 – 7.80 (m, 2H), 7.67 – 7.51 (m, 2H), 7.28 – 7.13 (m, 1H). ¹³C NMR (100 MHz, DMSO) δ 150.56, 147.75, 143.57, 130.02, 129.65, 129.59, 128.99, 126.29, 123.27, 123.20.

NMR SPECTRA OF FREE LIGANDS (L¹-L⁵)

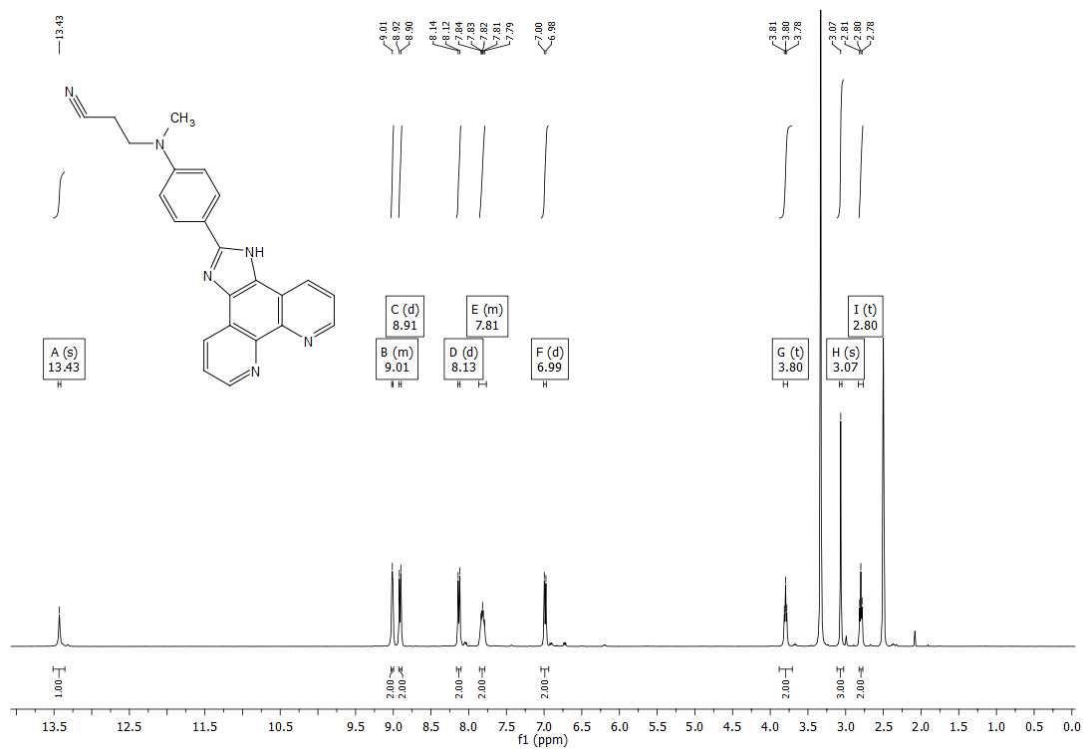


(a)

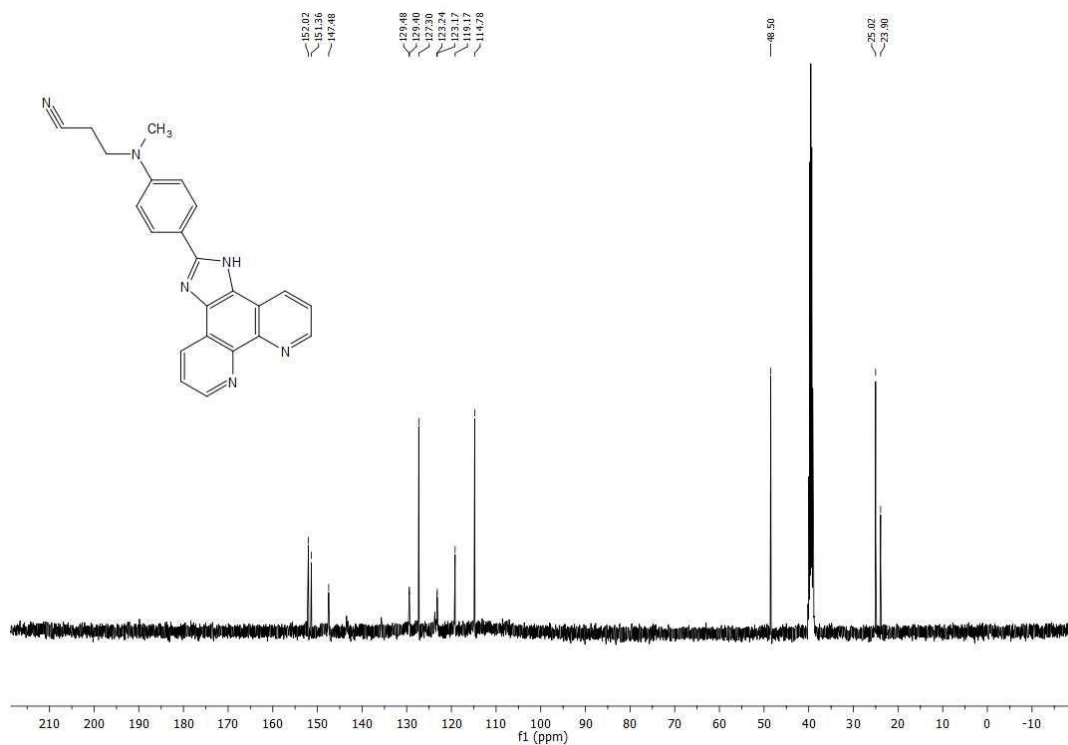


(b)

Figure S1. ¹H NMR (a) and ¹³C NMR (b) of 2-(4-[N,N-dimethylamino]phenyl)-1H-imidazo[4,5-f][1,10]phenanthroline (**L¹**).

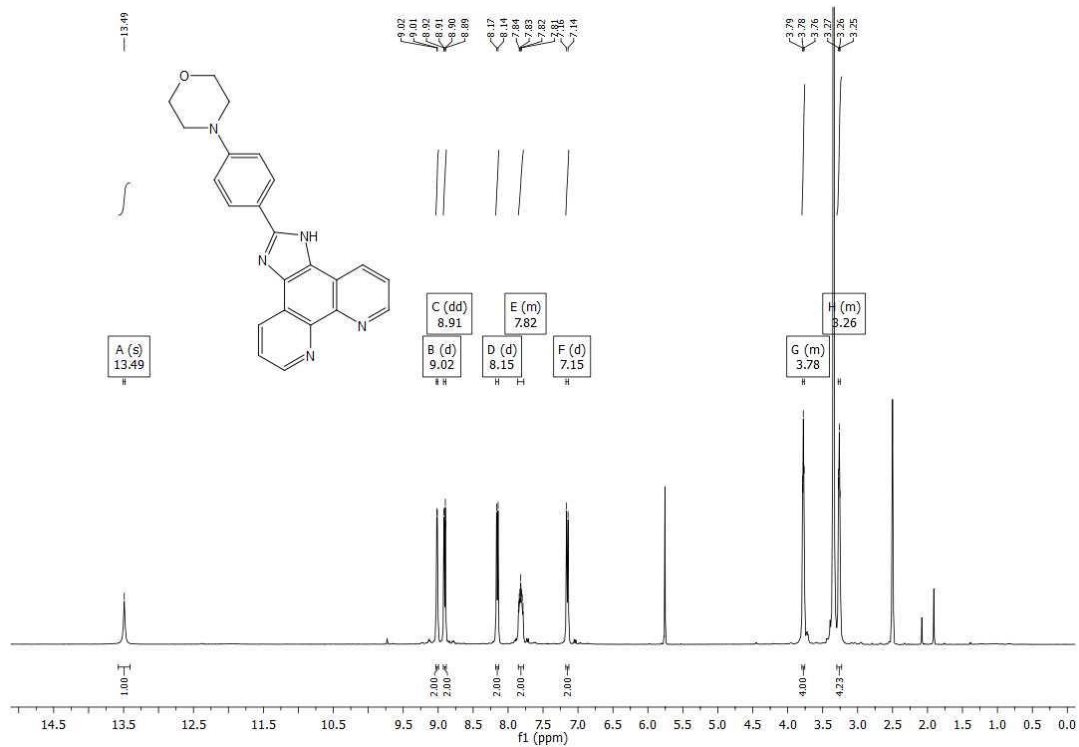


(a)

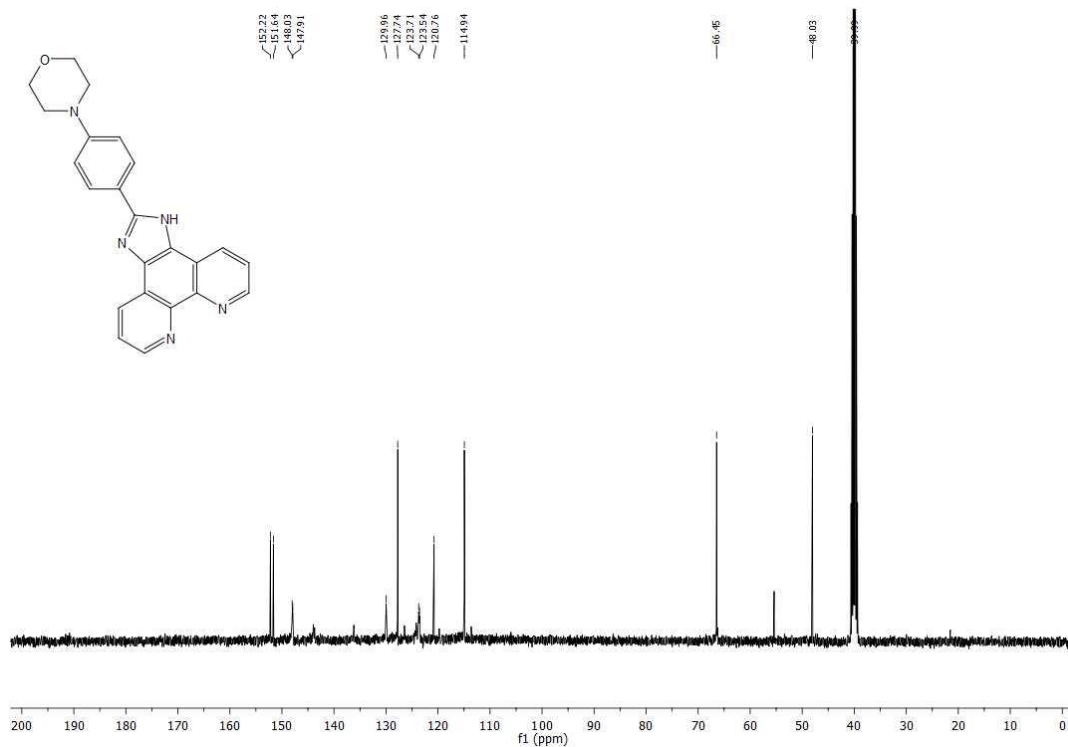


(b)

Figure S2. ¹H NMR (a) and ¹³C NMR (b) of 2-(4-[(2-cyanoethyl)methylamino]phenyl)-1H-imidazo[4,5-f][1,10]phenanthroline (**L²**).

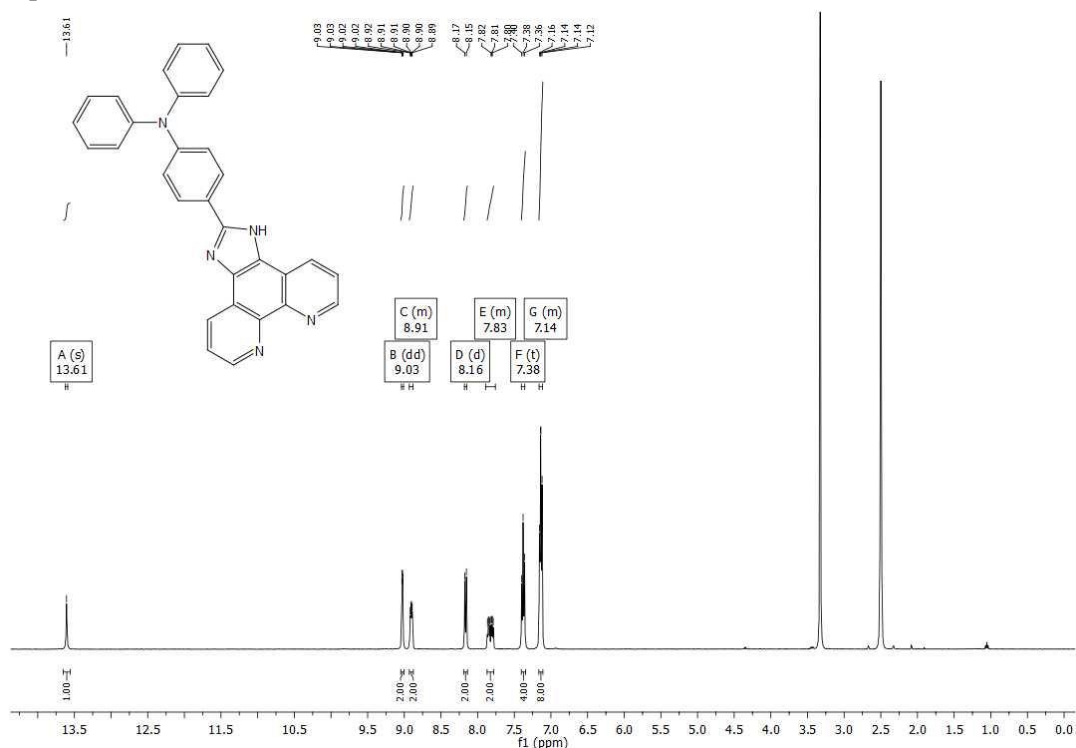


(a)

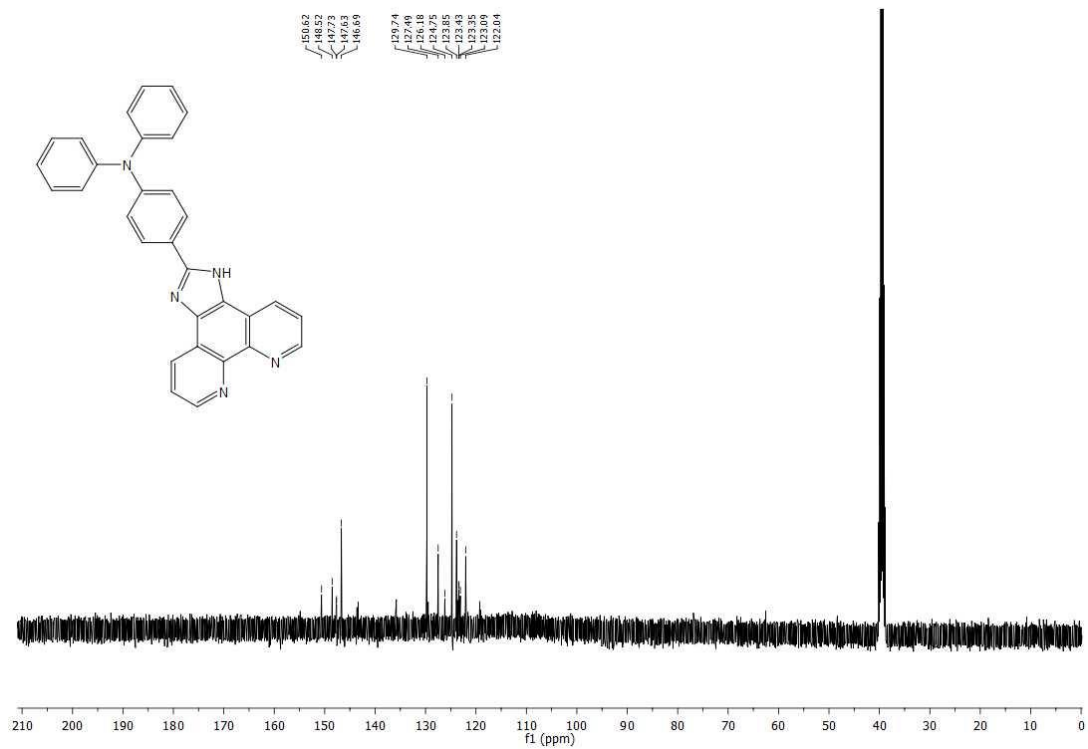


(b)

Figure S3. ^1H NMR (a) and ^{13}C NMR (b) of 2-(4-morpholinophenyl)-1H-imidazo[4,5-f][1,10]phenanthroline (L^3).

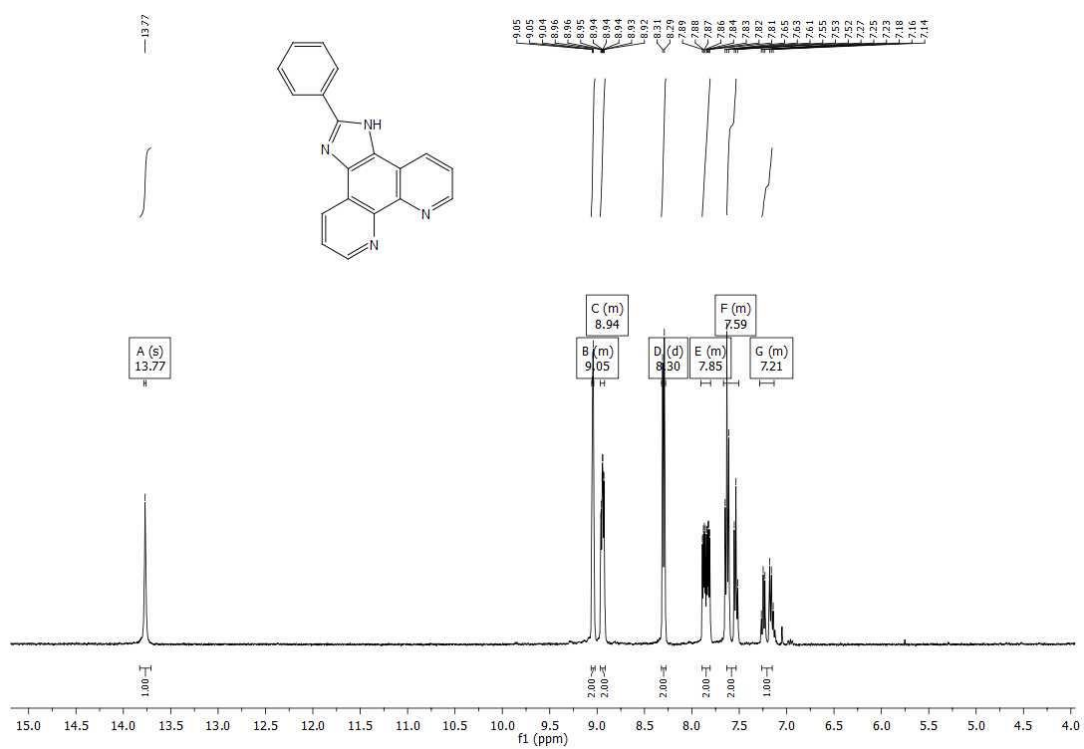


(a)

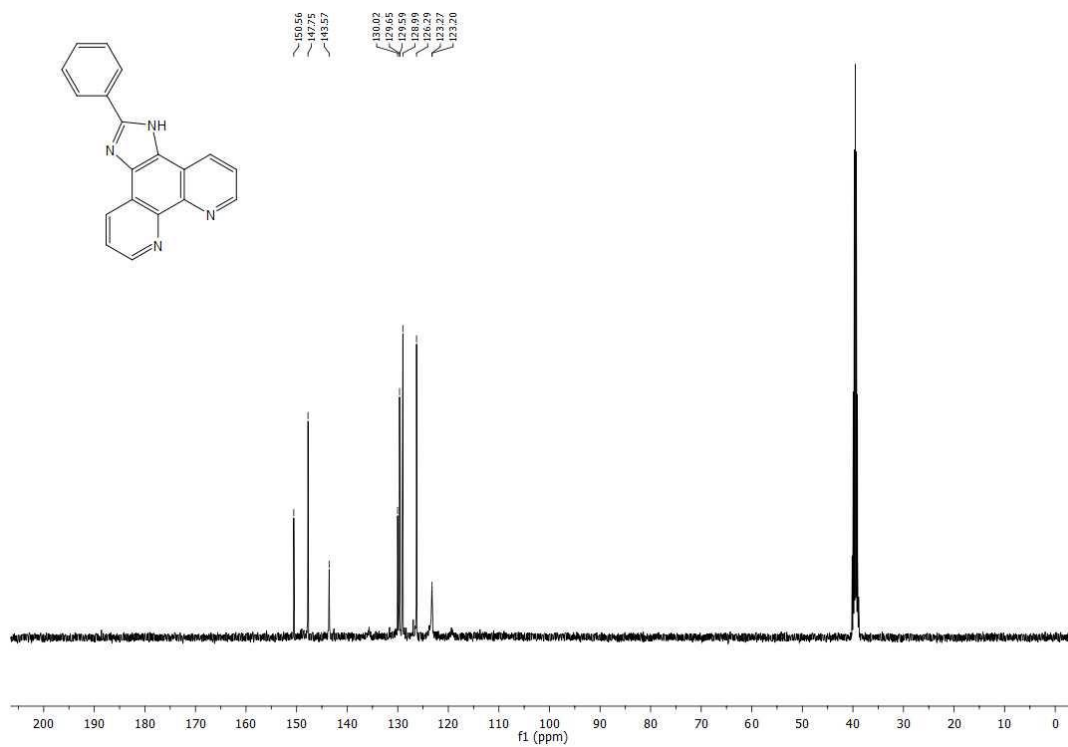


(b)

Figure S4. ^1H NMR (a) and ^{13}C NMR (b) of 2-(4-[N,N-diphenylamino]phenyl)-1H-imidazo[4,5-f][1,10]phenanthroline (L^4).



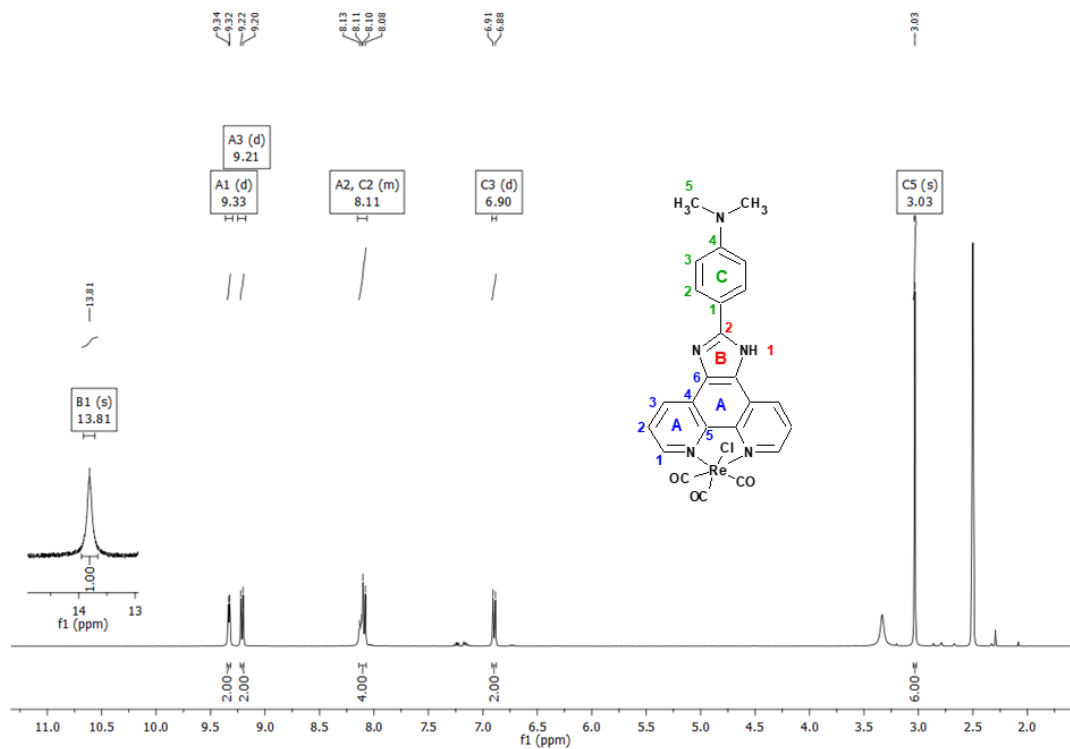
(a)



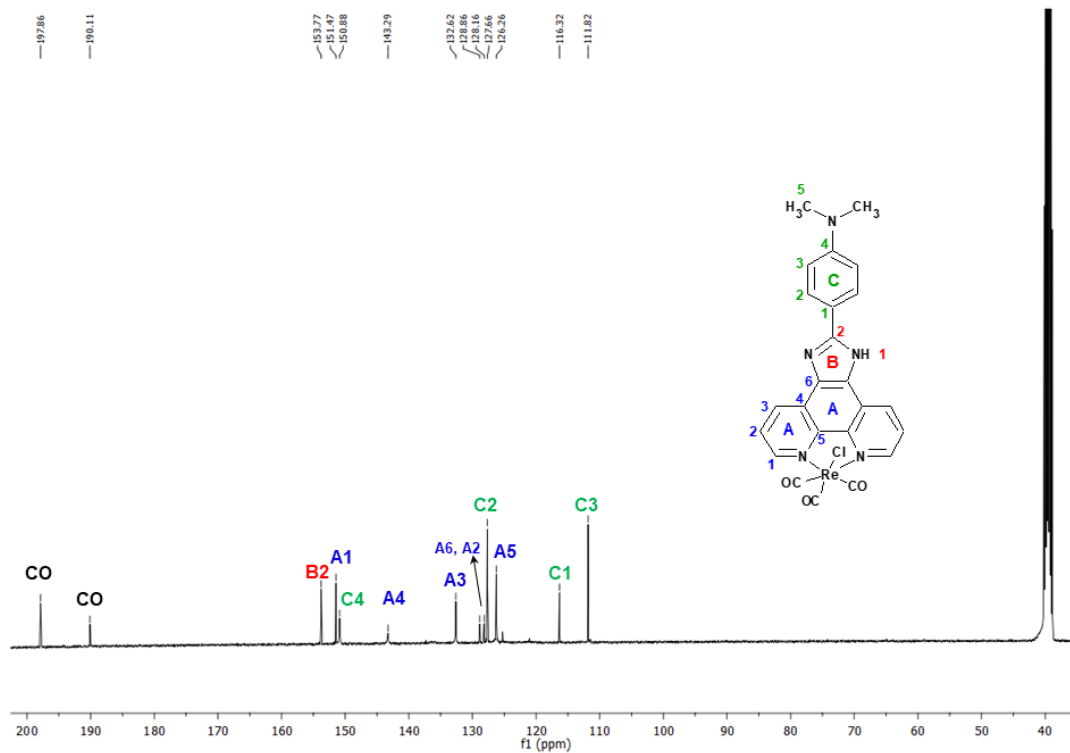
(b)

Figure S5. ¹H NMR (a) and ¹³C NMR (b) of 2-phenyl-1H-imidazo[4,5-f][1,10]phenanthroline (**L**⁵).

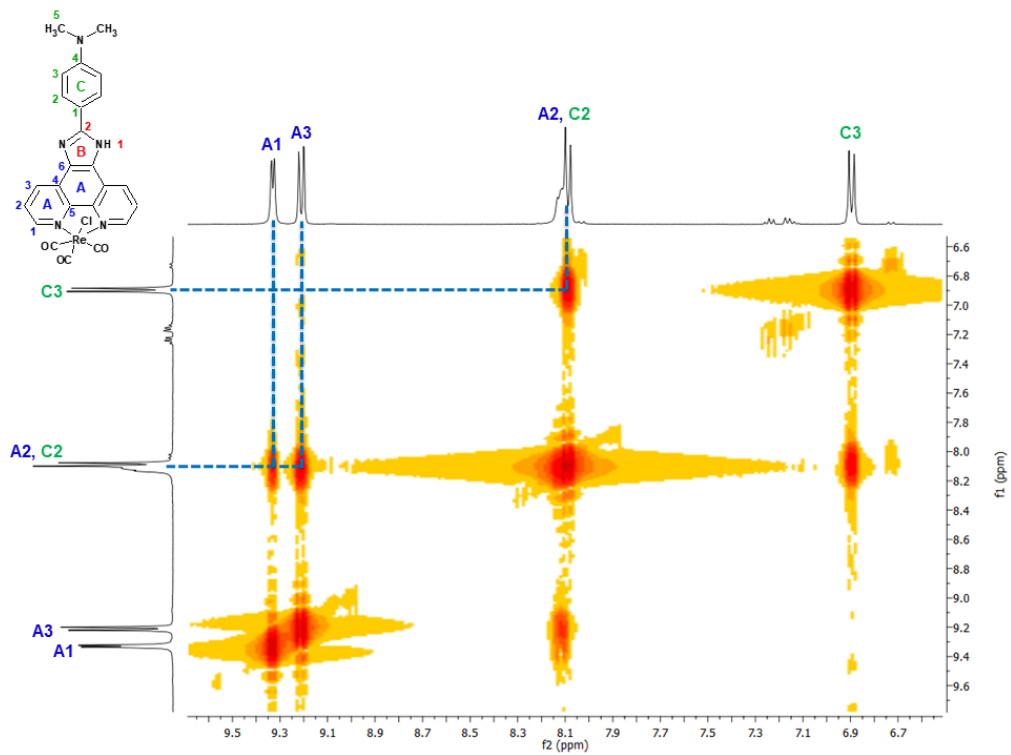
NMR SPECTRA OF RHENIUM(I) COMPLEXES (1-5)



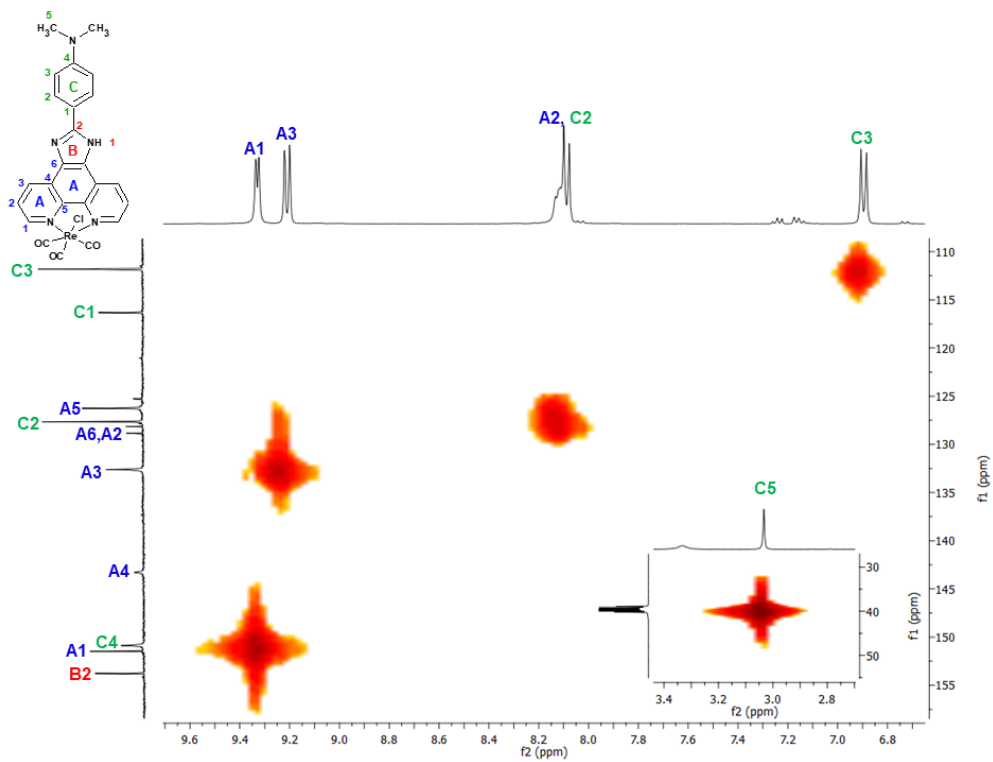
(a)



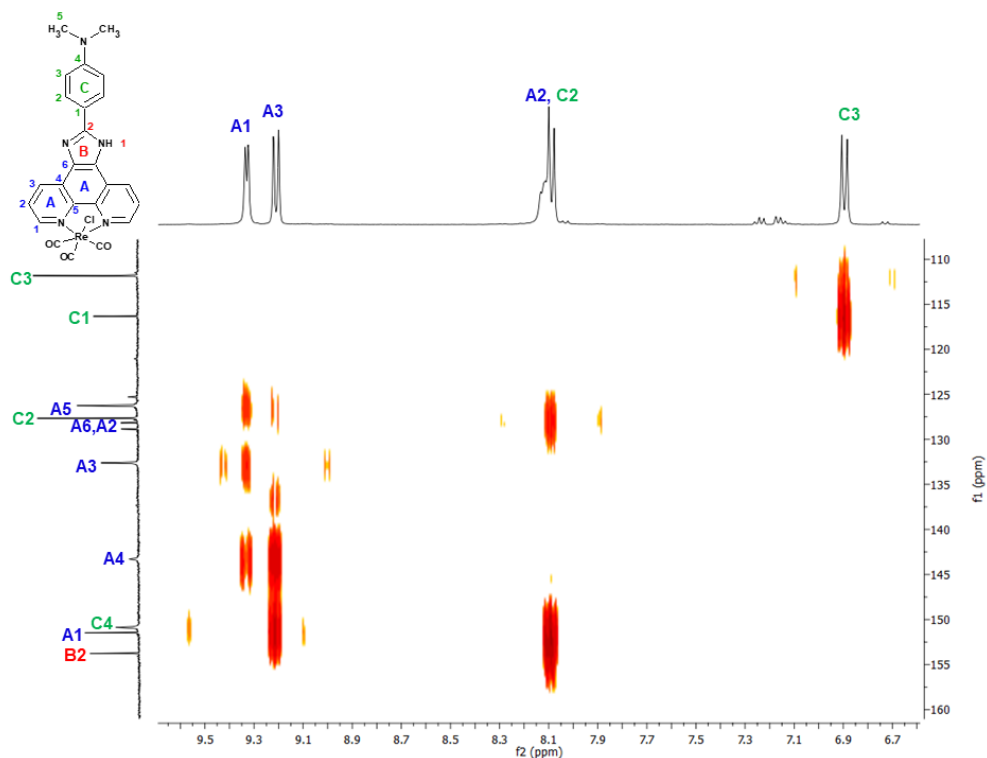
(b)



(c)

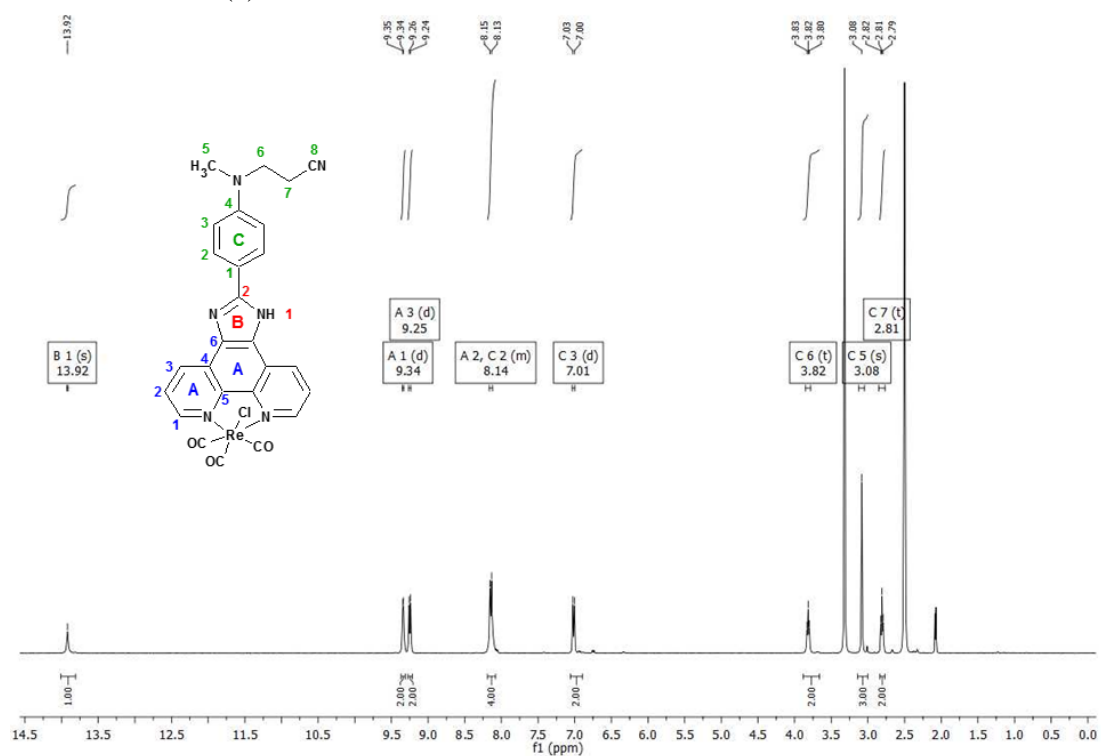


(d)

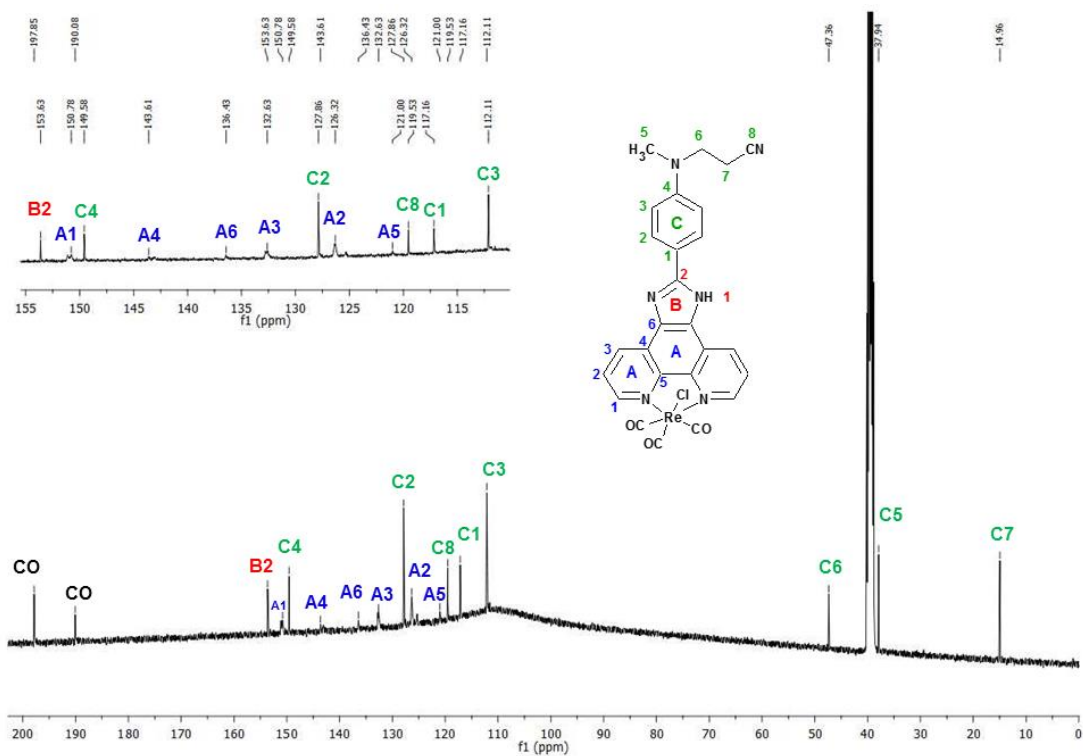


(e)

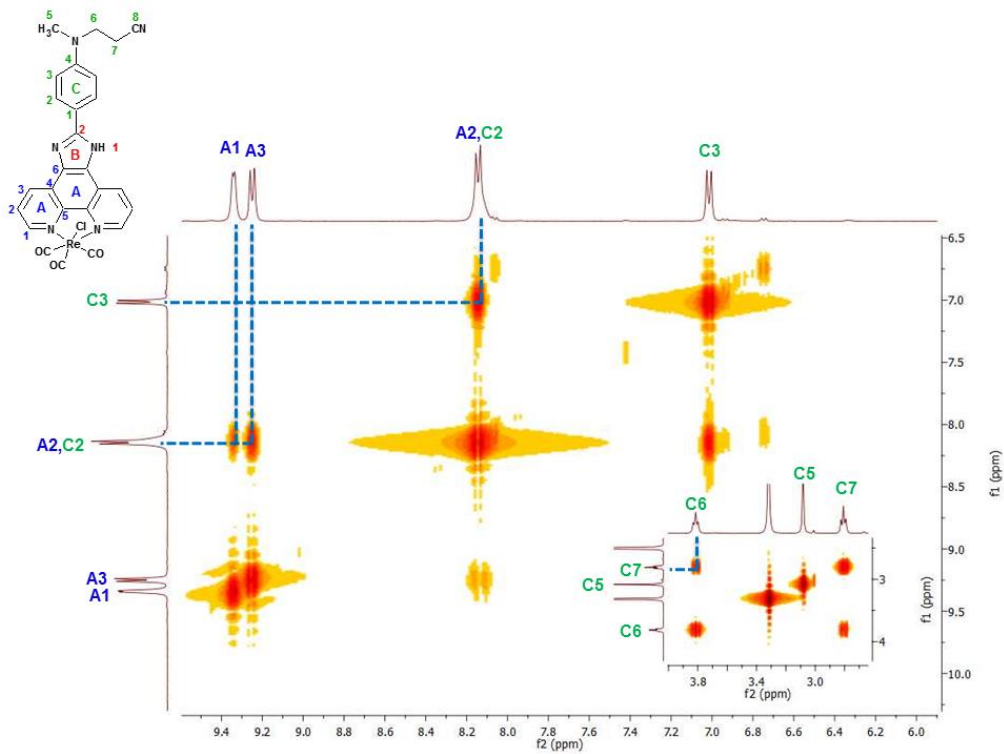
Figure S6. NMR spectra of **1**: ^1H NMR (a), ^{13}C NMR (b), ^1H - ^1H COSY (c) ^1H - ^{13}C HMQC (d), ^1H - ^{13}C HMBC (e)



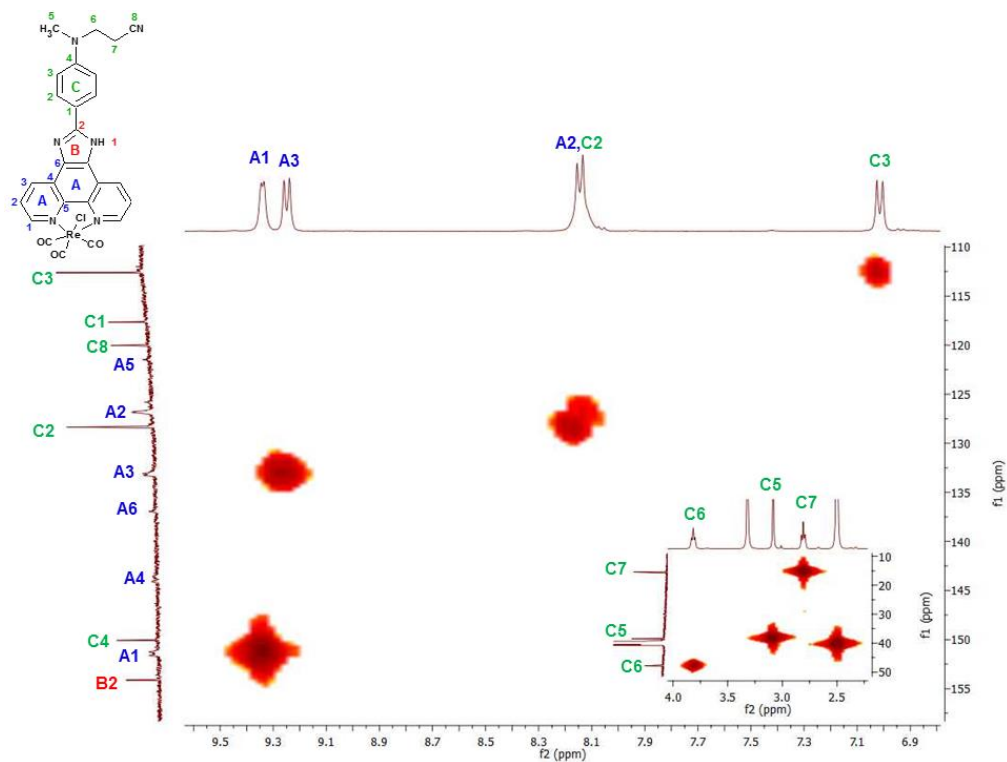
(a)



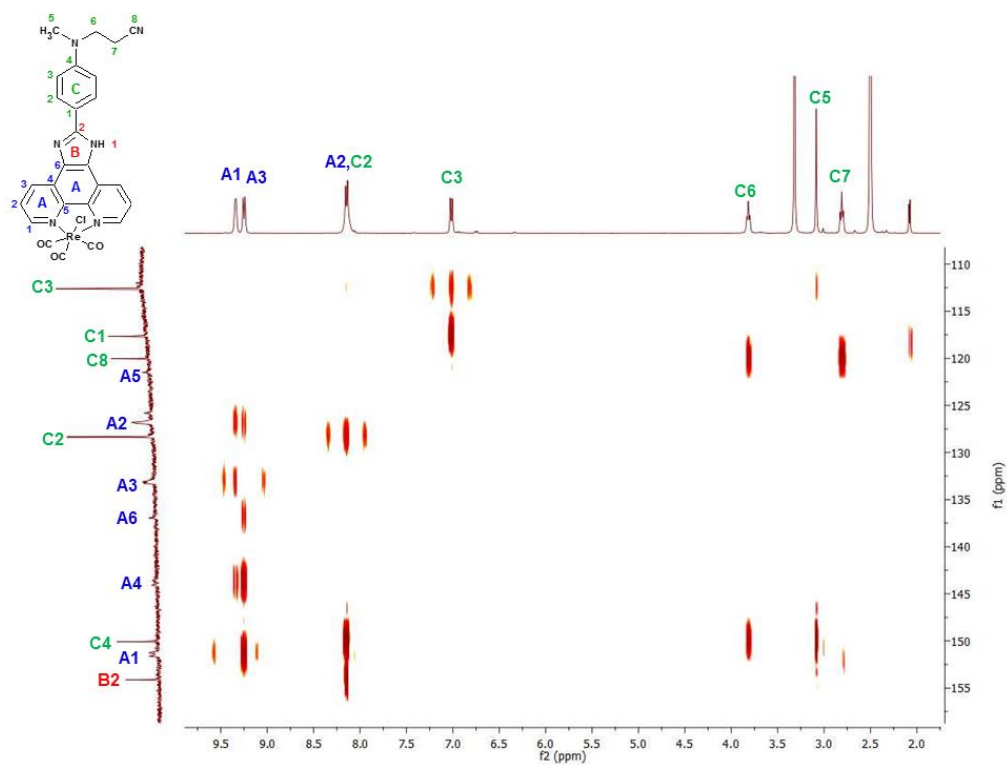
(b)



(c)

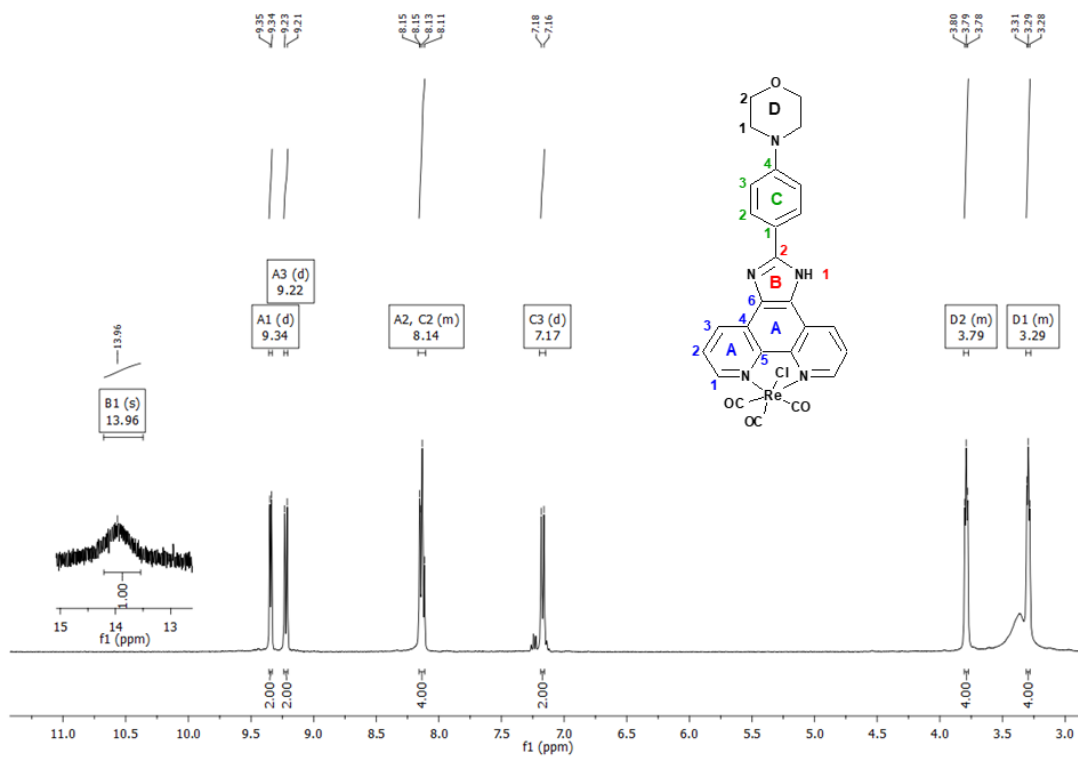


(d)

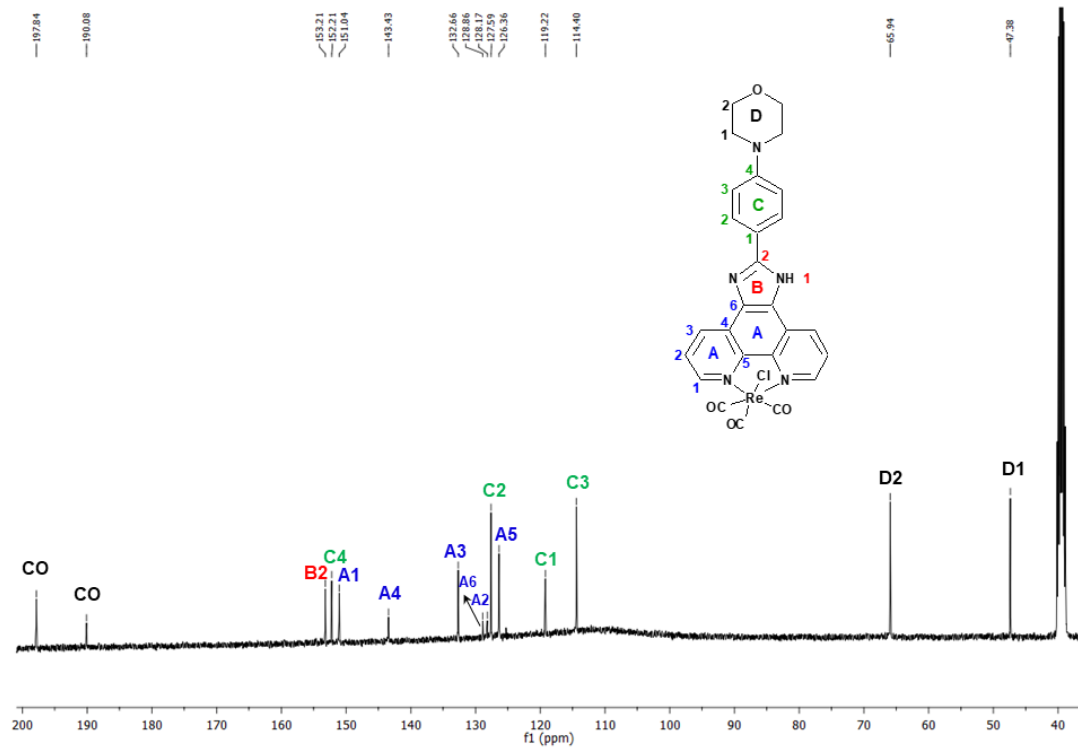


(e)

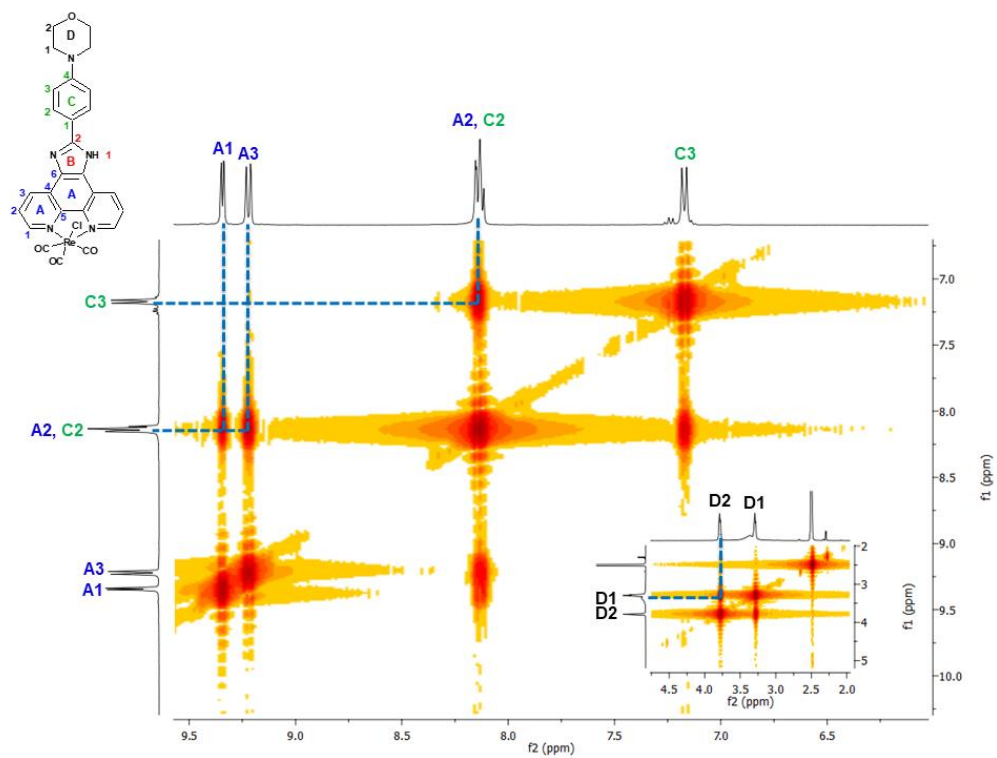
Figure S7. NMR spectra of **2**: ^1H NMR (a), ^{13}C NMR (b), ^1H - ^1H COSY (c) ^1H - ^{13}C HMQC (d), ^1H - ^{13}C HMBC (e)



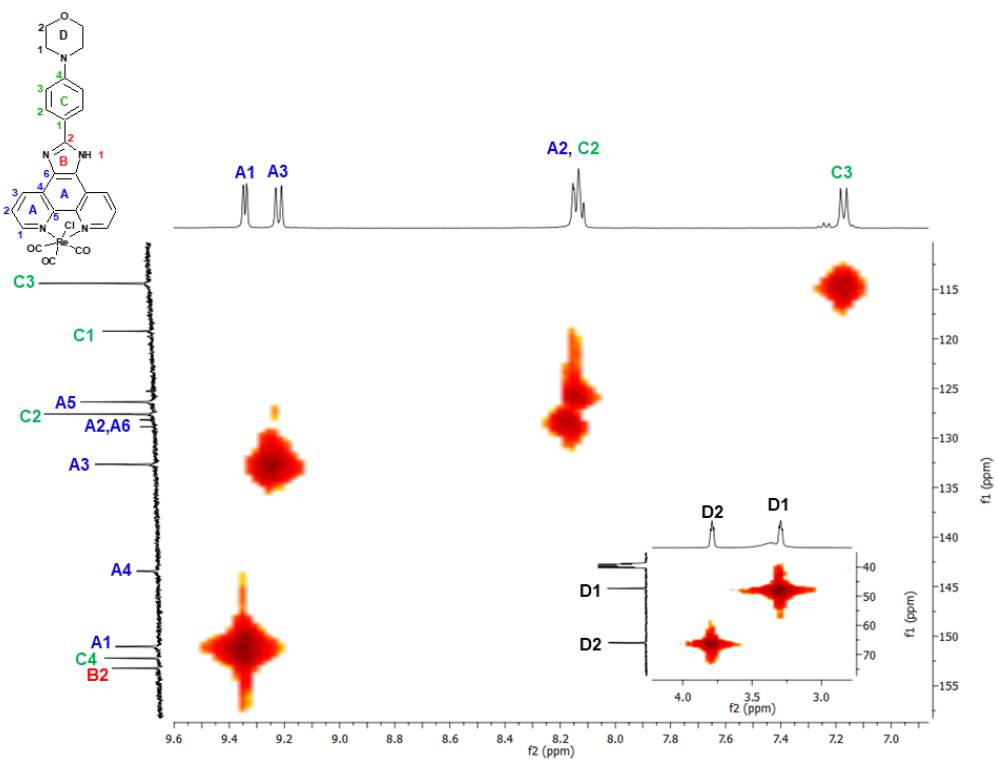
(a)



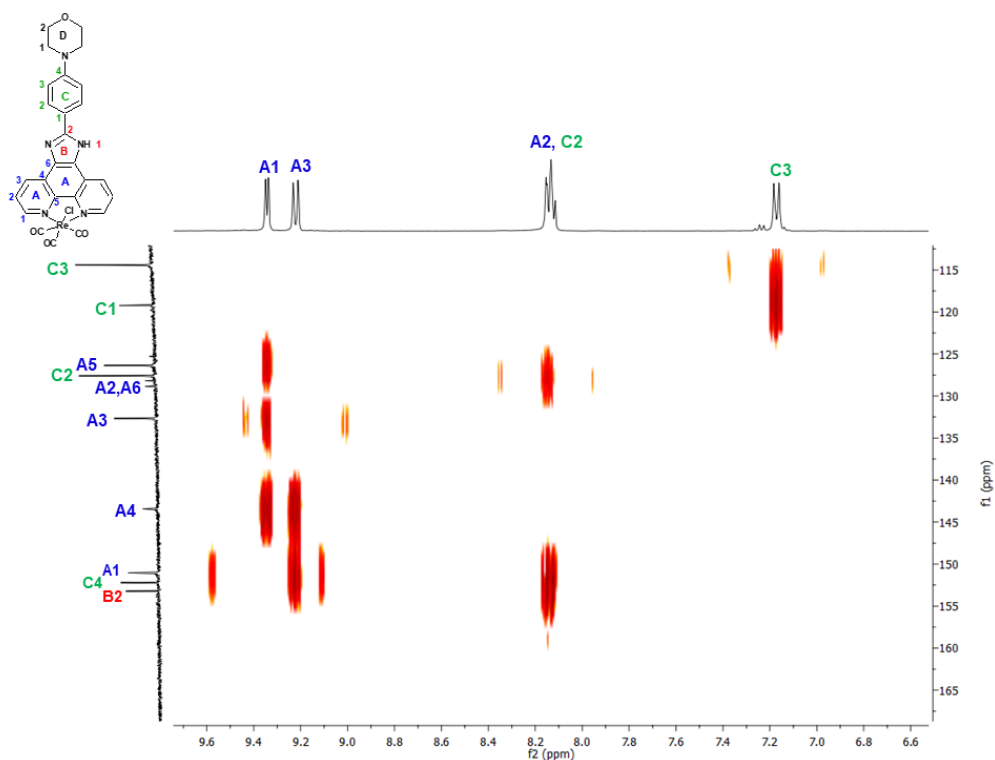
(b)



(c)

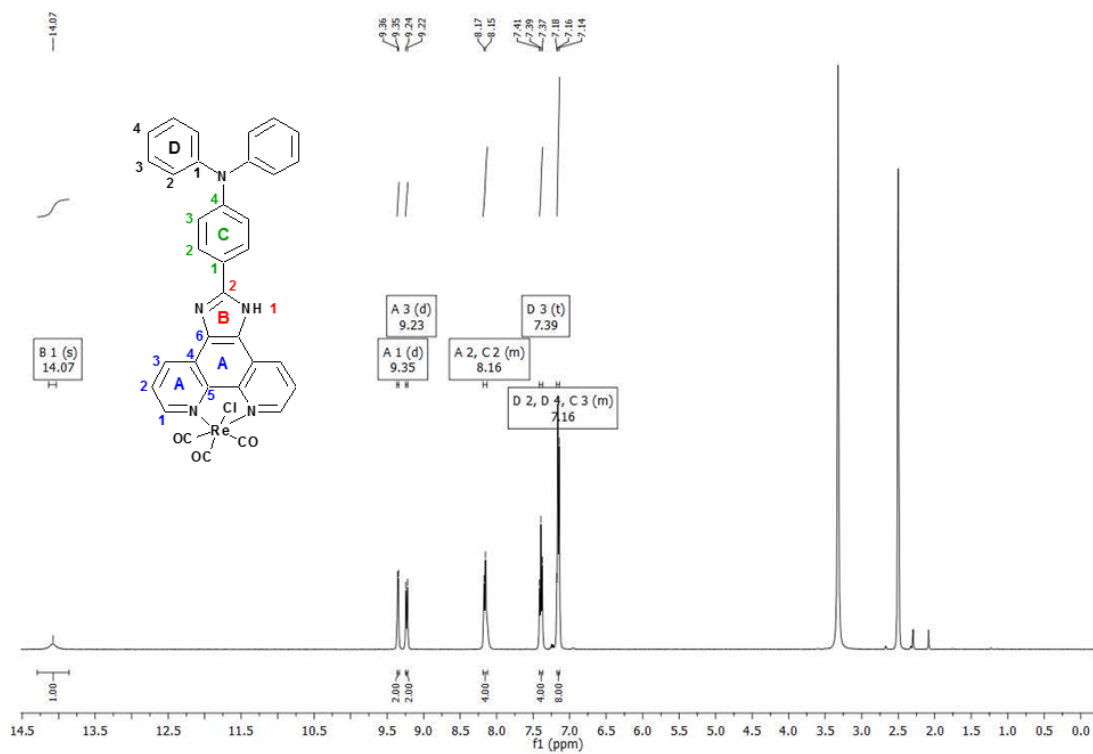


(d)

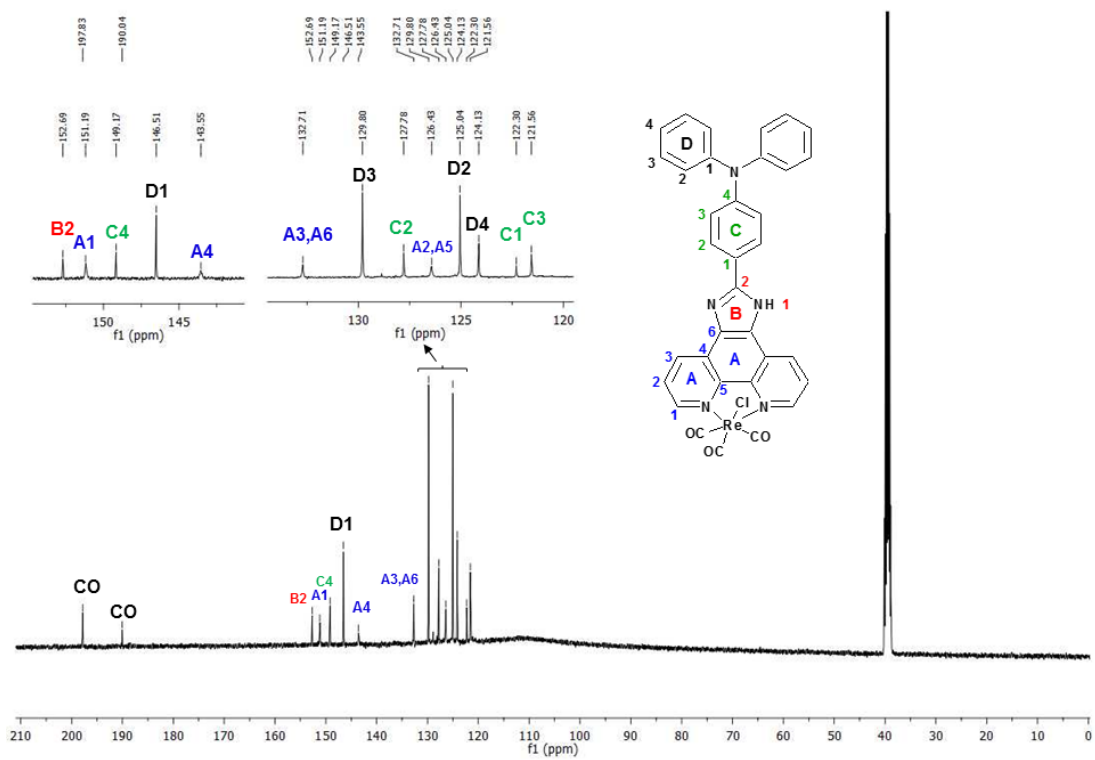


(e)

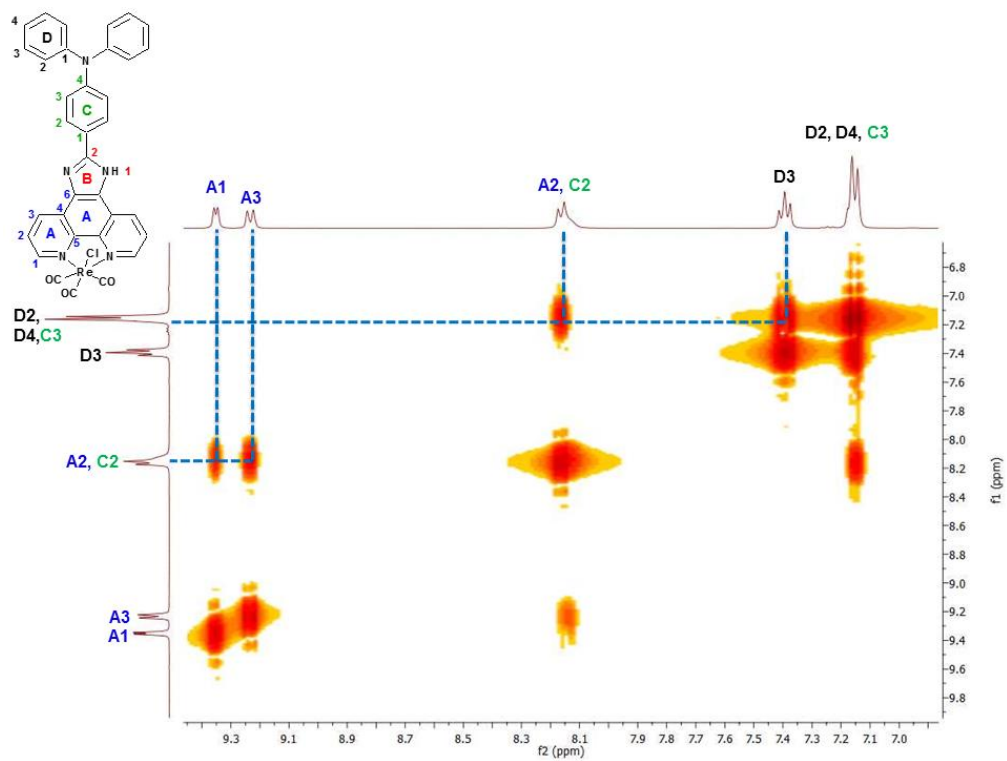
Figure S8. NMR spectra of **3**: ^1H NMR (a) ^{13}C NMR (b), ^1H - ^1H COSY (c) ^1H - ^{13}C HMQC (d), ^1H - ^{13}C HMBC (e)



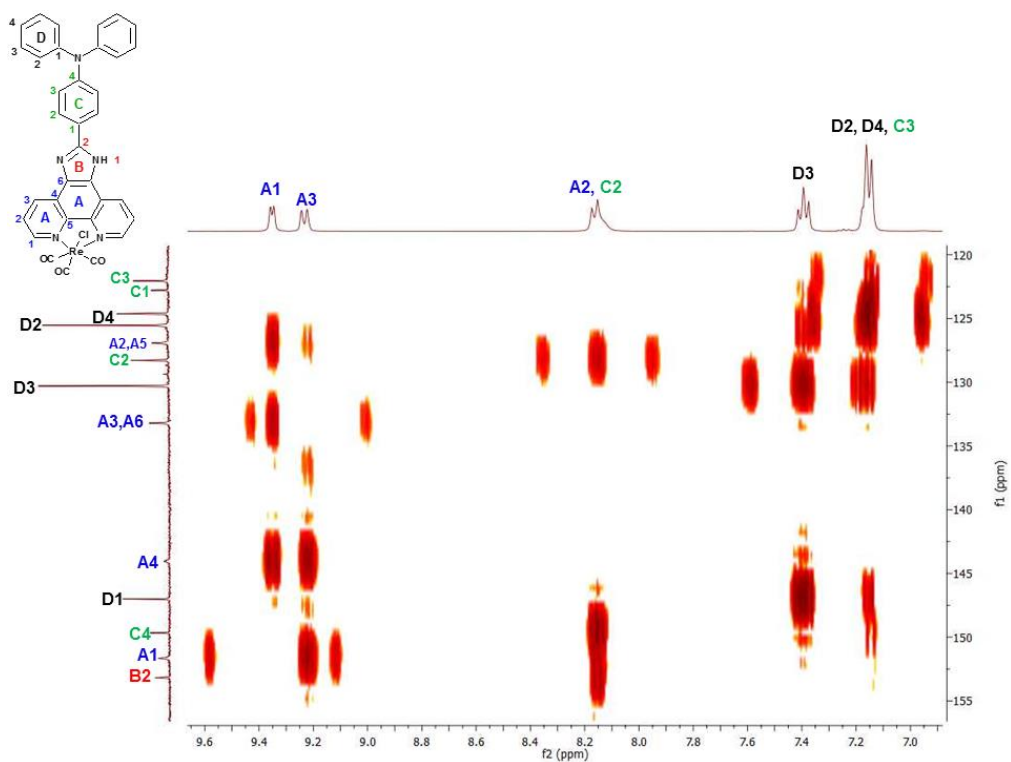
(a)



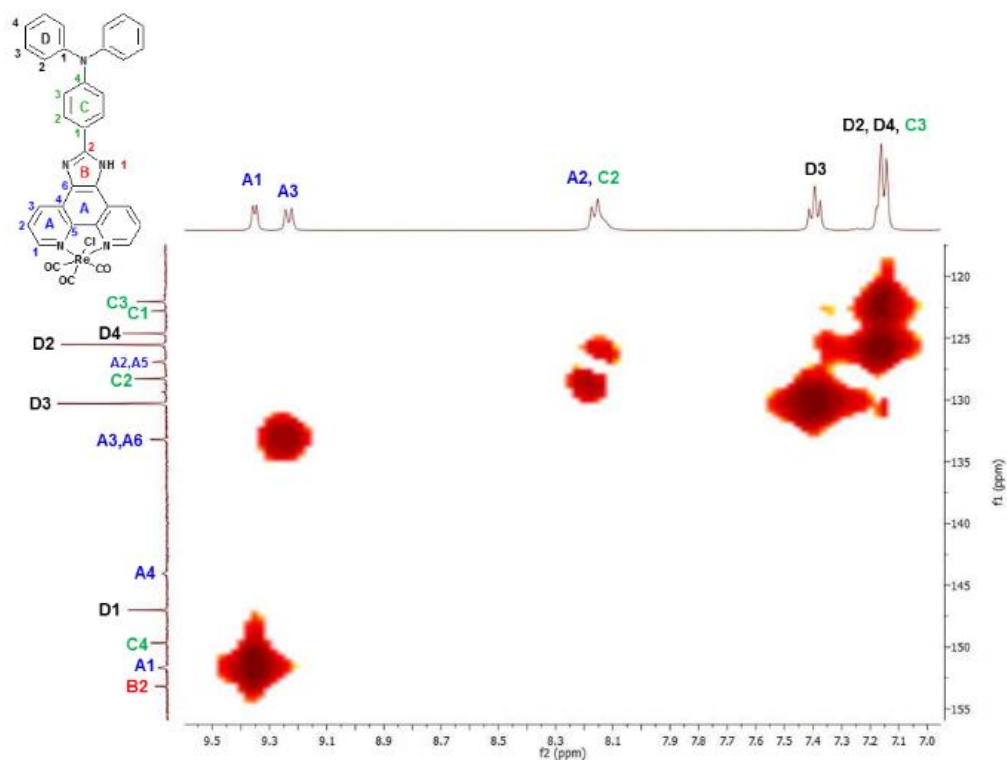
(b)



(c)

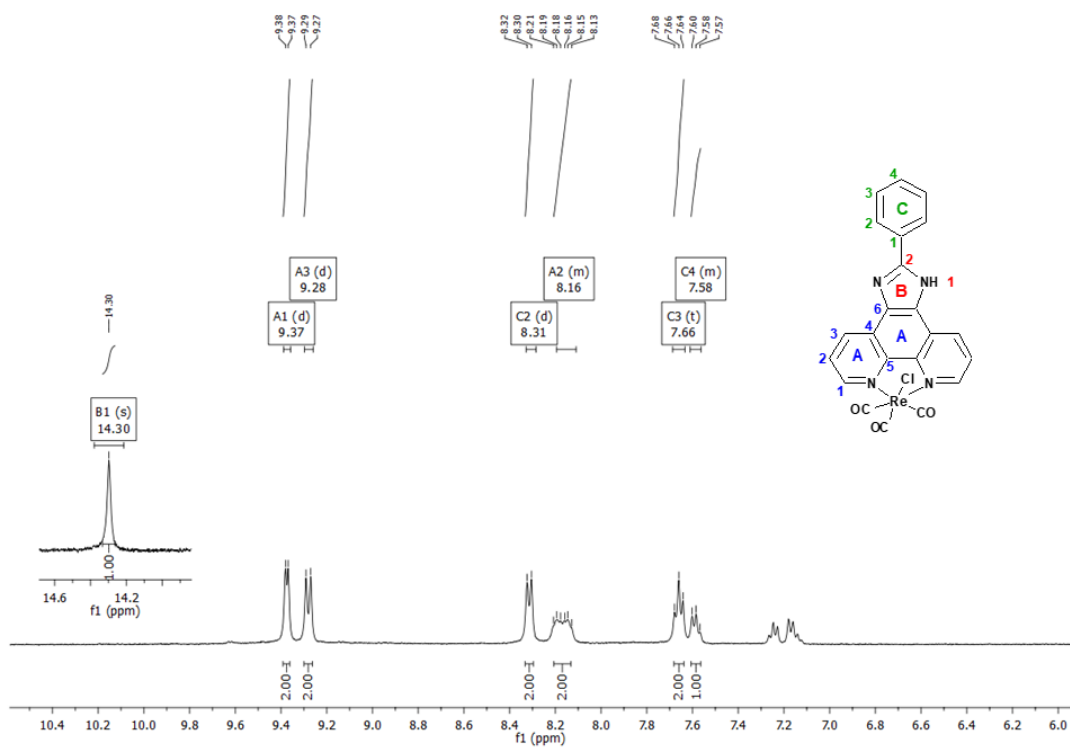


(d)

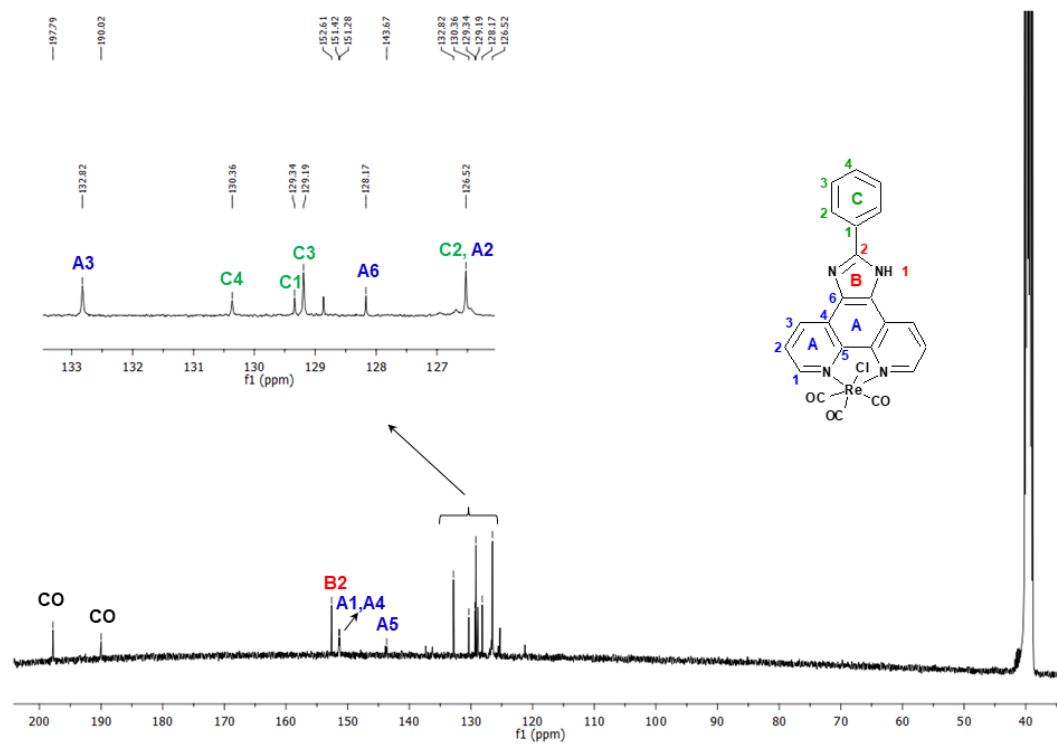


(e)

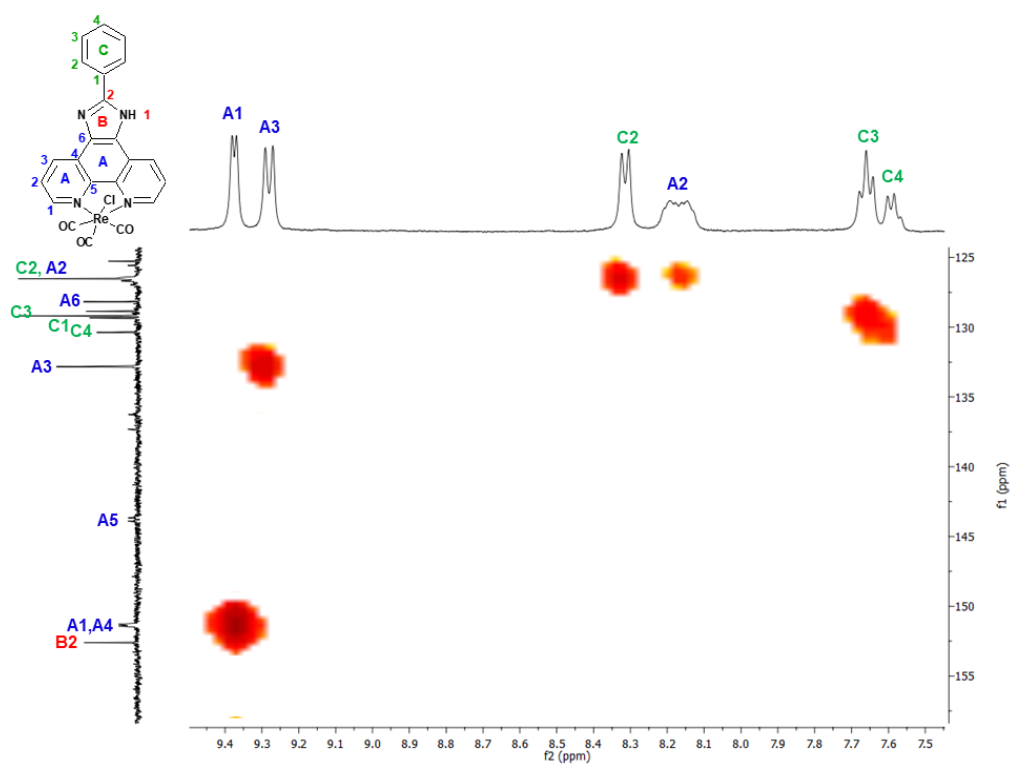
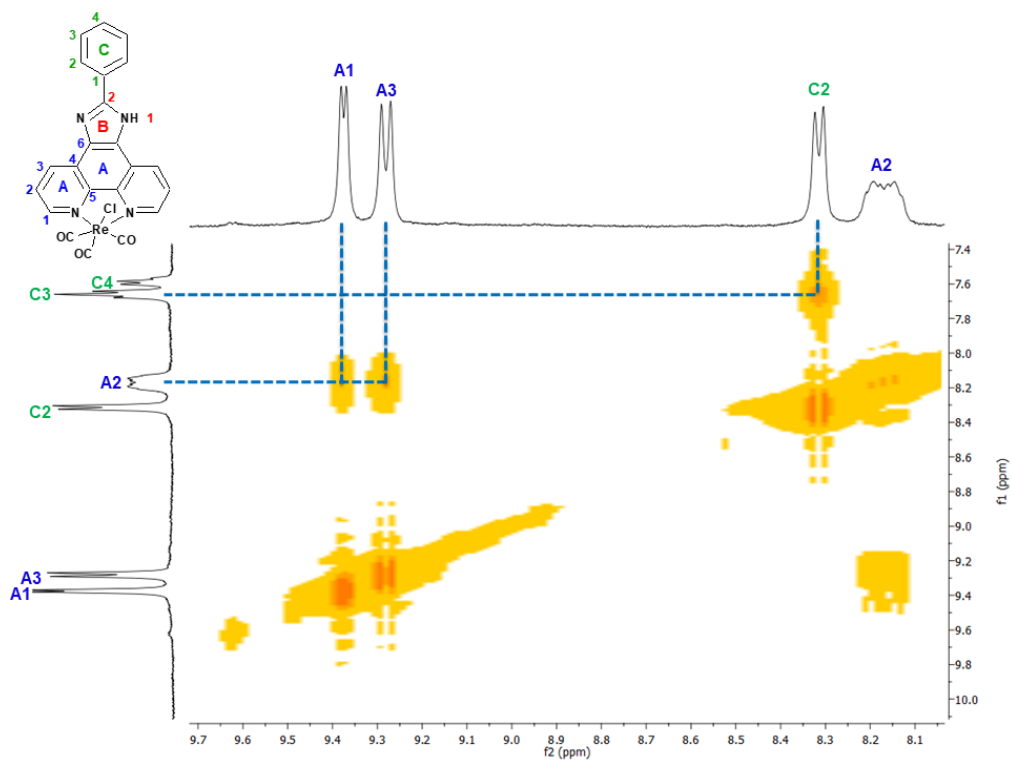
Figure S9. NMR spectra of **4**: ^1H NMR (a) ^{13}C NMR (b), ^1H - ^1H COSY (c) ^1H - ^{13}C HMQC (d), ^1H - ^{13}C HMBC (e)

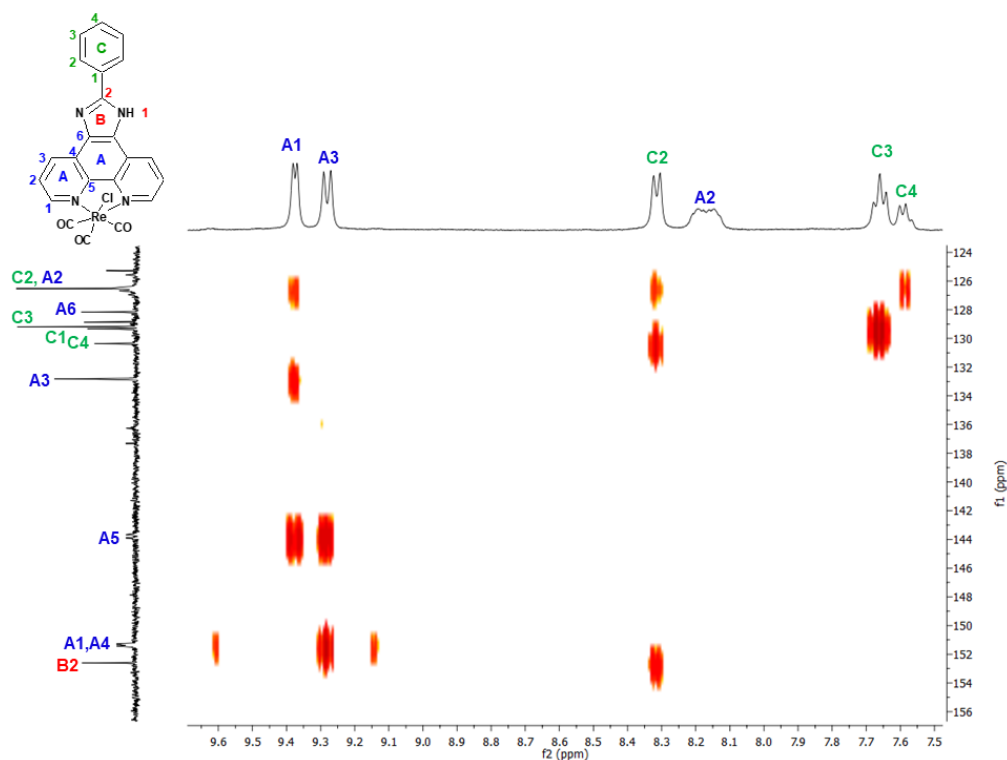


(a)



(b)

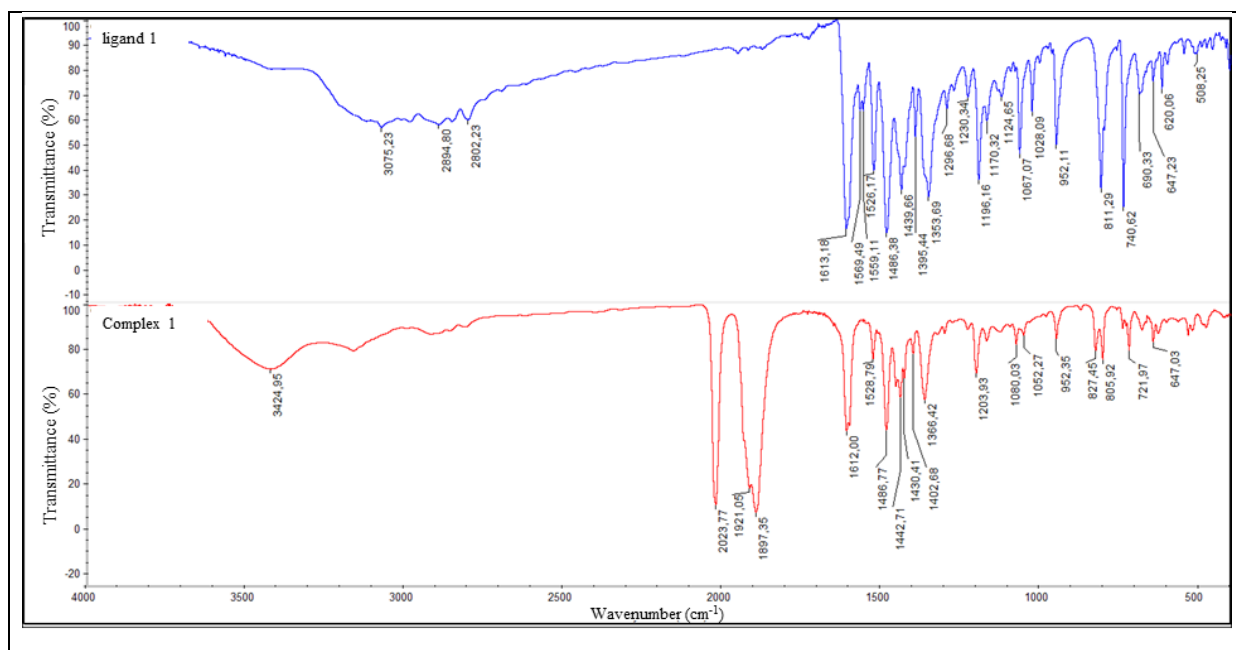


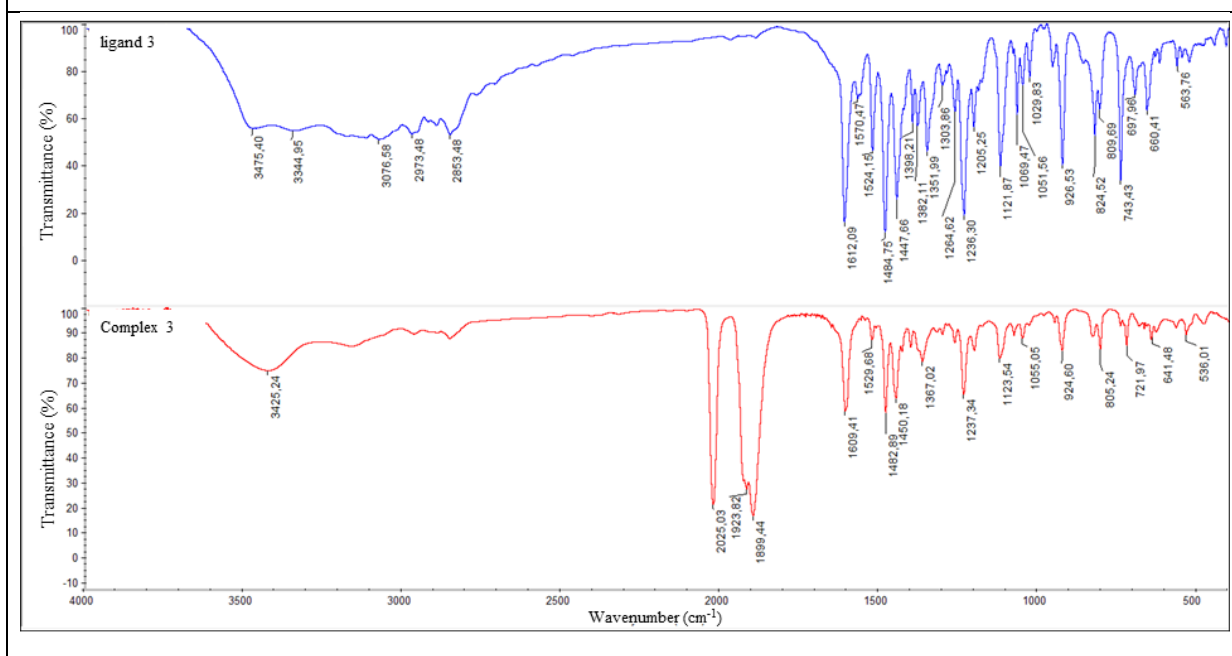
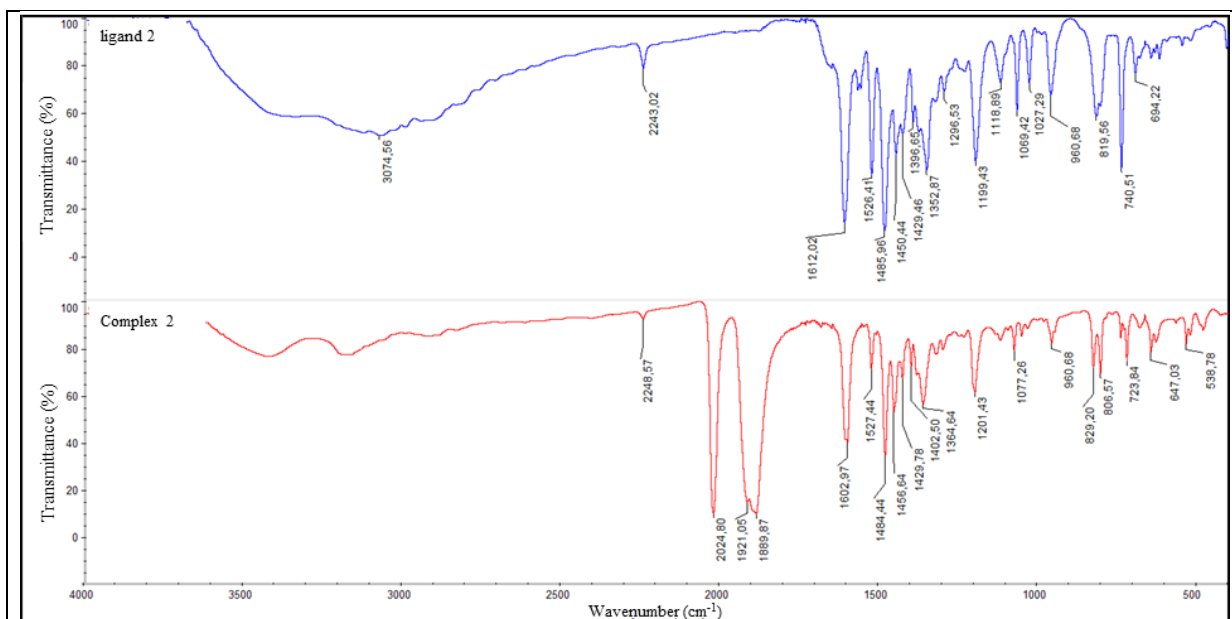


(e)

Figure S10. NMR spectra of **5**: ^1H NMR (a) ^{13}C NMR (b), ^1H - ^1H COSY (c) ^1H - ^{13}C HMQC (d), ^1H - ^{13}C HMBC (e)

IR SPECTRA OF RHENIUM(I) COMPLEXES (1–5)





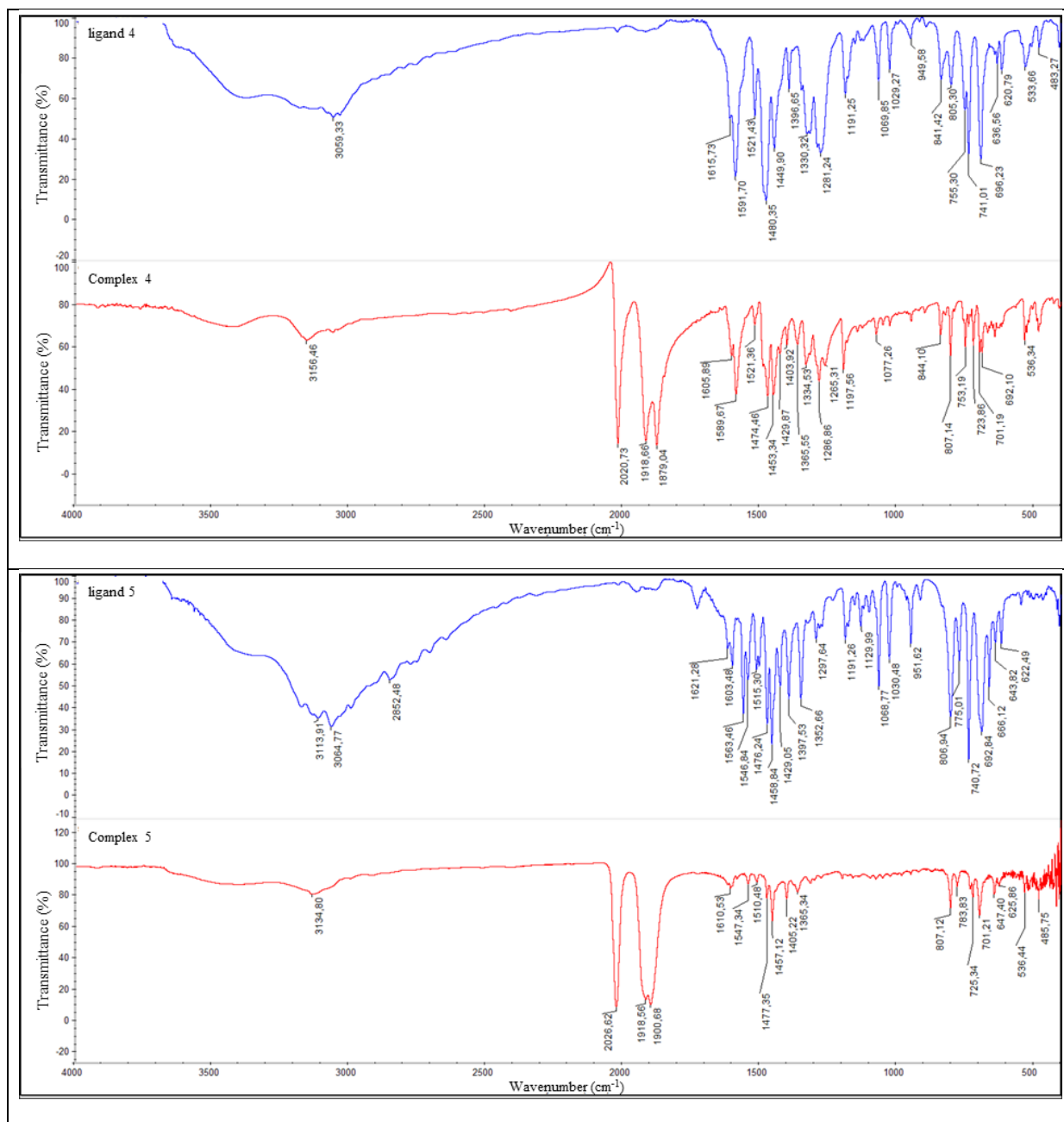
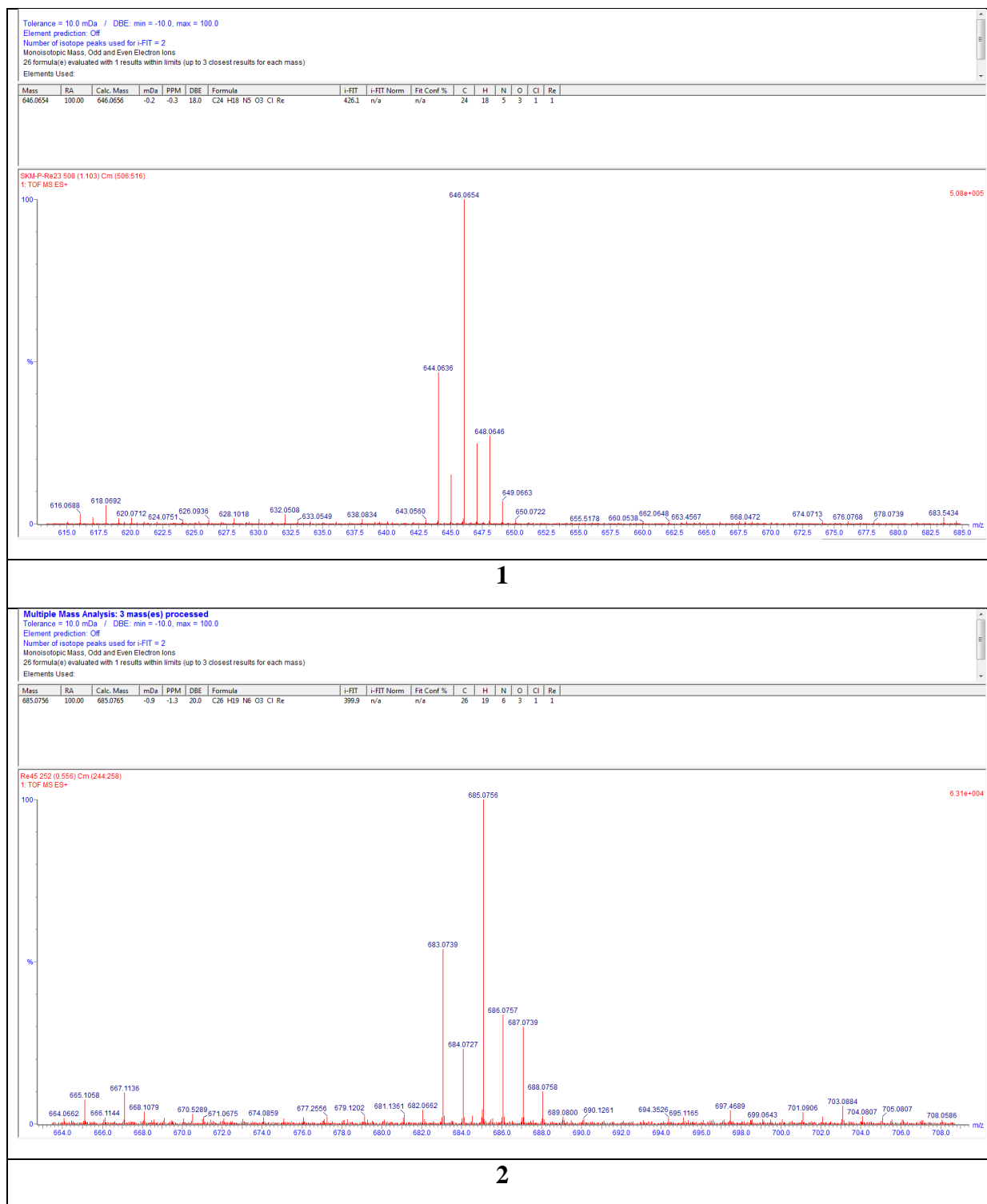


Figure S11. FT-IR spectra of **1-5** (red line) along with FT-IR spectra of the free ligands **L¹-L⁵** (blue line).

Table S1. Carbonyl stretching frequencies for complexes **1-5**

Compound	ν_{CO} [cm ⁻¹]	ν_{CO} [cm ⁻¹]	ν_{CO} [cm ⁻¹]	ν_{average} [cm ⁻¹]
1	2023.77	1921.05	1897.35	1947.39
2	2024.80	1921.05	1889.87	1945.24
3	2025.03	1923.82	1899.44	1949.43
4	2020.73	1918.66	1879.04	1939.48
5	2026.62	1918.56	1900.68	1948.62

HMRS SPECTRA OF RHENIUM(I) COMPLEXES (1-5)



Tolerance = 10.0 mDa / DBE: min = -10.0, max = 100.0

Element prediction: Off

Number of isotope peaks used for i-FIT = 2

Monoisotopic Mass, Odd and Even Electron Ions

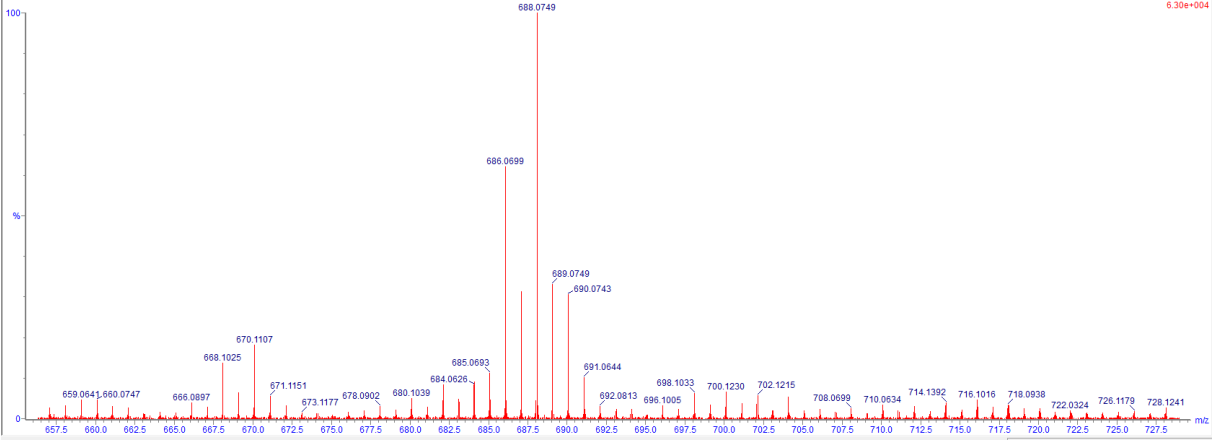
52 formula(e) evaluated with 1 results within limits (up to 3 closest results for each mass)

Elements Used:

Mass	RA	Calc. Mass	mDa	PPM	DBE	Formula	i-FIT	i-FIT Norm	Fit Conf %	C	H	N	O	Cl	Re
688.0749	100.00	688.0761	-1.2	-1.7	19.0	C ₂₆ H ₂₀ N ₅ O ₄ Cl ₁ Re	376.0	n/a	n/a	26	20	5	4	1	1

SKM-P-Re22 259 (0.580) Cm (259.270)

1. TOF MS ES+



3

Tolerance = 10.0 mDa / DBE: min = -10.0, max = 100.0

Element prediction: Off

Number of isotope peaks used for i-FIT = 2

Monoisotopic Mass, Odd and Even Electron Ions

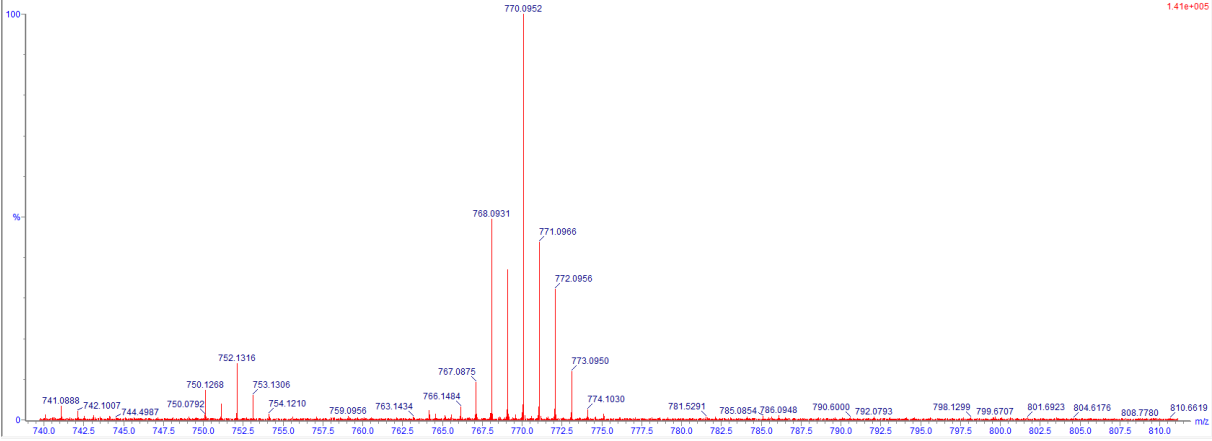
60 formula(e) evaluated with 1 results within limits (up to 3 closest results for each mass)

Elements Used:

Mass	RA	Calc. Mass	mDa	PPM	DBE	Formula	i-FIT	i-FIT Norm	Fit Conf %	C	H	N	O	Cl	Re
770.0952	100.00	770.0969	-1.7	-2.2	26.0	C ₃₄ H ₂₂ N ₅ O ₃ Cl ₁ Re	445.3	n/a	n/a	34	22	5	3	1	1

Re47 563 (1.227) Cm (560.575)

1. TOF MS ES+



4

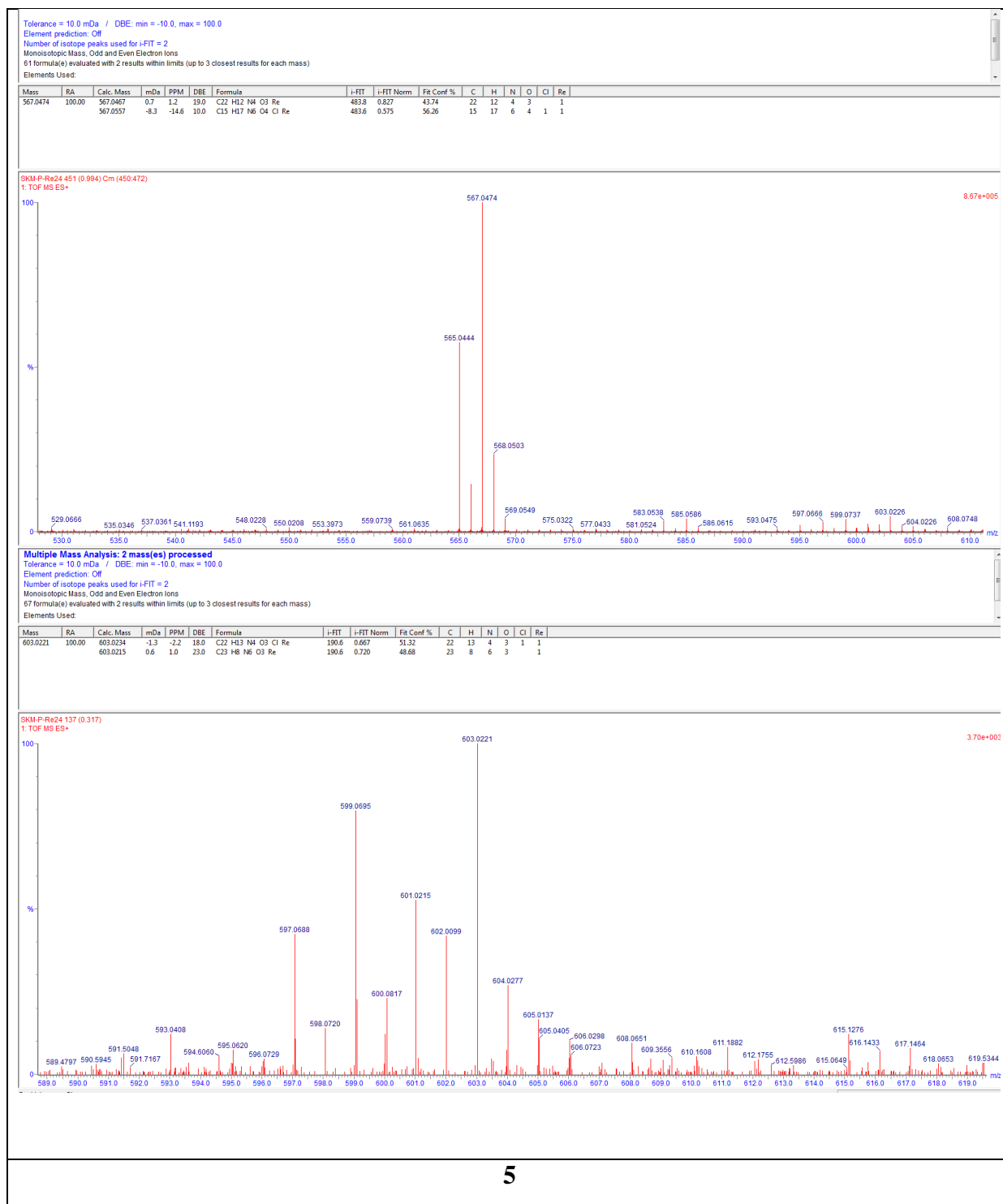


Figure S12. HRMS spectra of complexes **1–5**.

X-RAY ANALYSIS

Table S2. Crystal data and structure refinement of the complex **4**.

Empirical formula	C ₃₄ H ₂₁ ClN ₅ O ₃ Re
Formula weight	769.21
Temperature [K]	293(2) K
Wavelength [Å]	0.71073
Crystal system	Triclinic
Space group	$P\bar{1}$
Unit cell dimensions [Å, °]	$a = 9.2661(5)$ $b = 10.9770(5)$ $c = 15.4545(6)$ $\alpha = 95.821(4)$ $\beta = 98.126(4)$ $\gamma = 107.294(4)$
Volume [Å ³]	1468.59(12)
Z	2
Density (calculated) [Mg/m ³]	1.739
Absorption coefficient [mm ⁻¹]	4.273
F(000)	752.0
Crystal size [mm]	0.181×0.079×0.024
θ range for data collection [°]	3.5 to 25.1
Index ranges	-11 ≤ h ≤ 10 -13 ≤ k ≤ 13 0 ≤ l ≤ 18
Reflections collected	5198
Independent reflections	5198
Completeness to 2θ=50° [%]	99.78
Max. and min. transmission	1.000 and 0.540
Data / restraints / parameters	5198 / 0 / 398
Goodness-of-fit on F ²	1.158
Final R indices [I>2σ(I)]	R ₁ = 0.0377 wR ₂ = 0.0795
R indices (all data)	R ₁ = 0.0438 wR ₂ = 0.0815
Largest diff. peak and hole[eÅ ⁻³]	1.423 and -1.071
CCDC number	2192061

Table S3. Bond lengths [Å] and angles [°] of complex **4**

Bond lengths	[Å]	Bond angles	[°]
Re(1)–C(1)	1.906(7)	C(2)–Re(1)–C(1)	89.4(3)
Re(1)–C(2)	1.901(7)	C(3)–Re(1)–C(1)	89.6(3)
Re(1)–C(3)	1.893(7)	C(3)–Re(1)–C(2)	86.7(3)
Re(1)–N(1)	2.163(5)	C(1)–Re(1)–N(1)	170.3(3)
Re(1)–N(2)	2.166(5)	C(2)–Re(1)–N(1)	99.0(2)
Re(1)–Cl(1)	2.4859(17)	C(3)–Re(1)–N(1)	95.7(2)
C(1)–O(1)	1.153(8)	C(1)–Re(1)–N(2)	95.5(3)
C(2)–O(2)	1.170(8)	C(2)–Re(1)–N(2)	174.6(3)
C(3)–O(3)	1.156(8)	C(3)–Re(1)–N(2)	95.6(2)
		N(1)–Re(1)–N(2)	75.94(18)
		C(1)–Re(1)–Cl(1)	91.1(2)
		C(2)–Re(1)–Cl(1)	95.2(2)
		C(3)–Re(1)–Cl(1)	177.96(19)
		N(1)–Re(1)–Cl(1)	83.27(14)
		N(2)–Re(1)–Cl(1)	82.43(14)

Table S4. Short intra- and intermolecular hydrogen bonds for complex **4**.

D–H...A	D–H [Å]	H...A [Å]	D–A [Å]	D–H...A [°]
4				
N(3)–H(3)...Cl(1) ^a	0.86	2.40	3.205(5)	156.0
C(5)–H(5)...O(2) ^b	0.93	2.56	3.475(9)	169.0
C(11)–H(11)...O(3) ^c	0.93	2.45	3.368(10)	169.0
C(22)–H(22)...N(4)	0.93	2.59	2.904(9)	100.0
C(28)–H(28)...O(1) ^d	0.93	2.54	3.416(9)	157.0
C(34)–H(34)...O(1) ^a	0.93	2.53	3.213(10)	131.0

Symmetry codes: (a) = 2-x,2-y,1-z, (b) = 1-x,2-y,1-z, (c) = 1+x,y,z, (d) = 1+x,y,-1+z, (e) = 2-x,1-y,1-z

Table S5. X–Y...Cg(J)(π -ring) interactions for complex **4**.

Y–X(I)...Cg(J)	X(I)...Cg(J) [Å]	X-Perp [Å]	γ [°]	Y–X(I)...Cg(J) [°]
4				
C(3)–O(3)...Cg(1) ^a	3.747(6)	-3.290	28.58	154.1(5)
C(3)–O(3)...Cg(2) ^a	3.768(6)	-3.313	28.46	164.1(5)

γ = angle X(I)→Cg(J) vector and normal to plane J.

Cg(1) is the centroid of atoms N(1)/C(4)/C(5)/C(6)/C(7)/C(15); Cg(2) is the centroid of atoms C(7)/C(8)/C(9)/C(10)/C(14)/C(15)

Symmetry codes: (a) = 1-x, 1-y, 1-z

THERMAL STUDIES

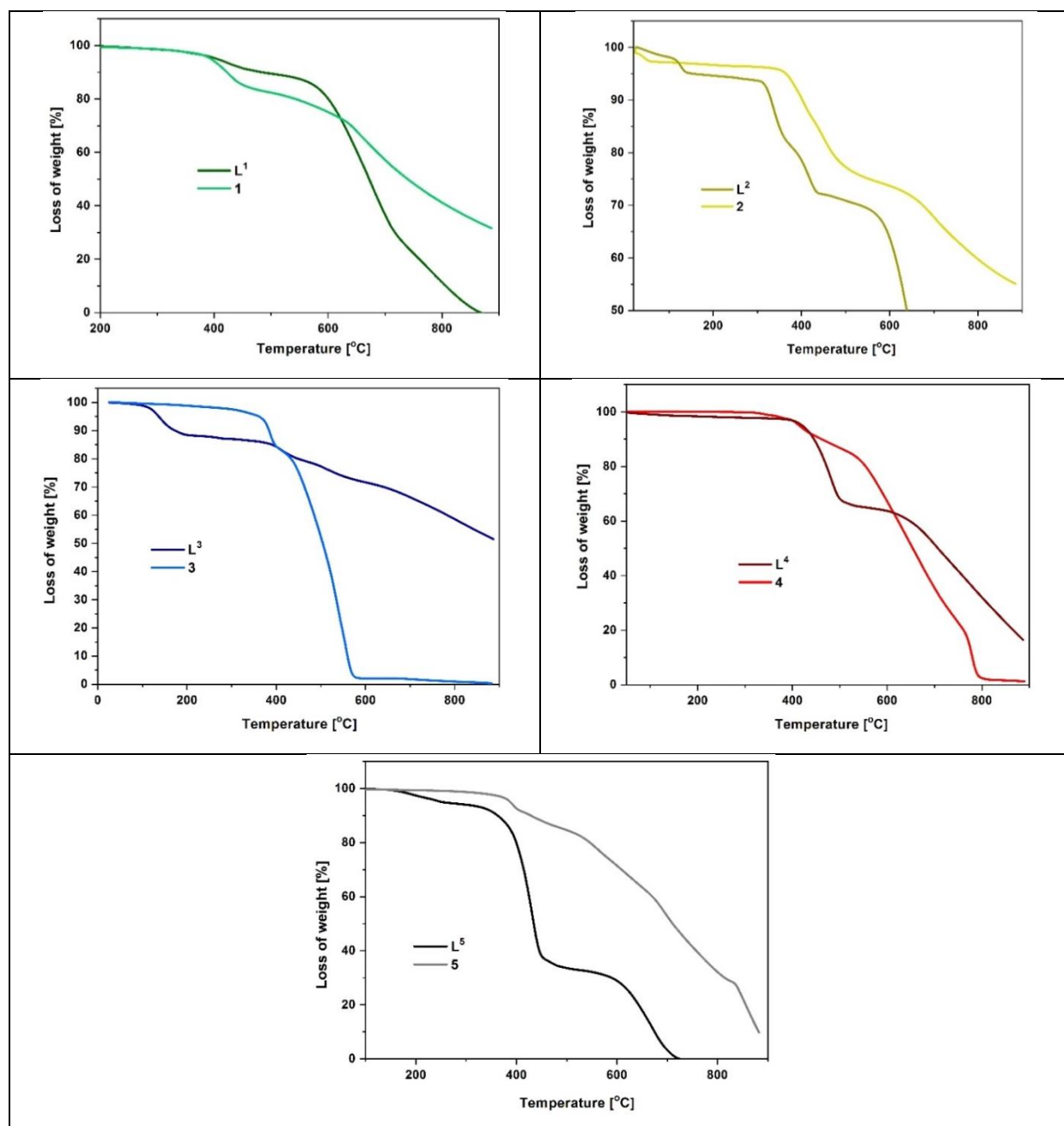


Figure S13. TGA thermograms of **1–5** and free ligands **L¹–L⁵**.

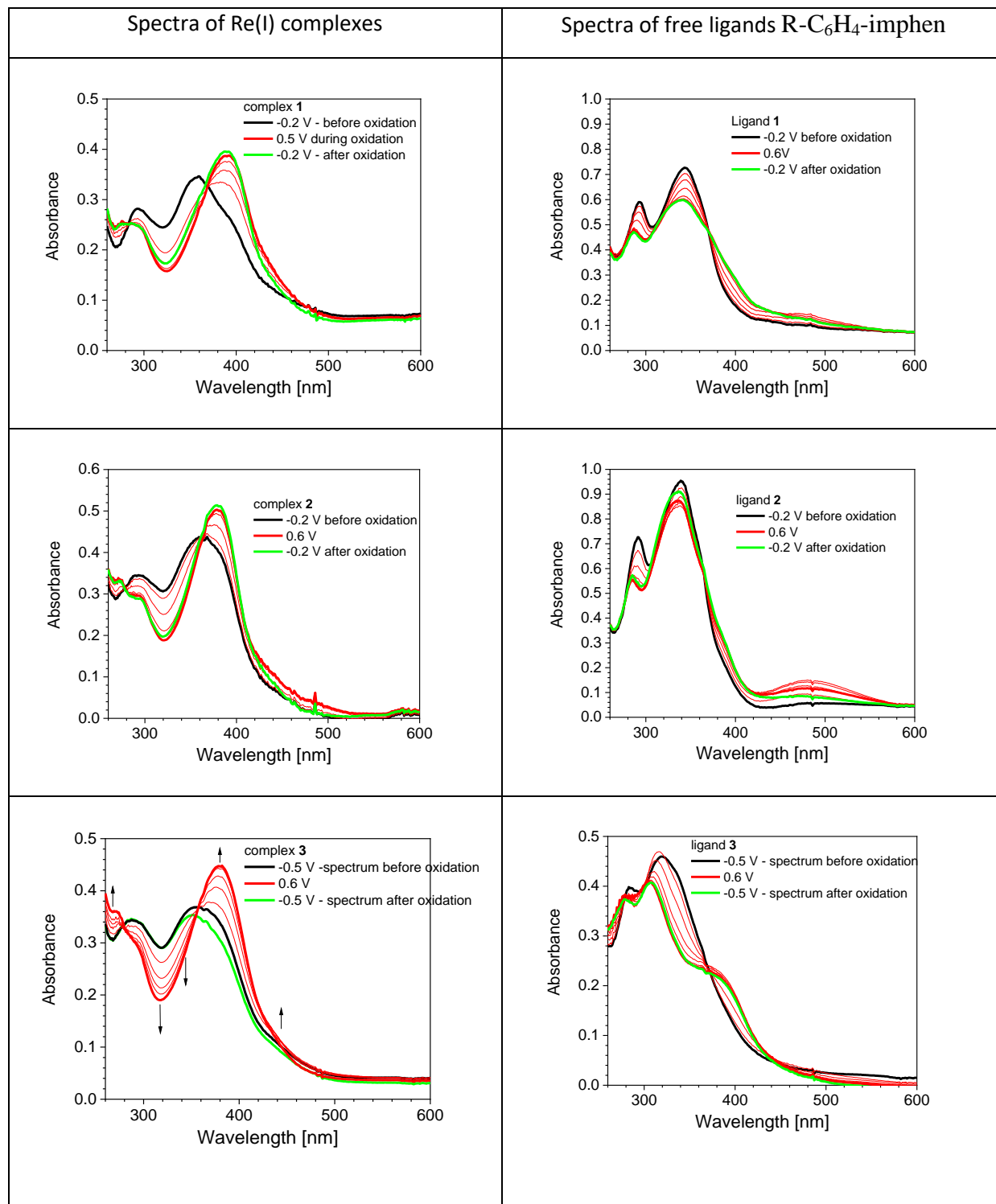
Table S6. Thermal stability of the synthesized compounds.

Code	T_5 [°C]	T_{10} [°C]	T_{max} [°C]
1	394	422	423, 656
2	364	401	405, 702
3	361	383	385, 555
4	414	461	628, 778
5	387	428	562, 691

T_5 and T_{10} temperature of 5% and 10% weight loss, respectively.

T_{max} temperature of maximum decomposition rate.

SPECTROELECTROCHEMISTRY



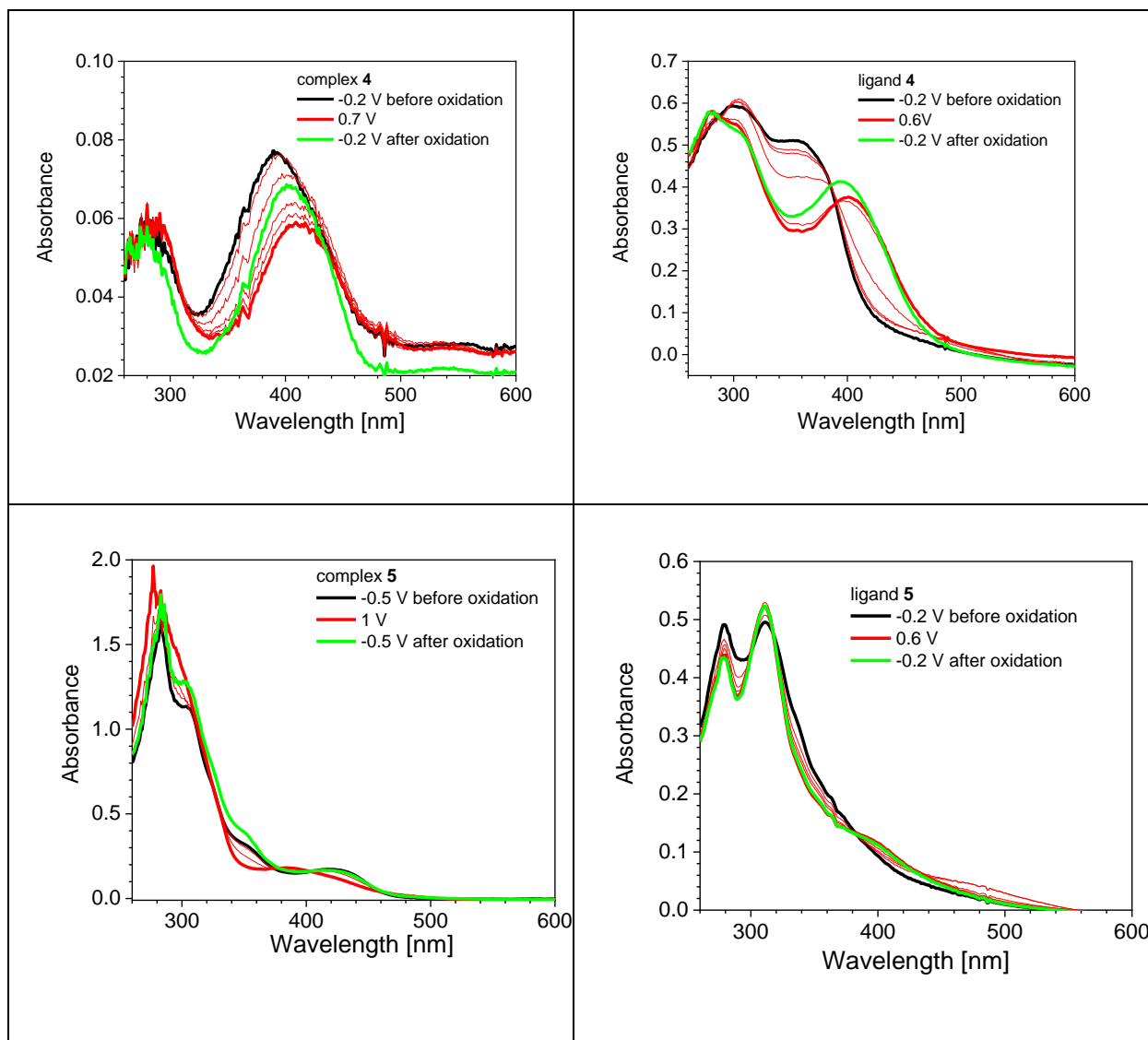


Figure S14. UV-VIS of complexes **1-5** and corresponding ligand in the solution $\text{CH}_2\text{Cl}_2/\text{Bu}_4\text{NPBF}_4$. Spectra recorded for different potentials related to: neutral state, first oxidation state and neutral state after oxidation process.

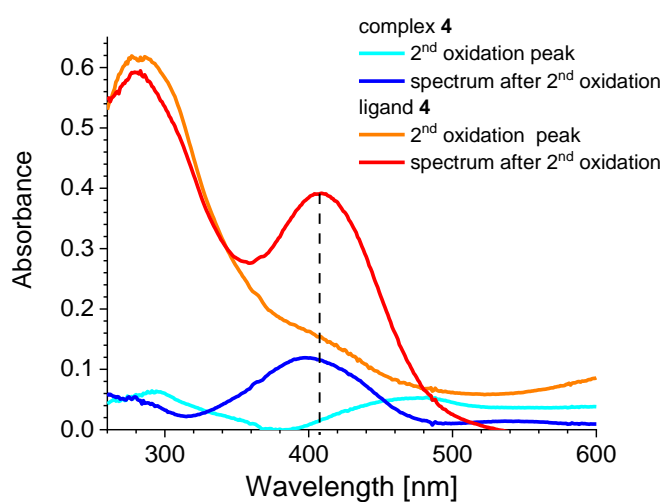
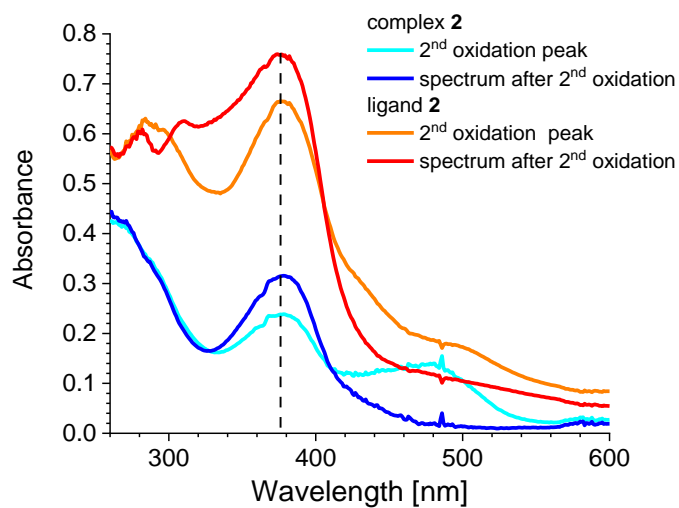
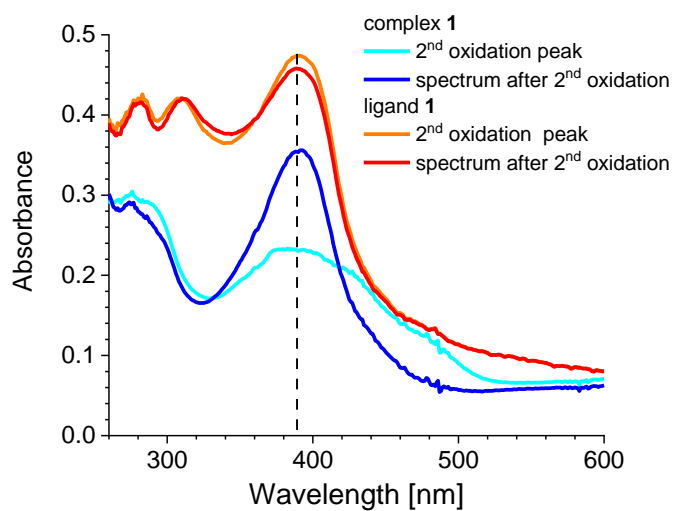
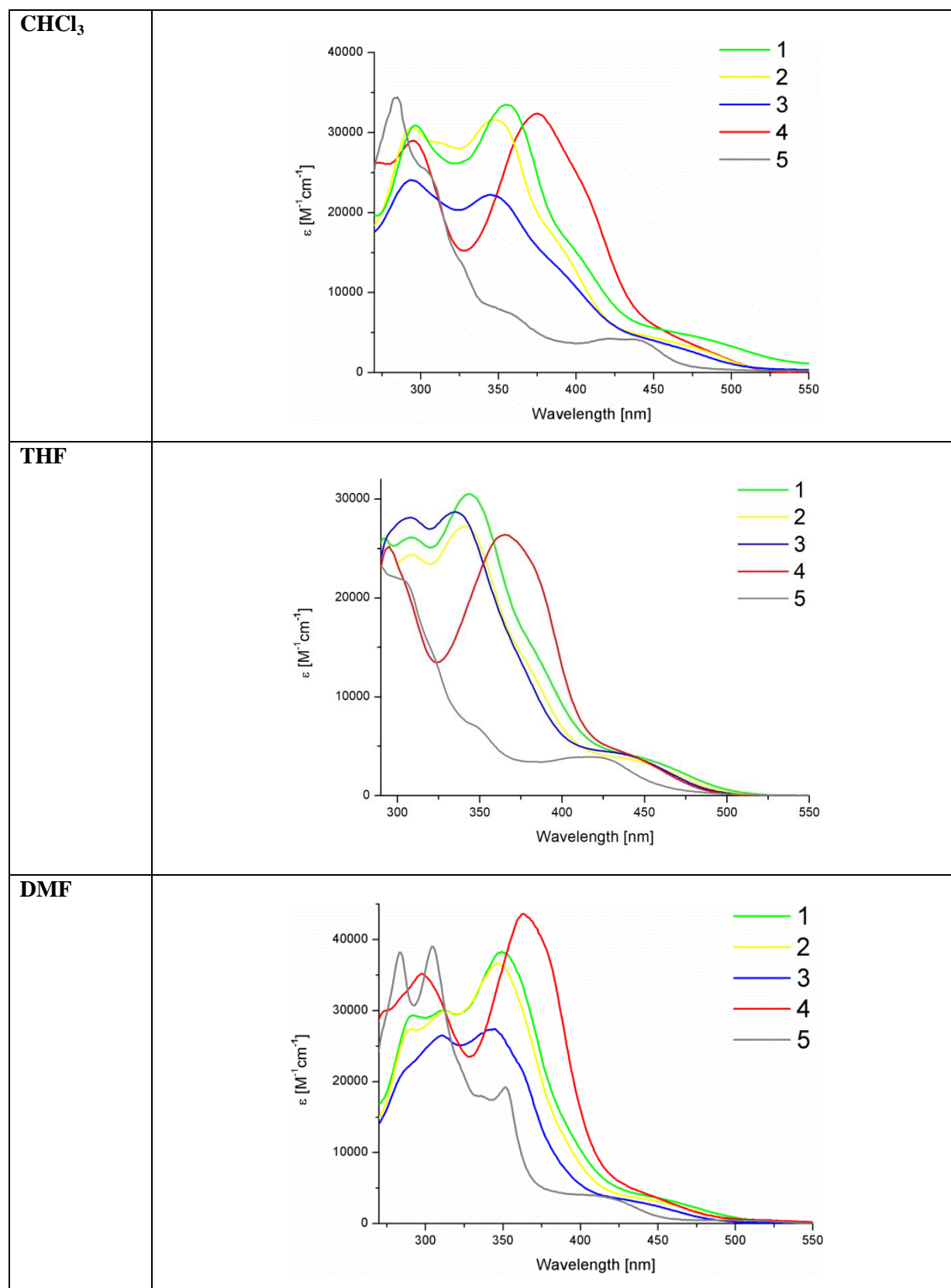


Figure S15. UV-VIS of complexes **1**, **2**, **4** and corresponding ligand in the solution $\text{CH}_2\text{Cl}_2/\text{Bu}_4\text{NPF}_6$. Spectra recorded for compounds at potential related to second oxidation state and potential related to neutral state after oxidation process.

UV-VIS SPECTROSCOPY



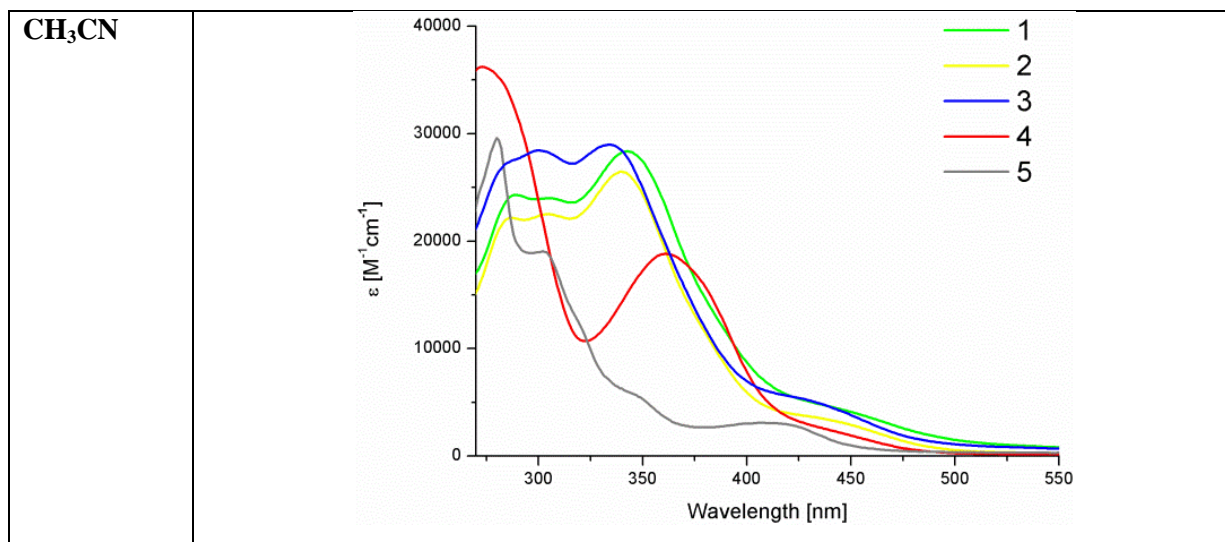


Figure S16. Absorption spectra of the complexes **1–5** in CHCl₃, THF, DMF, and CH₃CN.

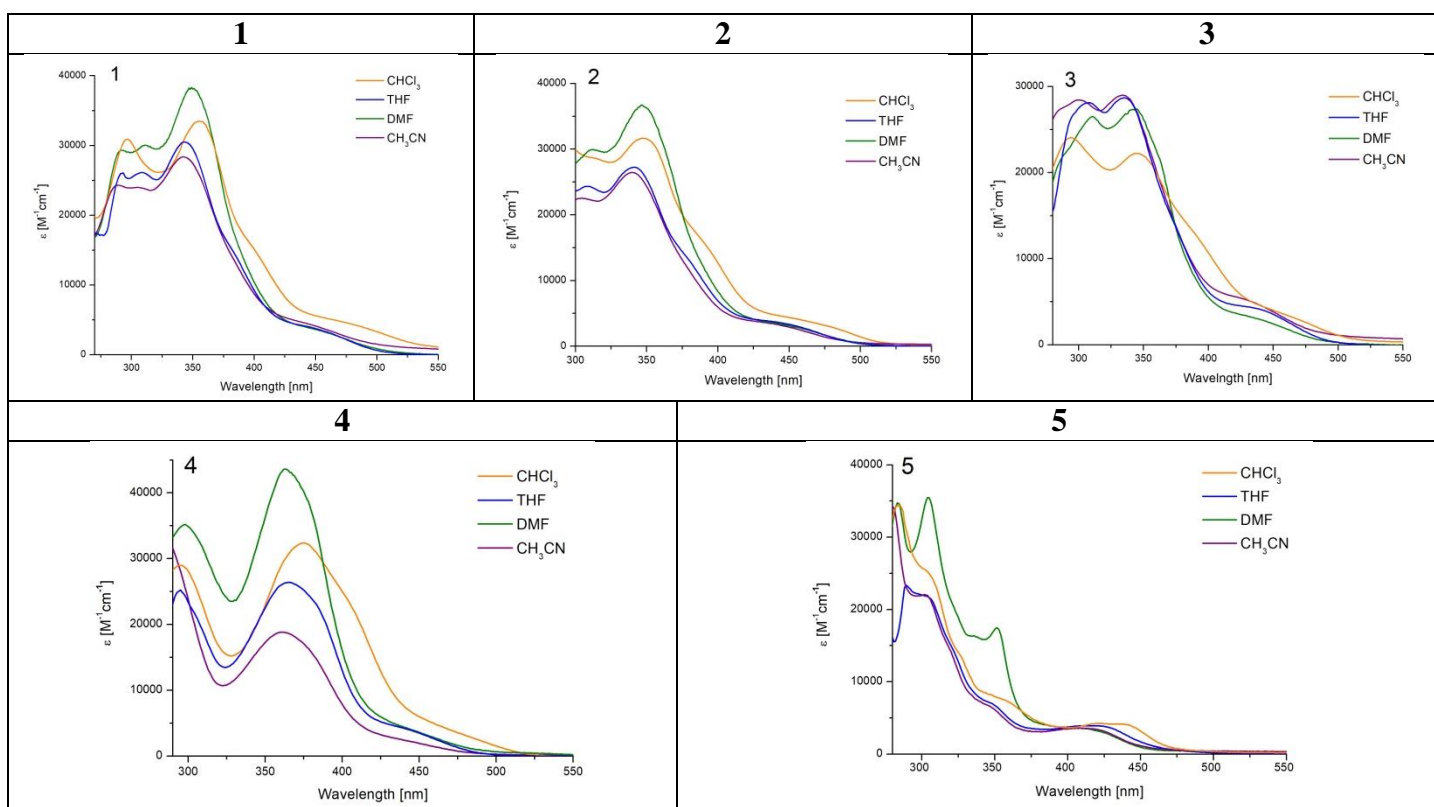


Figure S17. Impact of solvent polarity on UV-Vis spectra of complexes **1–5**.

Table S7. The absorption maxima and molar extinction coefficient for **1–5** in four solvents of different polarity.

Compound	Medium	λ (nm) (ϵ ($M^{-1}cm^{-1}$))
1	CHCl ₃	473 (4885), 391sh (17180), 355 (33510), 296 (31005)
	CH ₃ CN	447 (4250), 342 (28440), 305 (24150), 287 (24255)
	DMF	457 (3305), 349 (38175), 310 (30135), 290 (29395)
	THF	444 (3971), 343 (30582), 308 (26085), 292 (26084)
2	CHCl ₃	461(3795), 379sh (18380), 347 (31450), 309 (28940), 293 (30690)
	CH ₃ CN	441 (3270), 339 (26355), 303 (22395), 285 (22170)
	DMF	452 (3055), 346 (36695), 310 (29885), 289 (27420)
	THF	443 (3643), 341 (27408), 308 (24491)
3	CHCl ₃	455 (3685), 374sh (15765), 344 (22300), 293 (24045)
	CH ₃ CN	427 (5245), 335 (28985), 300 (28440), 282 (26905)
	DMF	434 (3175), 344 (27290), 309 (26550), 284 (21110)
	THF	437 (4216), 334 (28691), 307 (28093)
4	CHCl ₃	468 (4015), 398sh (25780), 374 (32420), 294 (28835)
	CH ₃ CN	441(2495), 361 (18985), 274 (36355)
	DMF	446 (3930), 364 (43735), 297 (35090)
	THF	443 (4177), 364 (26433), 294 (25085)
5	CHCl ₃	433 (4120), 352 (7600), 302 (25570), 284 (34270)
	CH ₃ CN	415 (2940), 346 (5680), 303 (19090), 280 (29320)
	DMF	416 (3925), 352 (19250), 336 (17895), 304 (38790), 284 (38175)
	THF	425 (3841), 348 (7016), 303 (21844), 289 (23297)

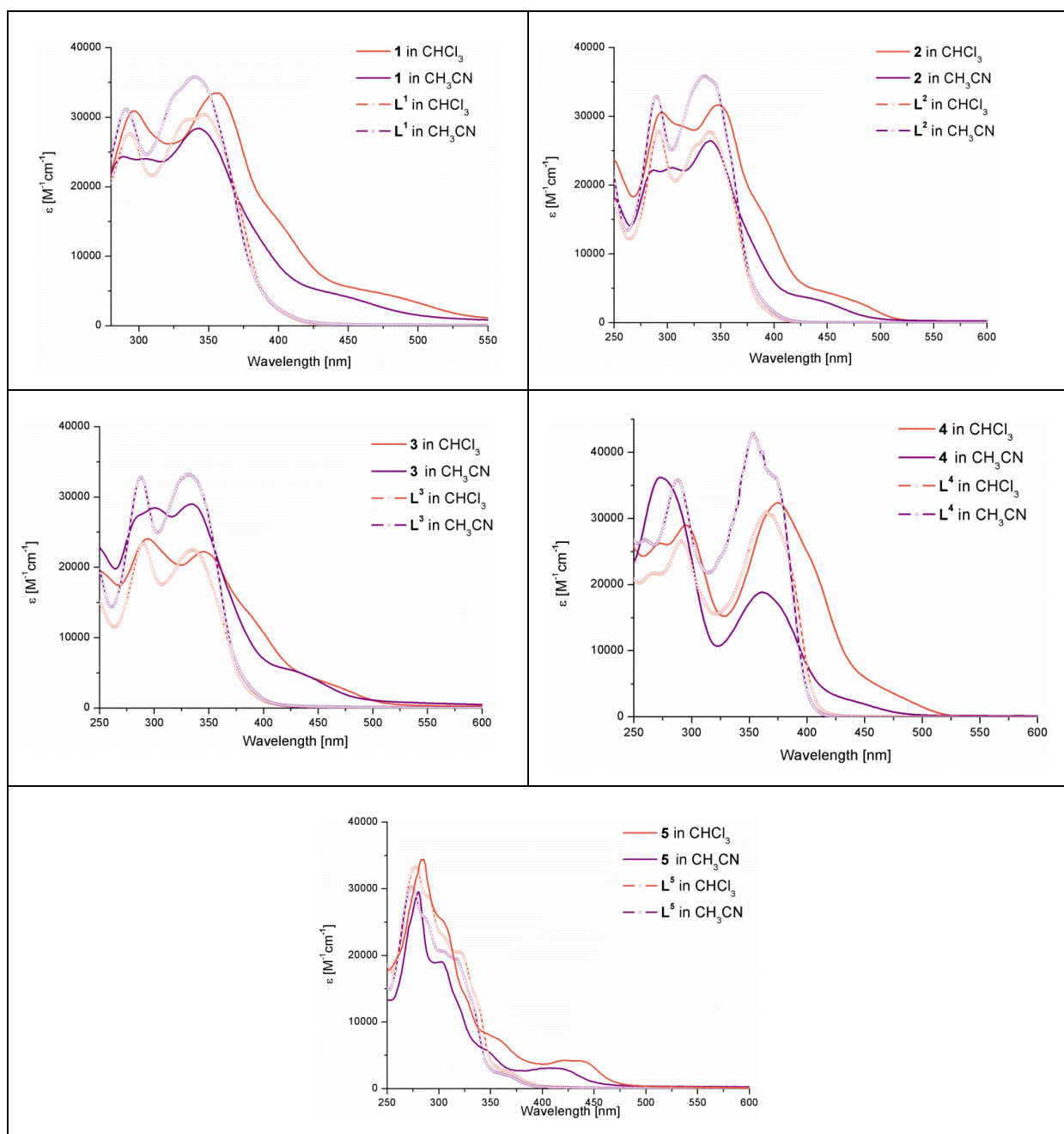


Figure S18. Comparison of UV–Vis spectra of complexes **1–5** with free ligands **L¹–L⁵**.

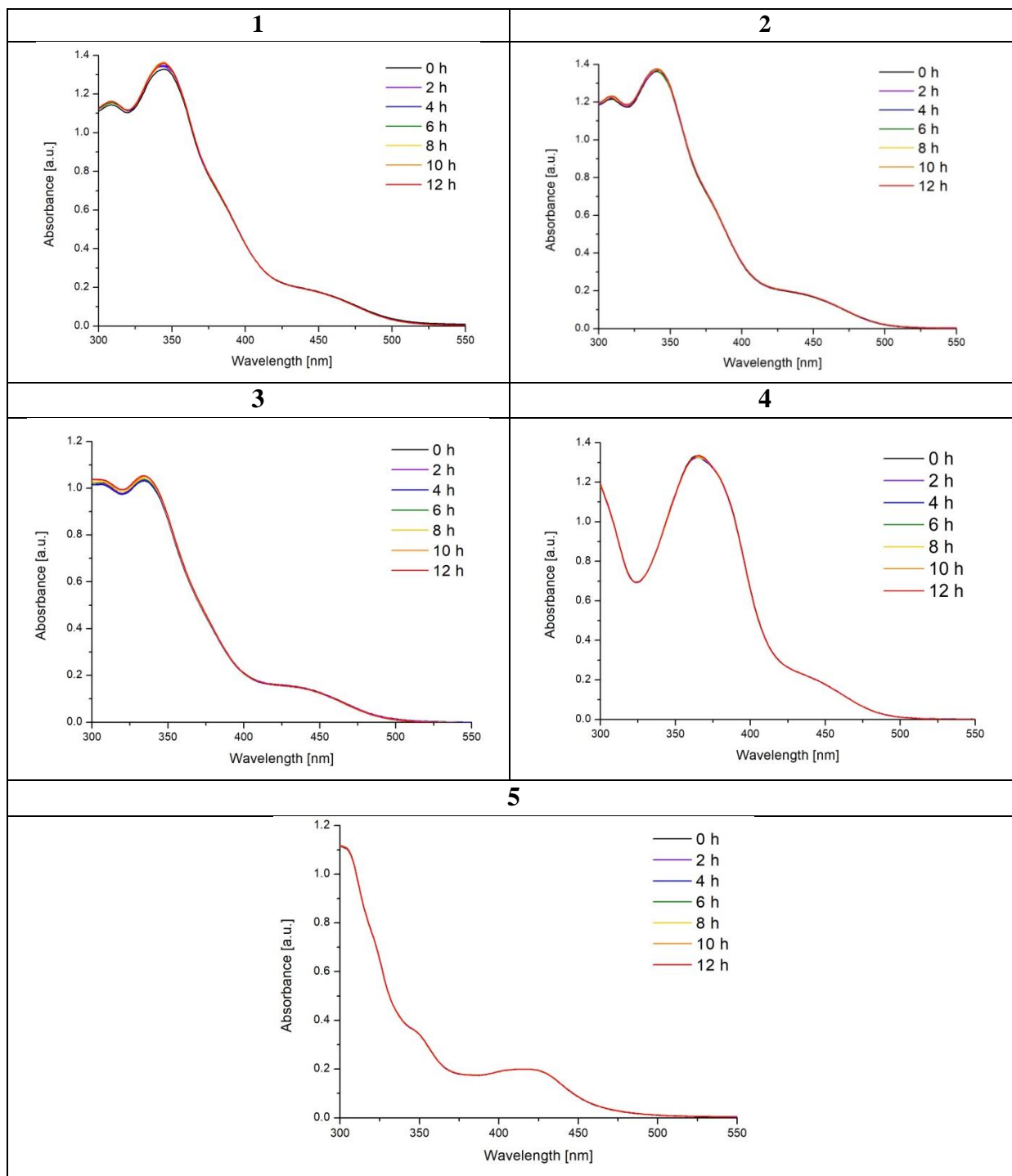


Figure S19. UV-Vis spectra of 1–5 in THF recorded once every two hours over 12h at room temperature.

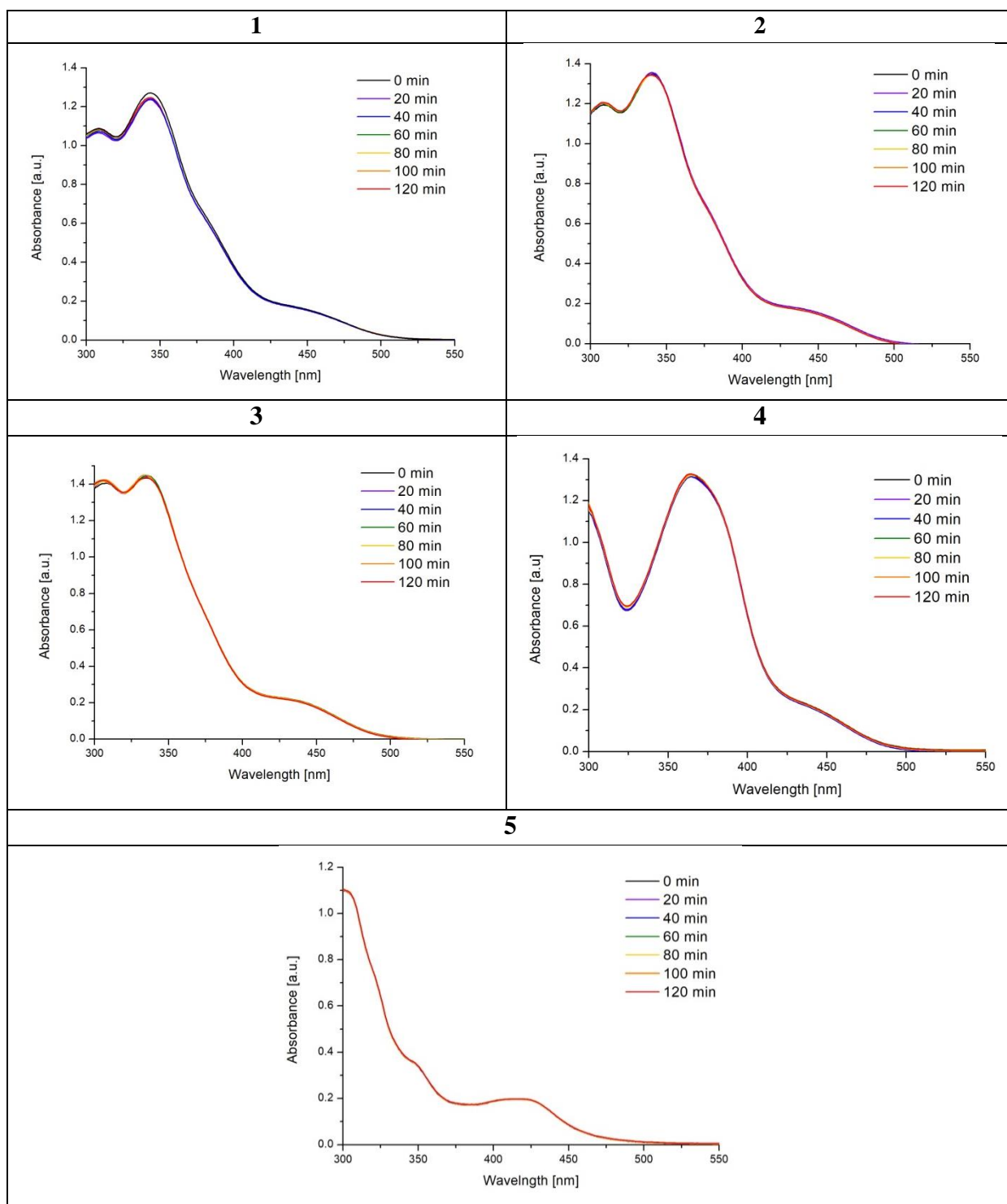
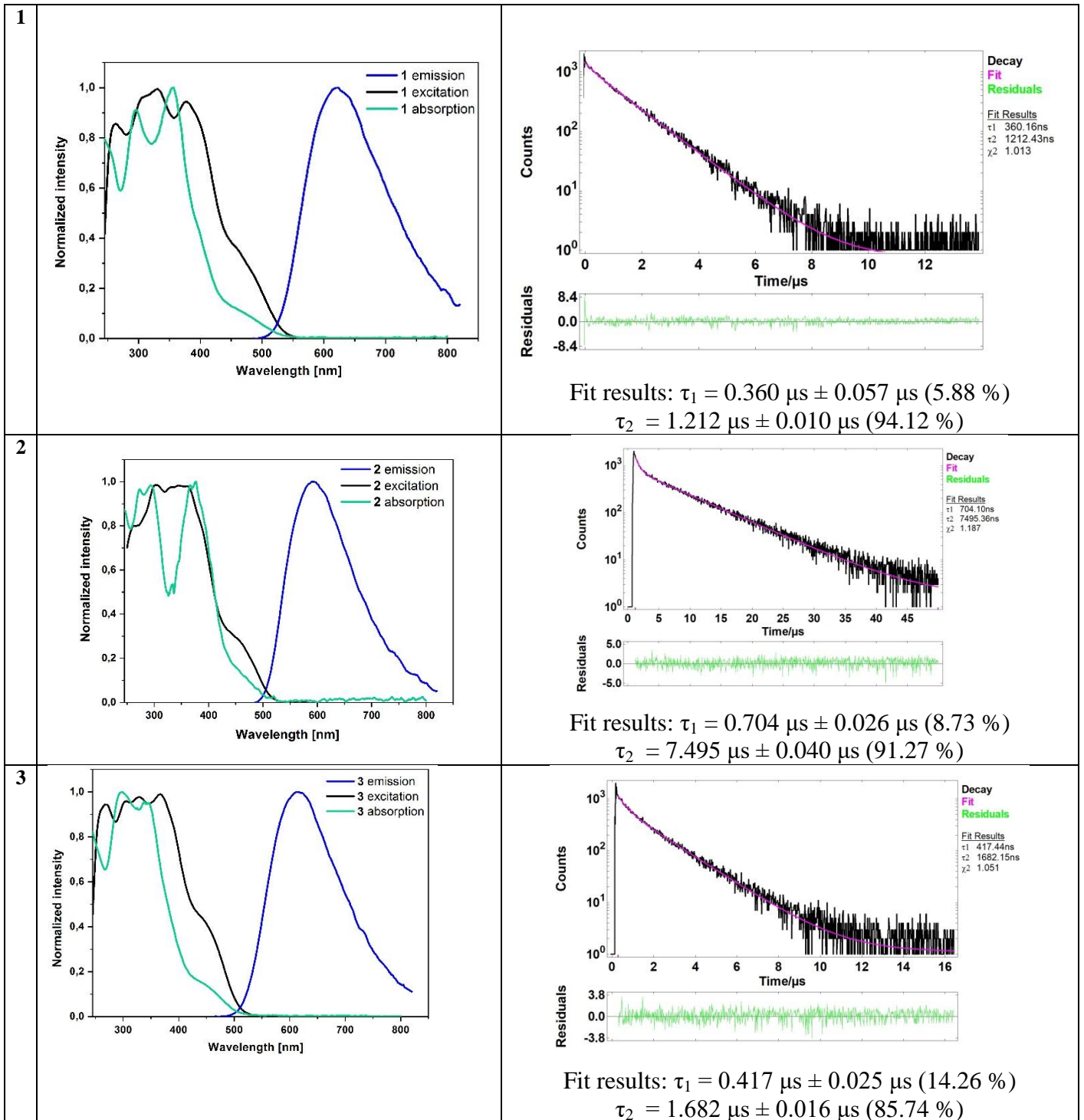


Figure S20. UV-Vis spectra of **1–5** in THF after sample exposure to light (440 nm).

PHOTOLUMINESCENCE



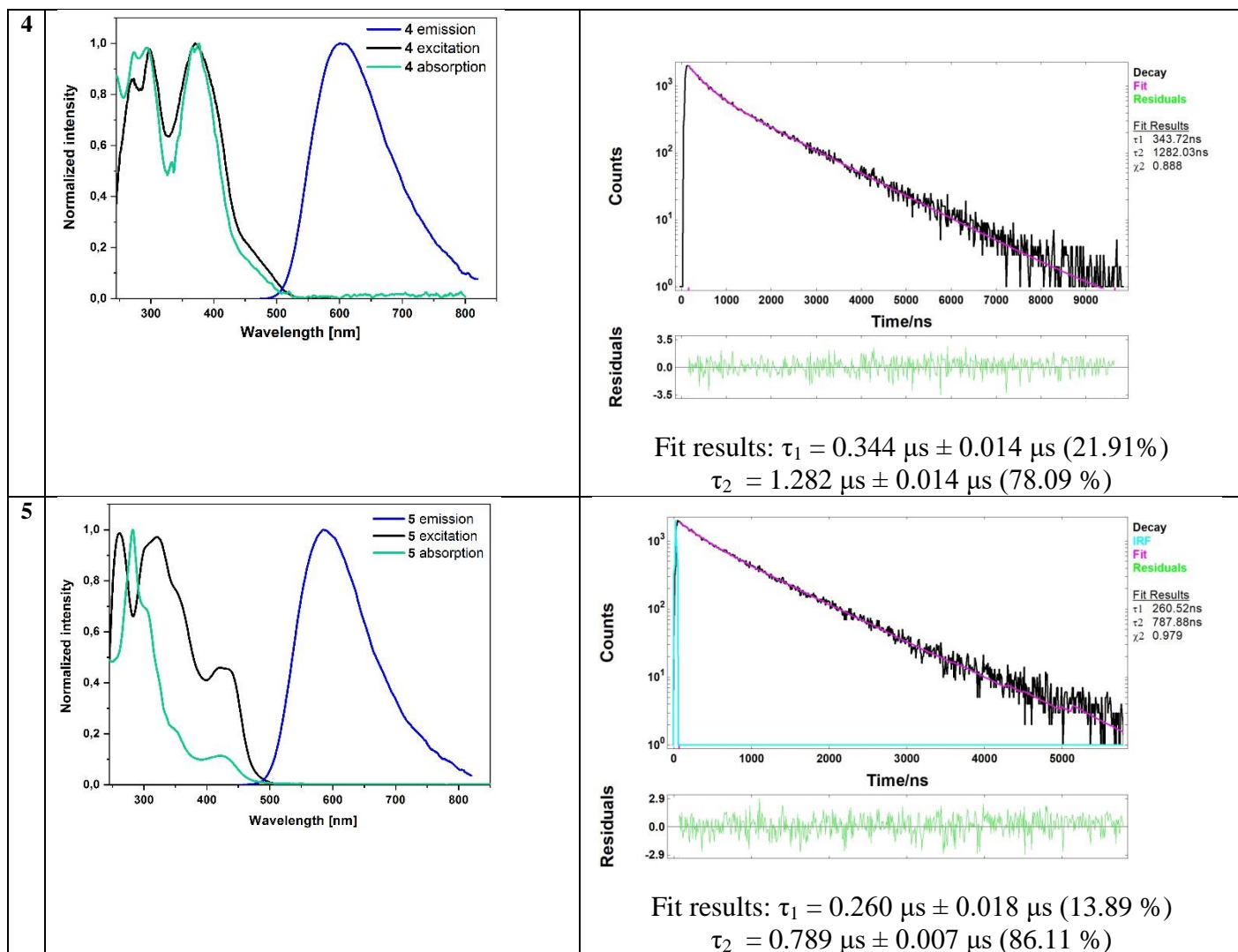
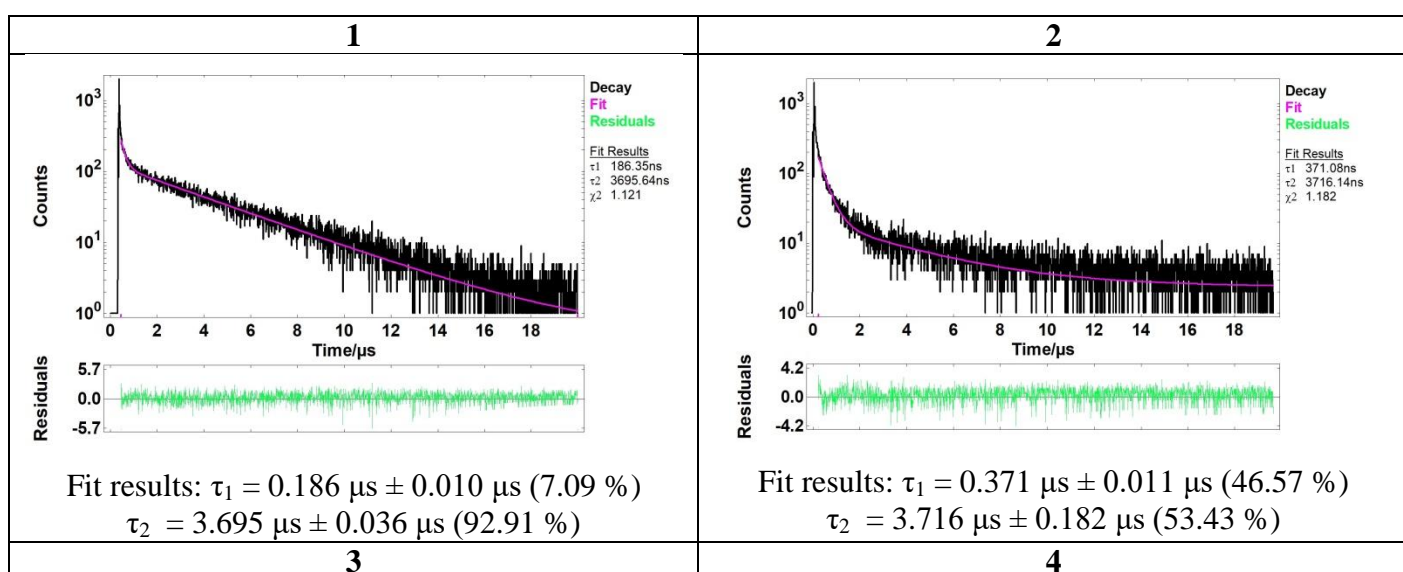


Figure S21. Absorption, excitation and emission steady-state spectra of **1–5** in deaerated chloroform solution along with the corresponding TCSPC decay curves.



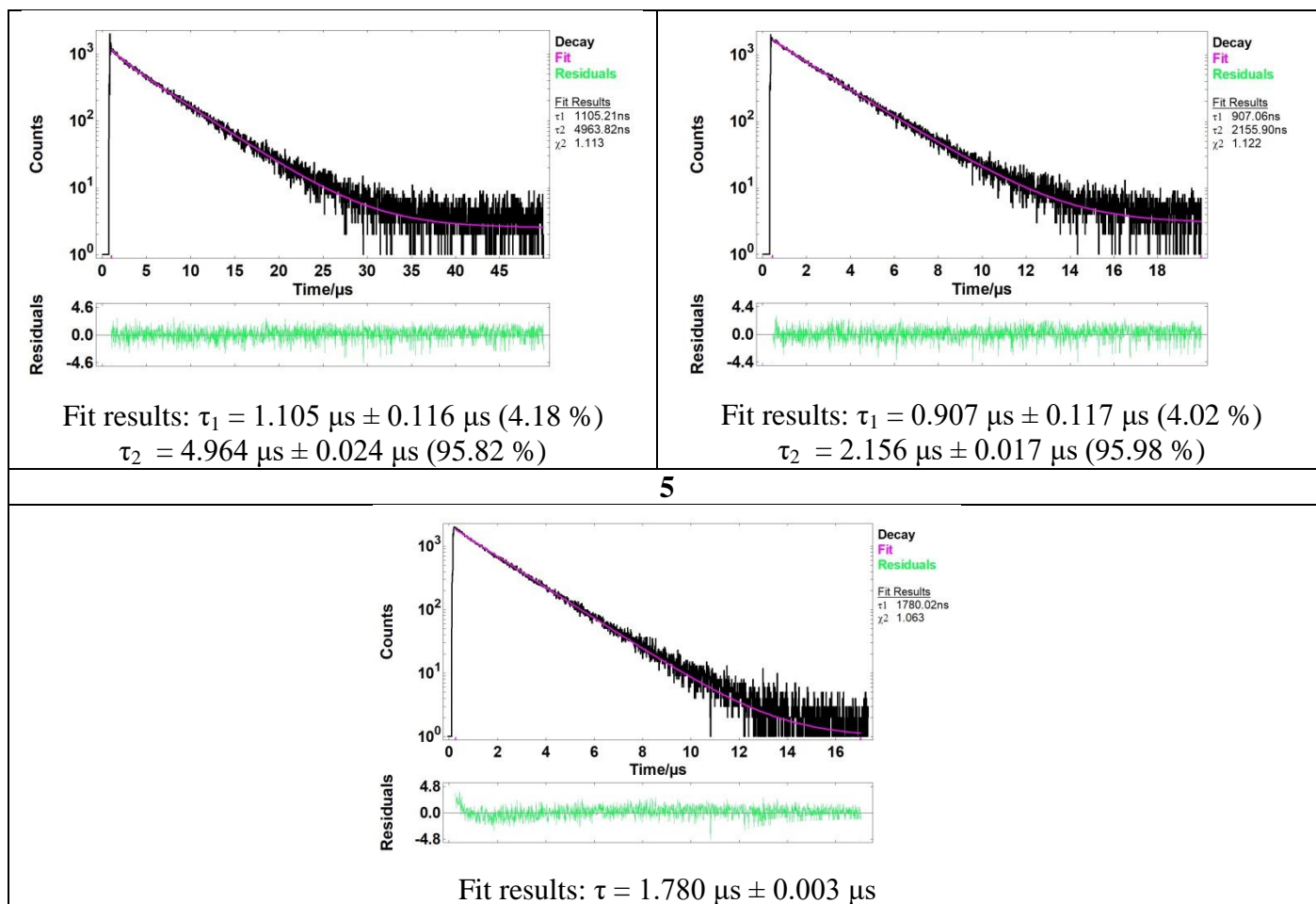
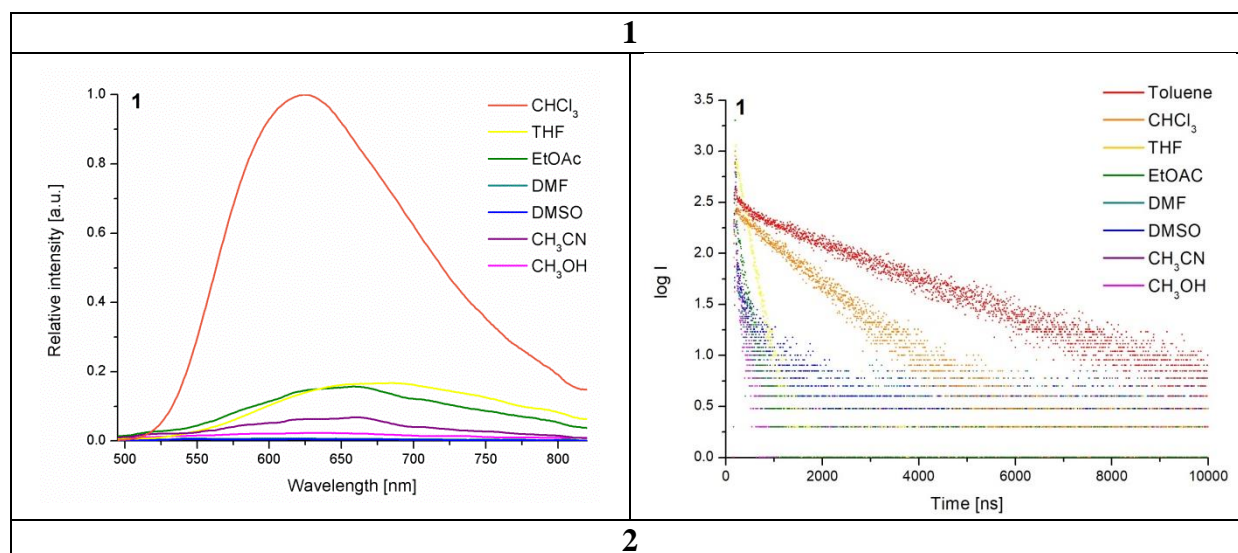
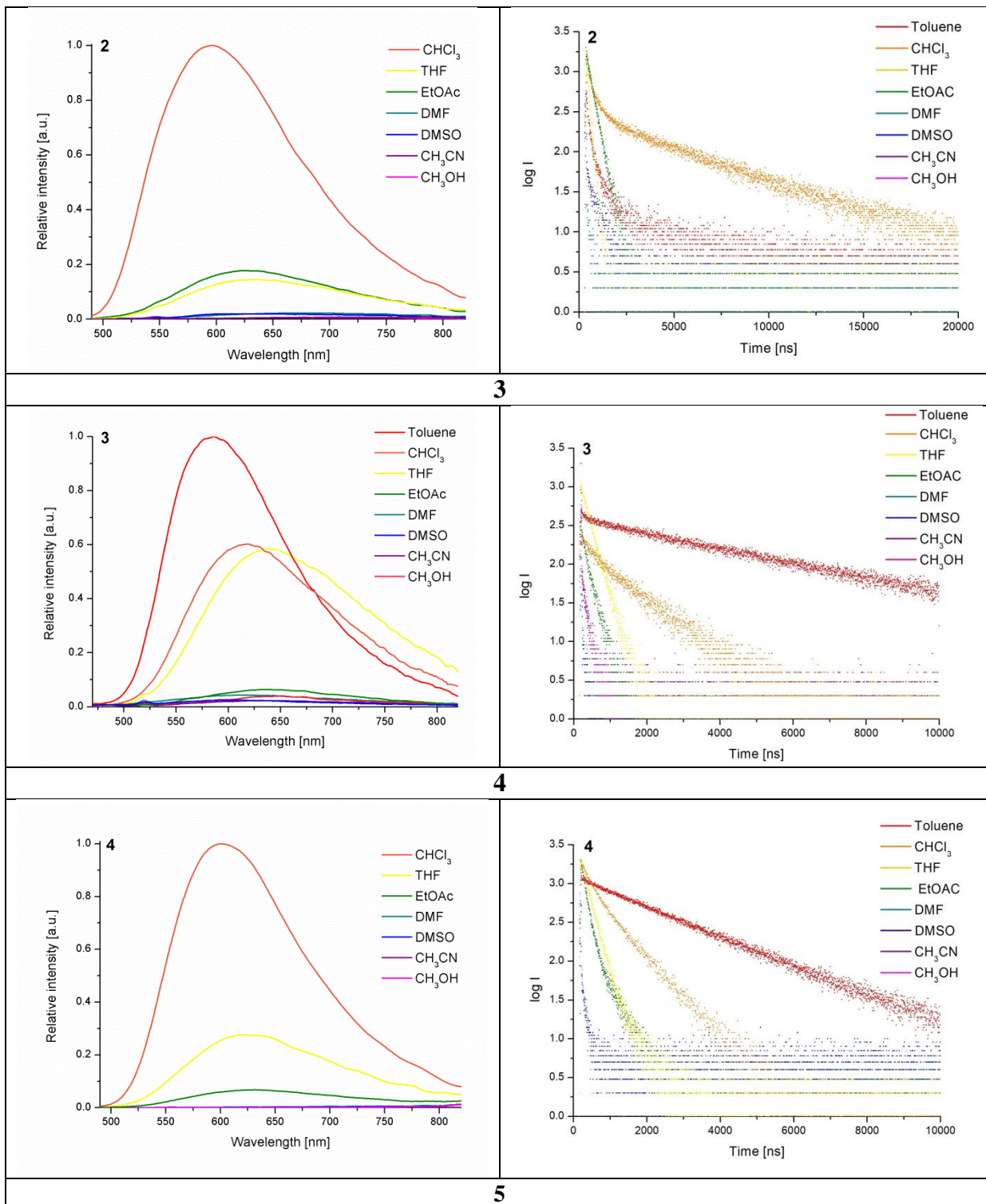


Figure S22. Decay curves of **1–5** in toluene at room temperature.





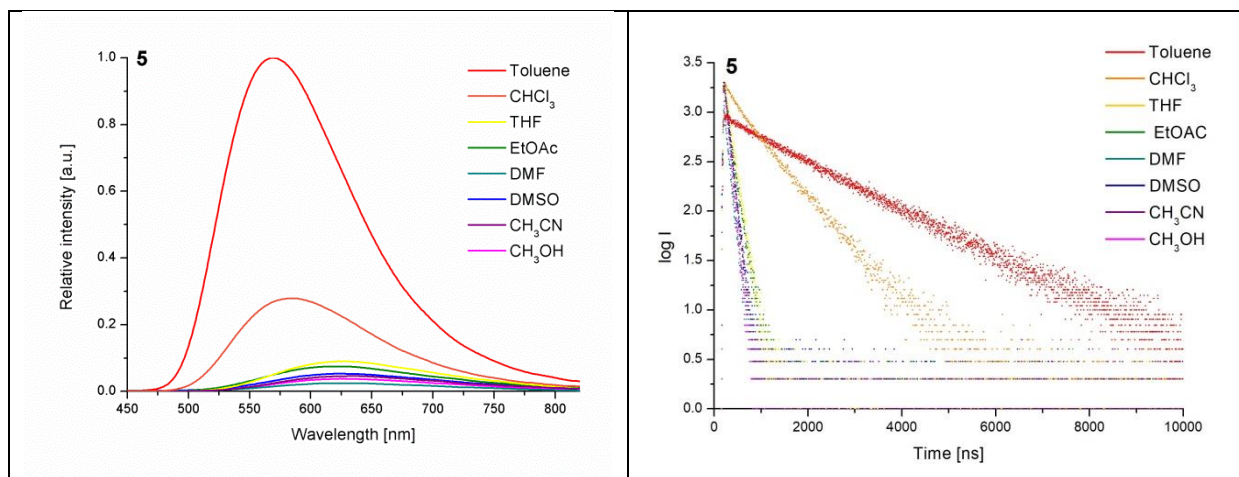


Figure S23. Emission spectra for compounds **1–5** in different solvents along with the corresponding TCSPC decay curves.

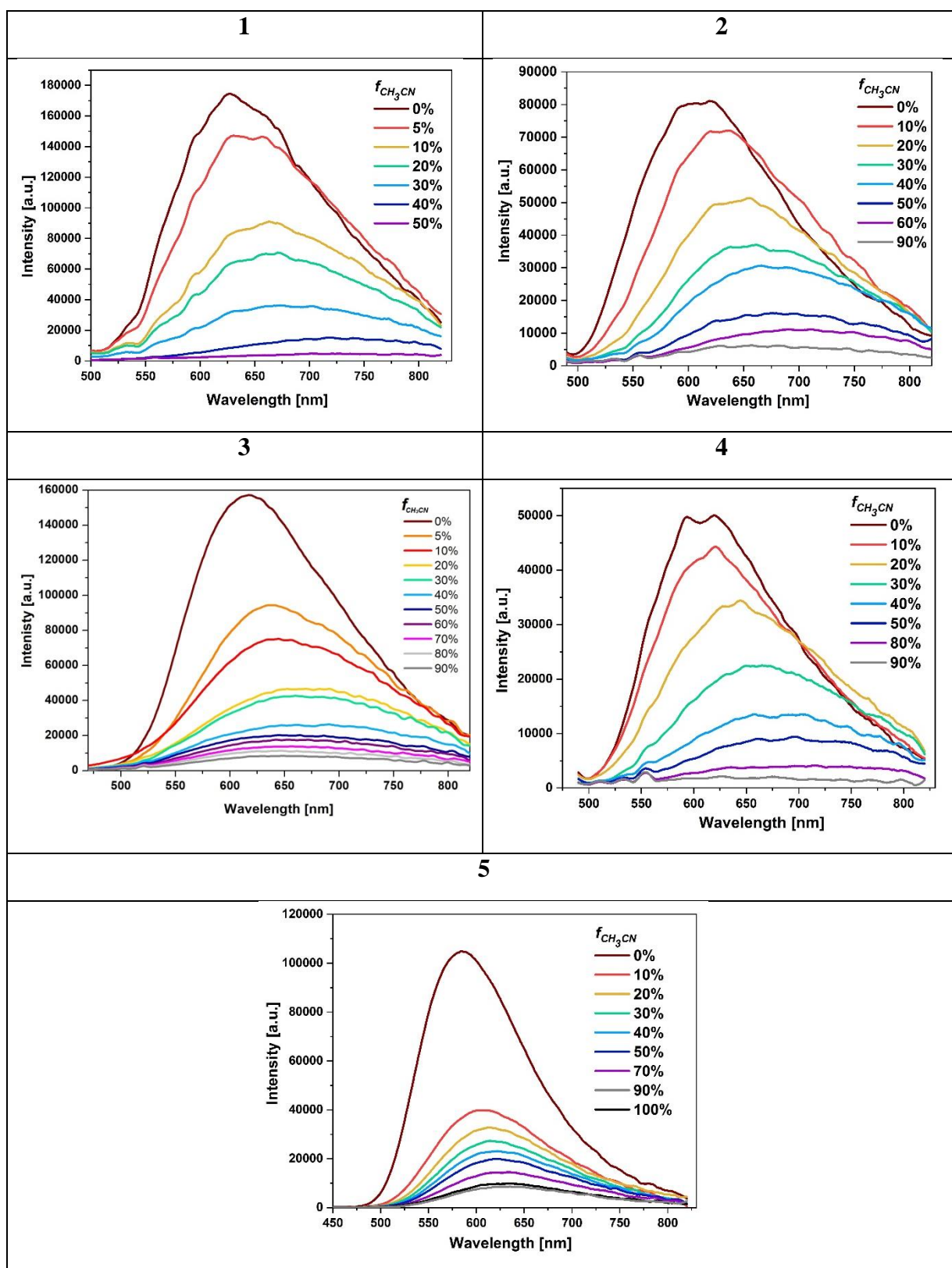
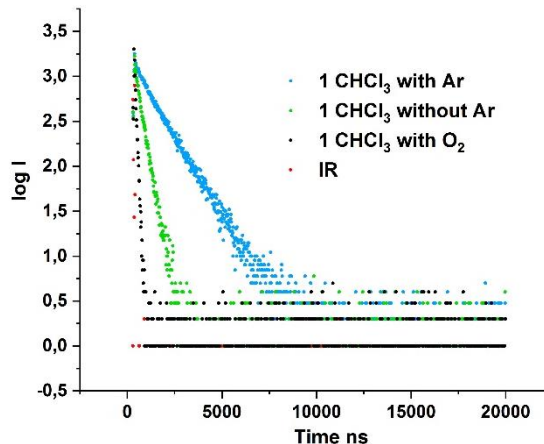
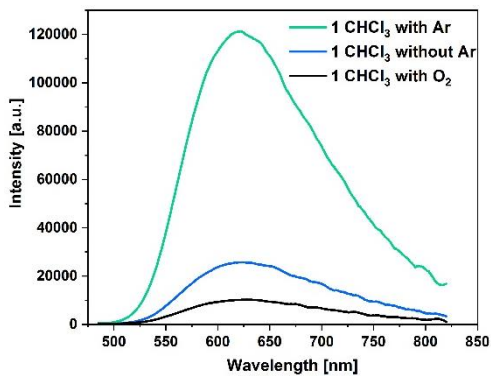
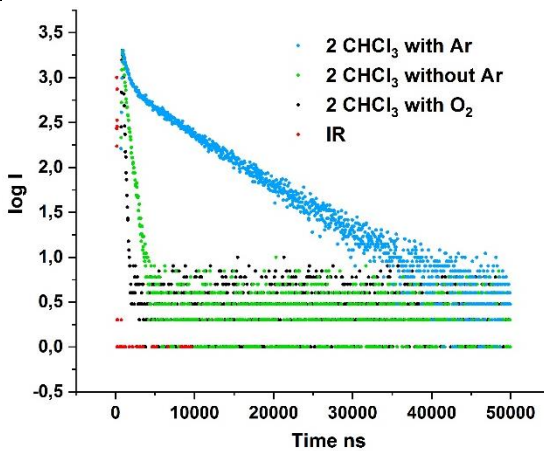
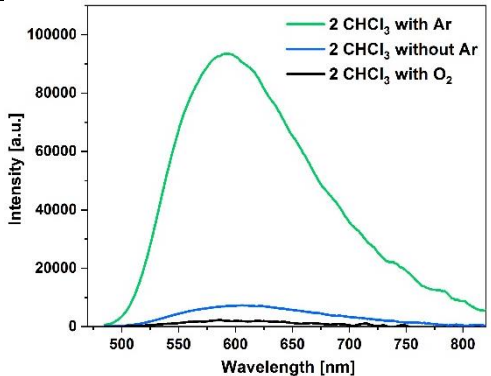


Figure S24. Emission spectra of 1–5 in $\text{CHCl}_3/\text{CH}_3\text{CN}$ mixture with different acetonitrile fraction ($f_{\text{CH}_3\text{CN}}$).

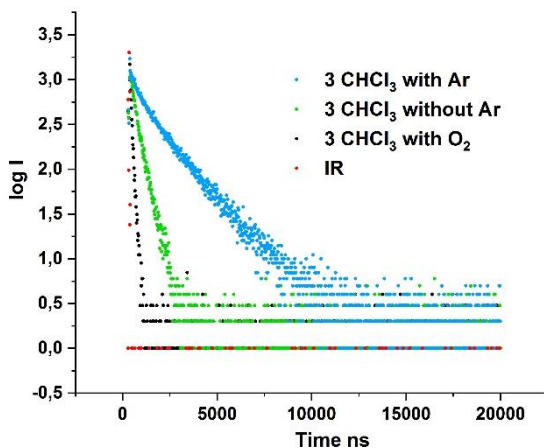
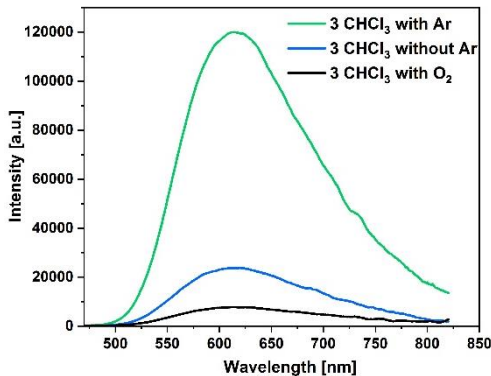
1



2



3



4

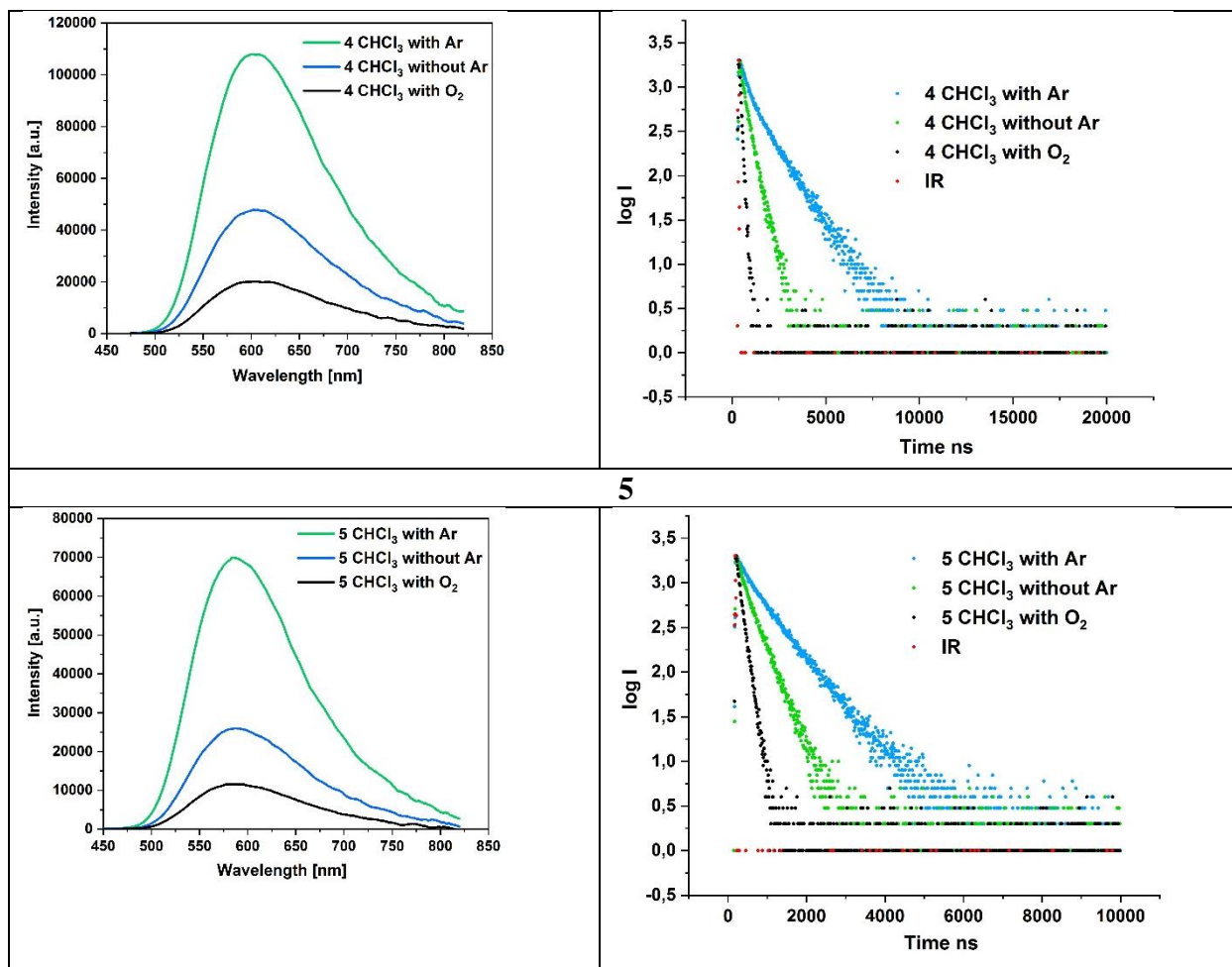


Figure S25. Emission spectra of **1–5** in air-equilibrated, degassed, and oxygenated chloroform solutions, along with decay curves.

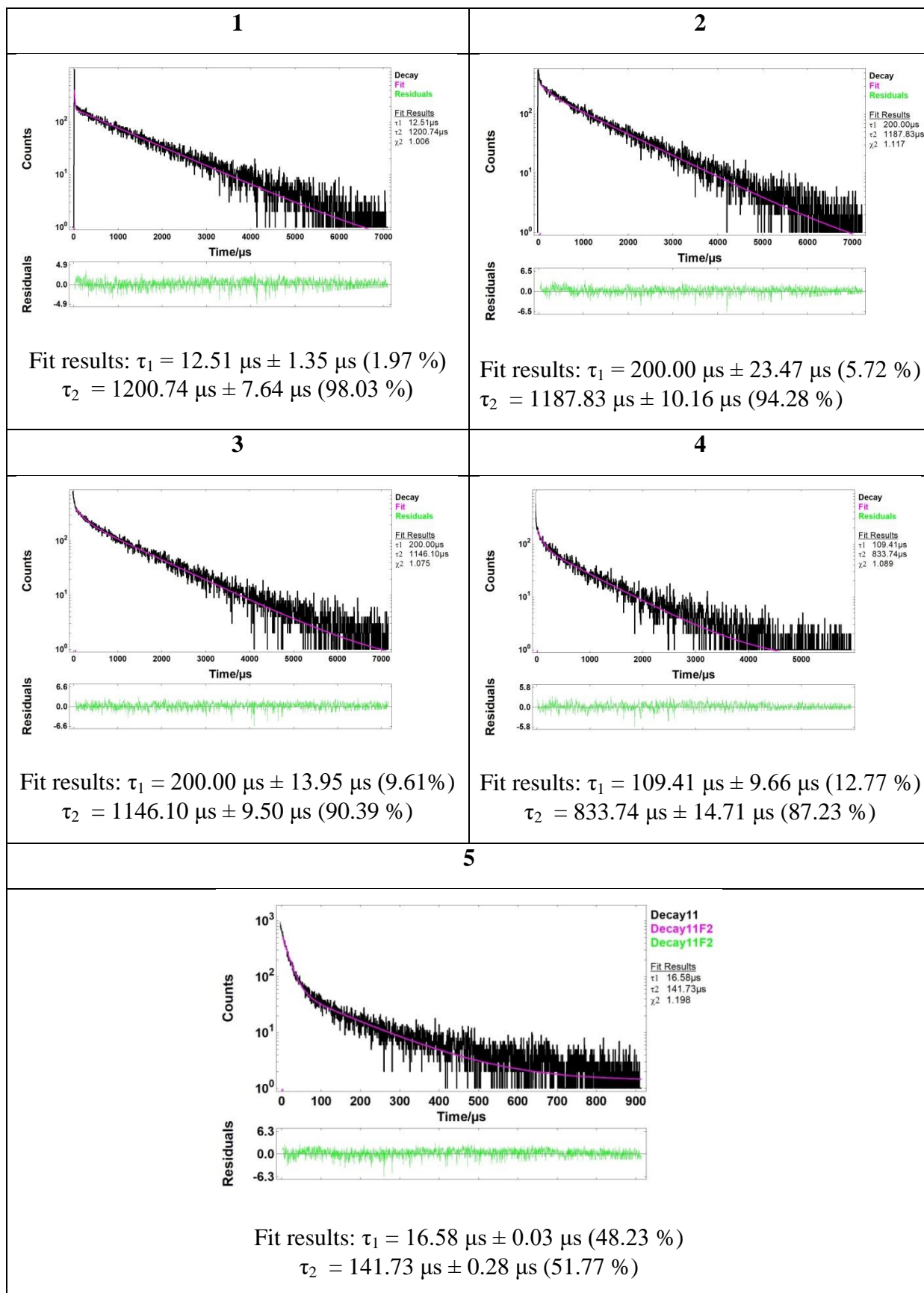
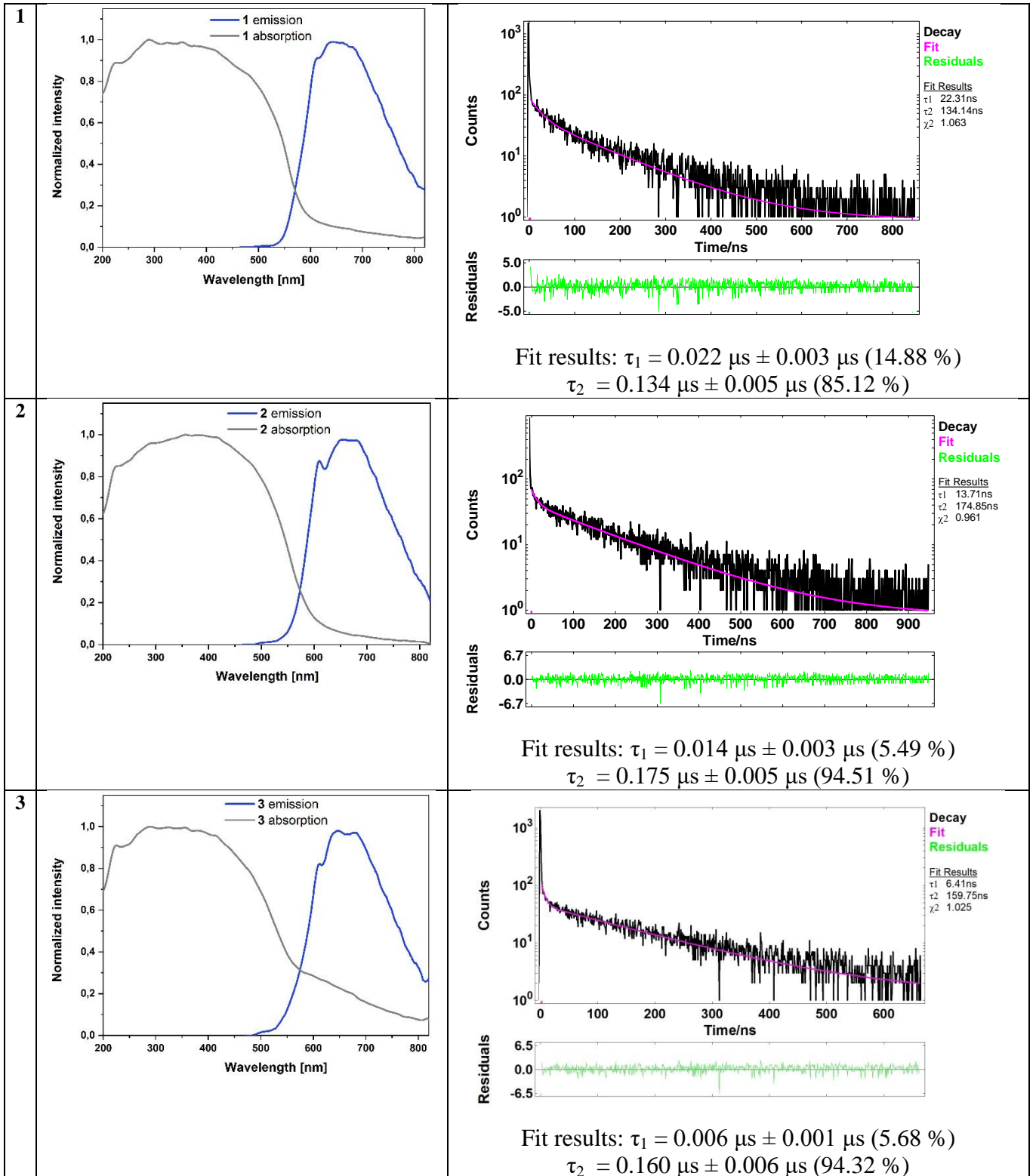


Figure S26. Decay curves of 1–5 in ethanol-methanol rigid-glass matrix (77K).



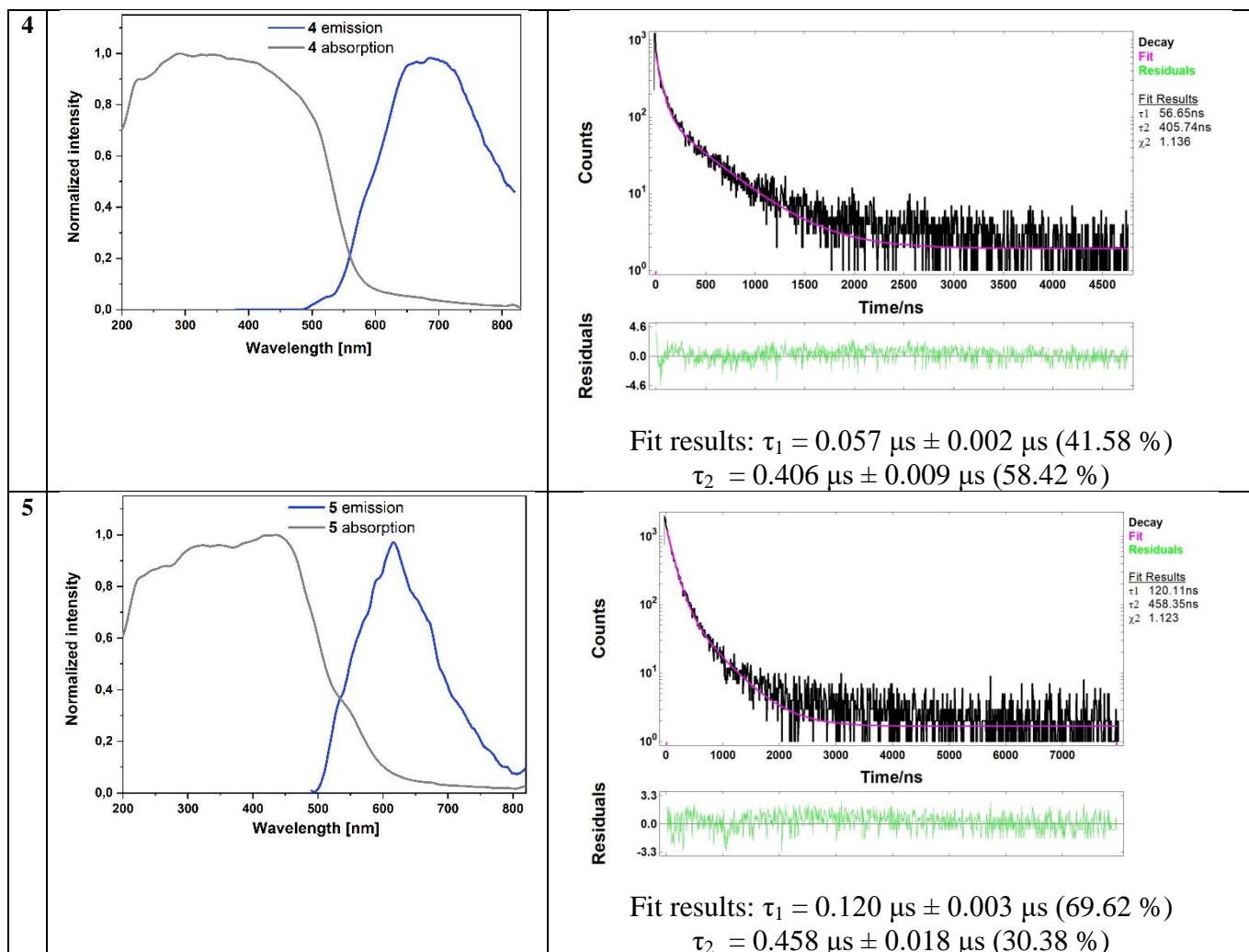


Figure S27. Absorption and emission steady-state spectra of **1–5** in solid state along with the corresponding TCSPC decay curves.

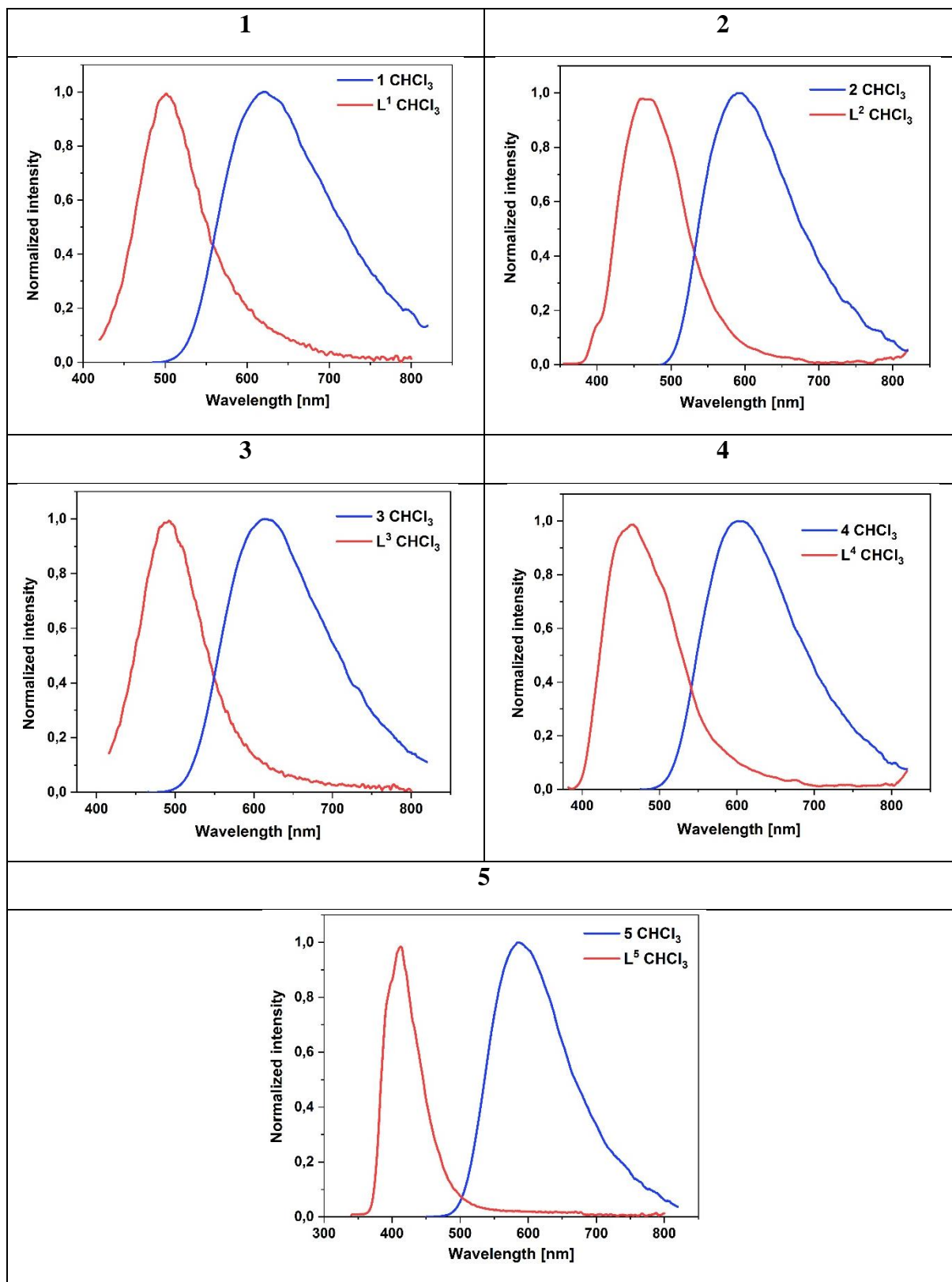


Figure S28. Normalized emission spectra of **1-5** in CHCl_3 , along with the emission spectra of free ligands.

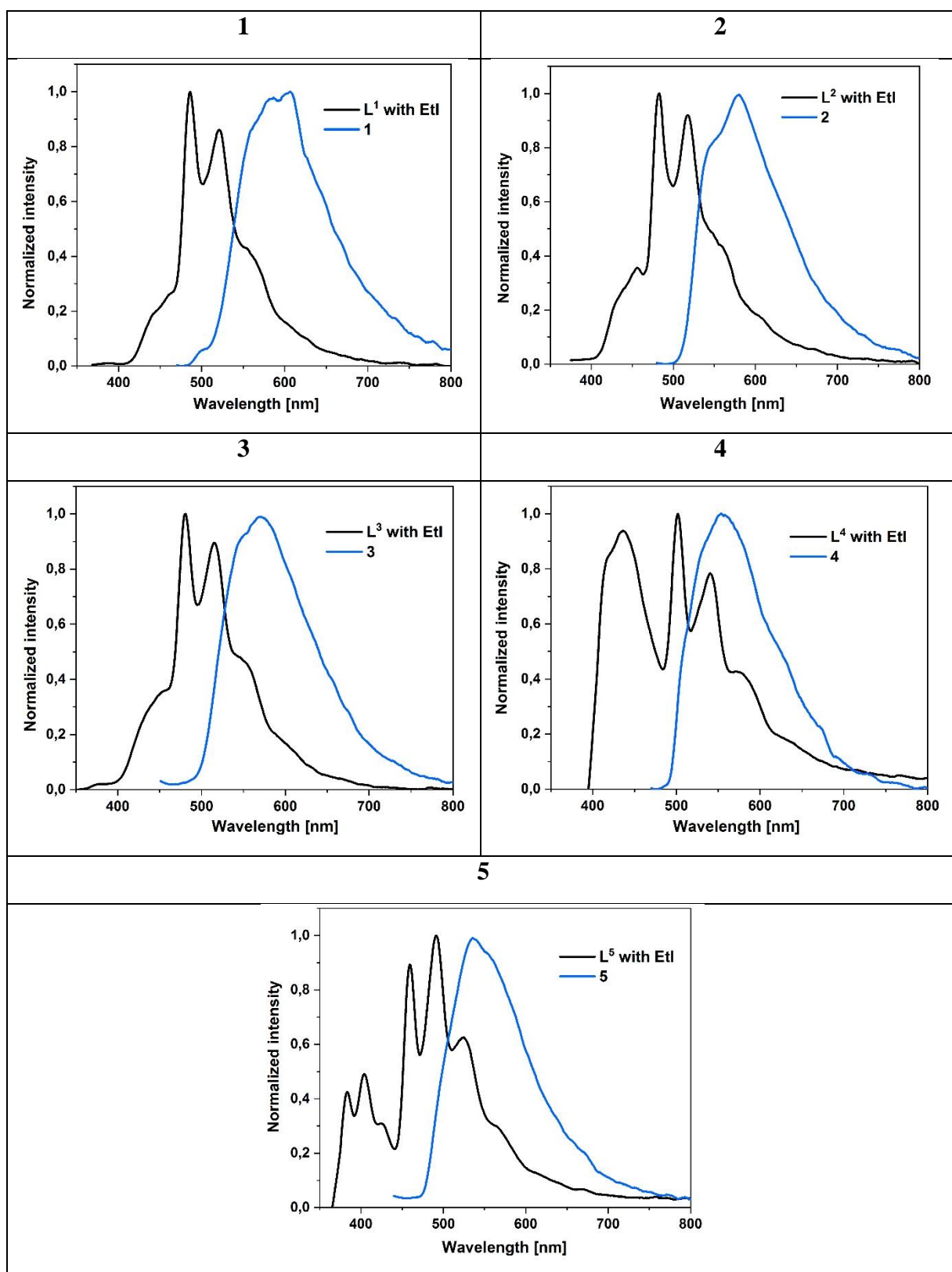
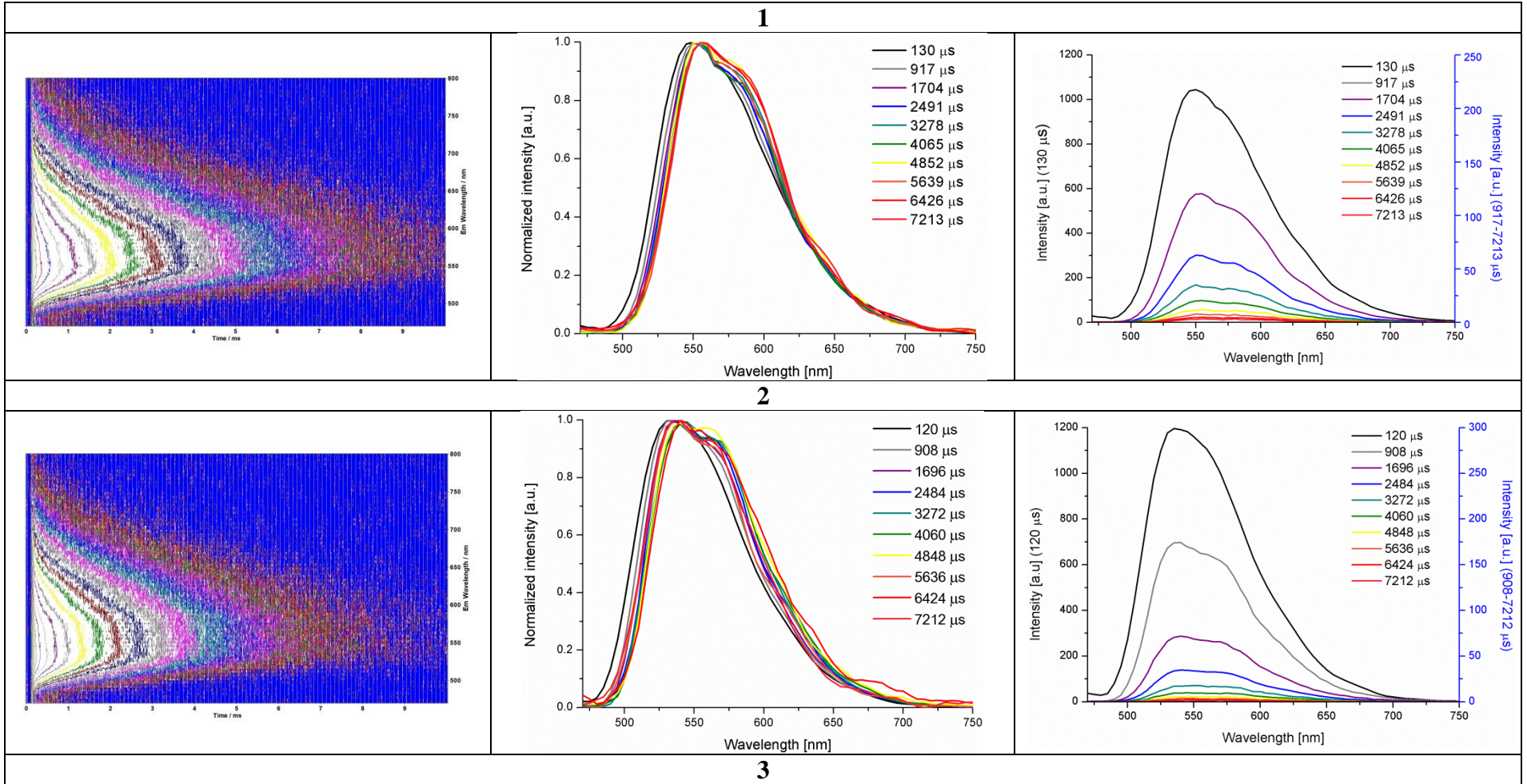
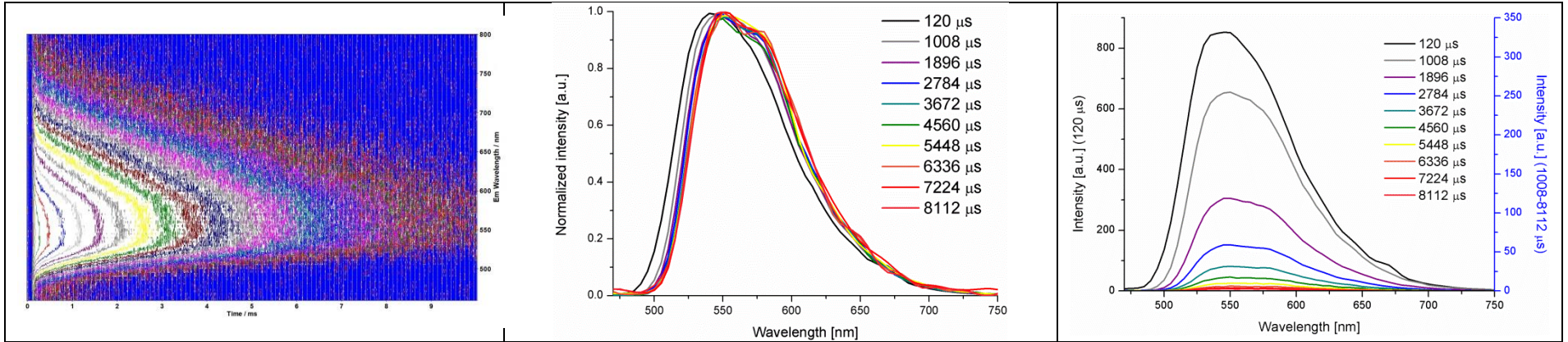
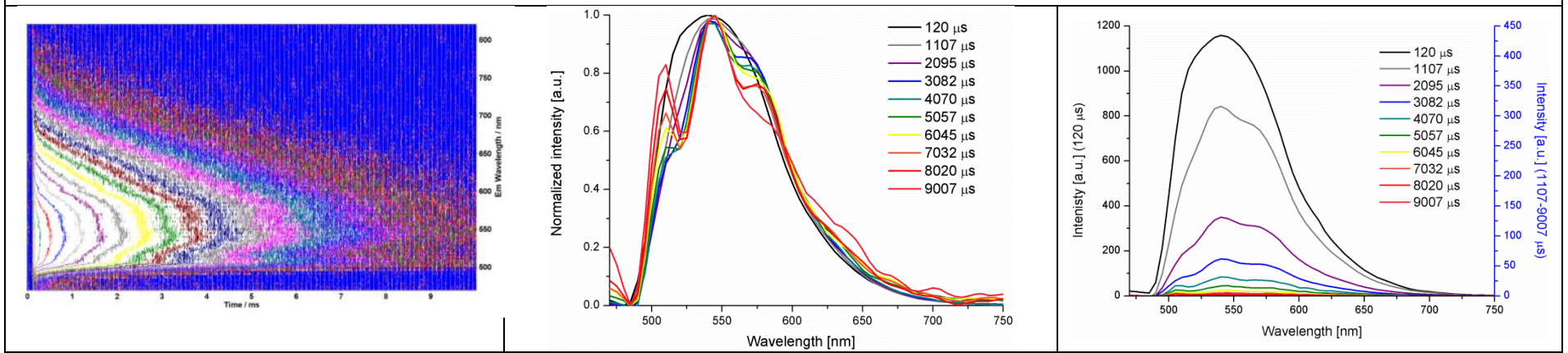


Figure S29. Phosphorescence spectra of 1–5 versus phosphorescence of the appropriate free ligand at 77 K in EtOH:MeOH rigid matrix. The triplet ligand emissions were induced by addition of 10% ethyl iodide.





4



5

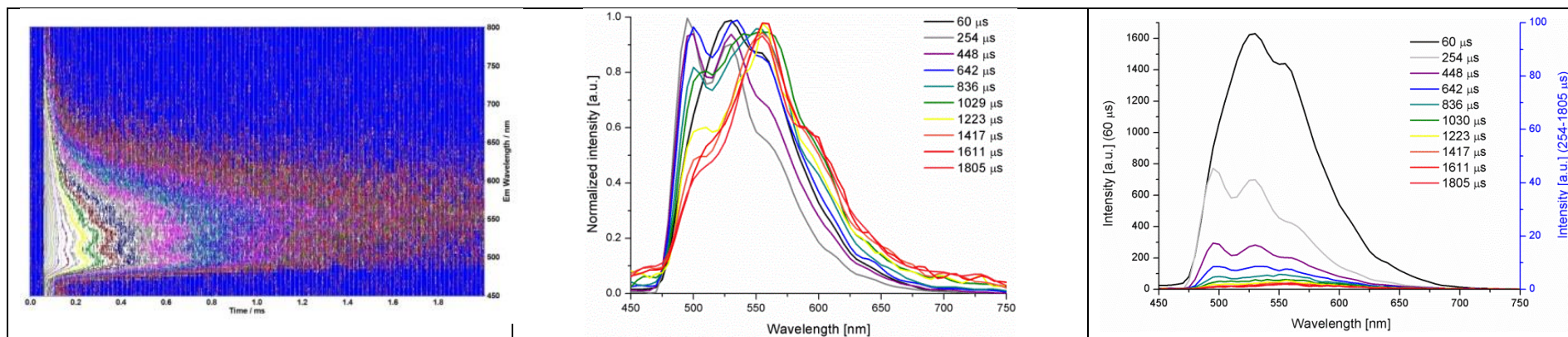


Figure S30. Time-resolved emission spectra of **1-5** at 77 K.

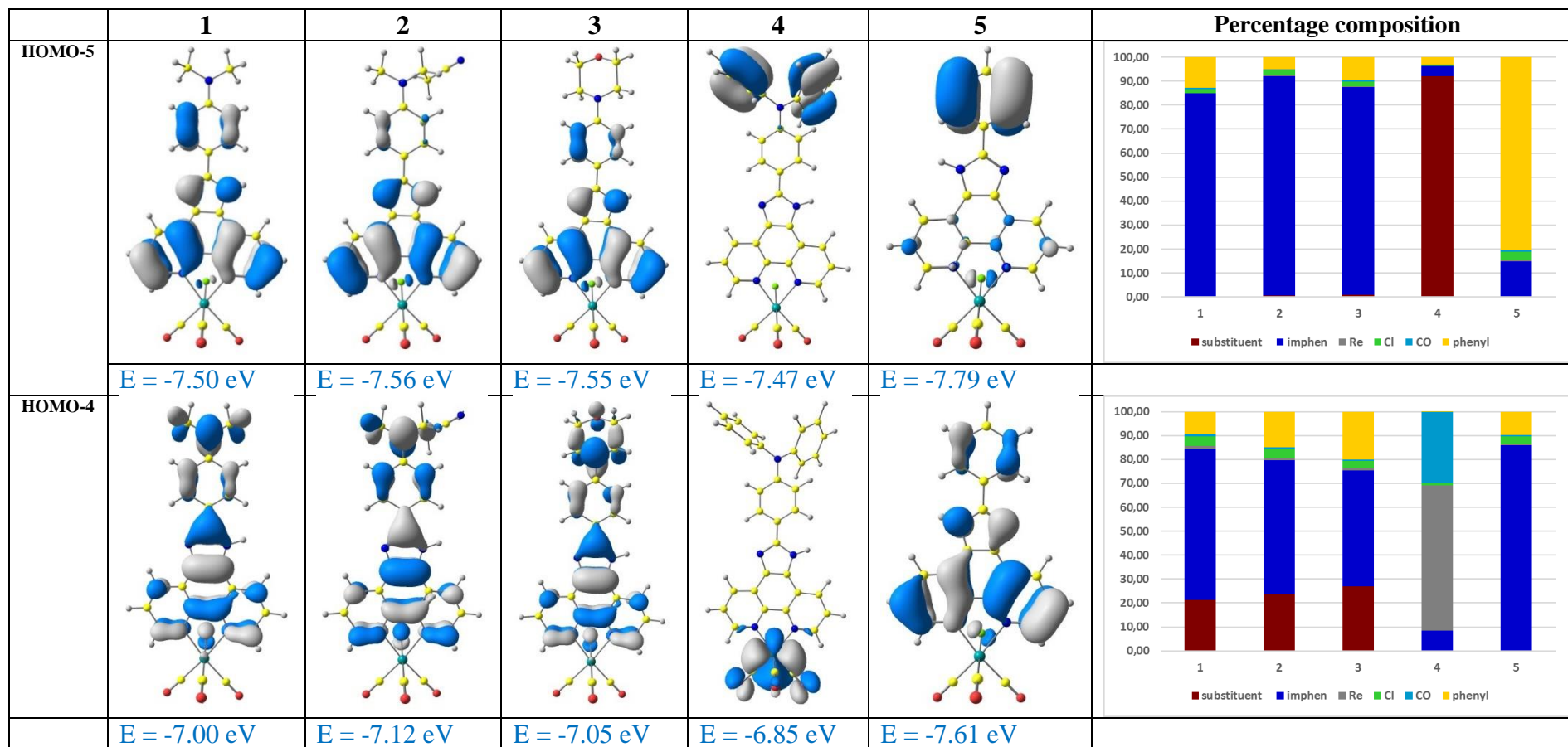
DFT AND TD-DFT CALCULATIONS

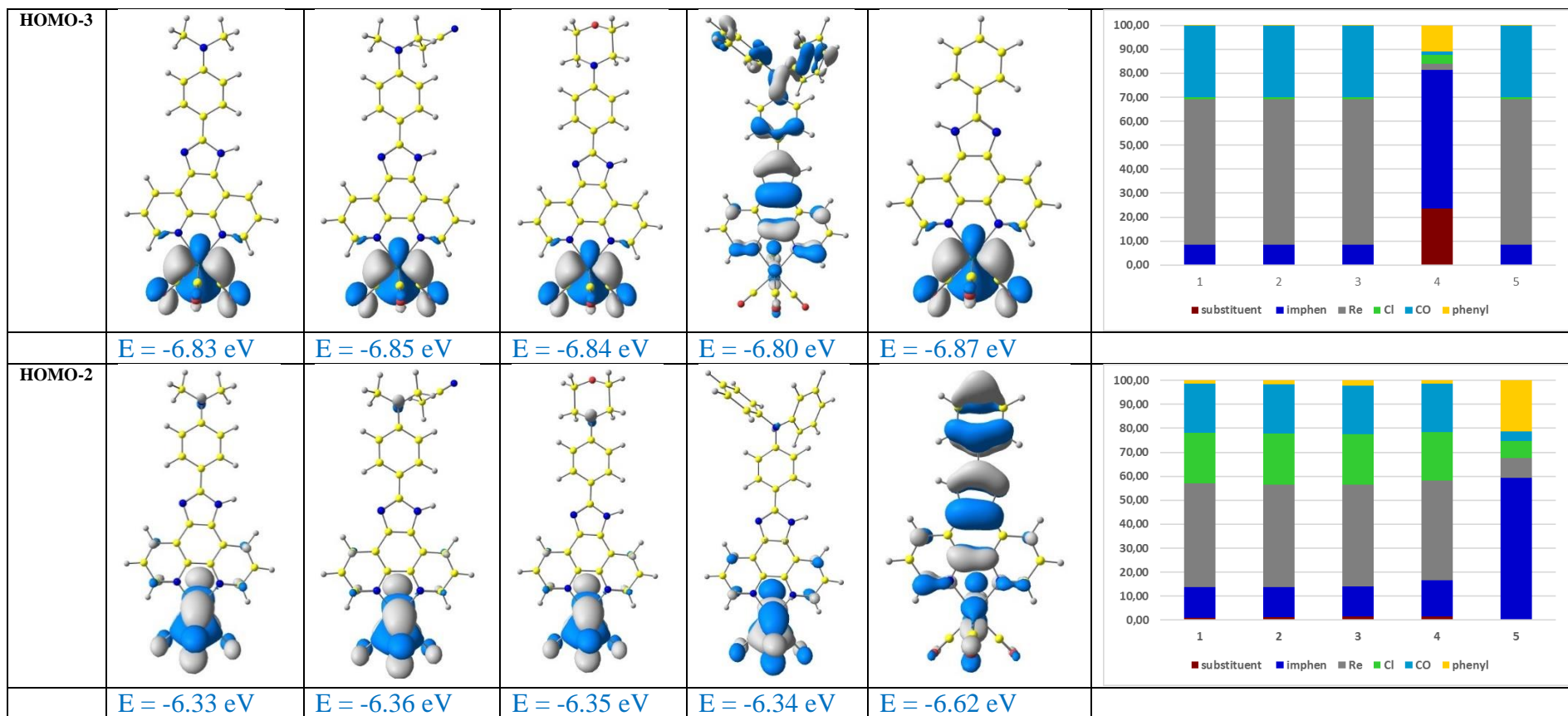
Table S8. Theoretical bond lengths [\AA] and angles [$^\circ$] for **1–5**, along with the experimental bond lengths [\AA] and angles [$^\circ$] for **4** and $[\text{ReCl}(\text{CO})_3(\text{Br-thiophene-imphen})]$ (ref. code XUMGAQ). The structural parameters for $[\text{ReCl}(\text{CO})_3(\text{Br-thiophene-imphen})]$ were taken from the Cambridge Structural Database [1]. The calculations were performed at DFT/PBE0/def2-TZVPD/def2-TZVP level with the use of the PCM model at polarities corresponding to CHCl_3 .

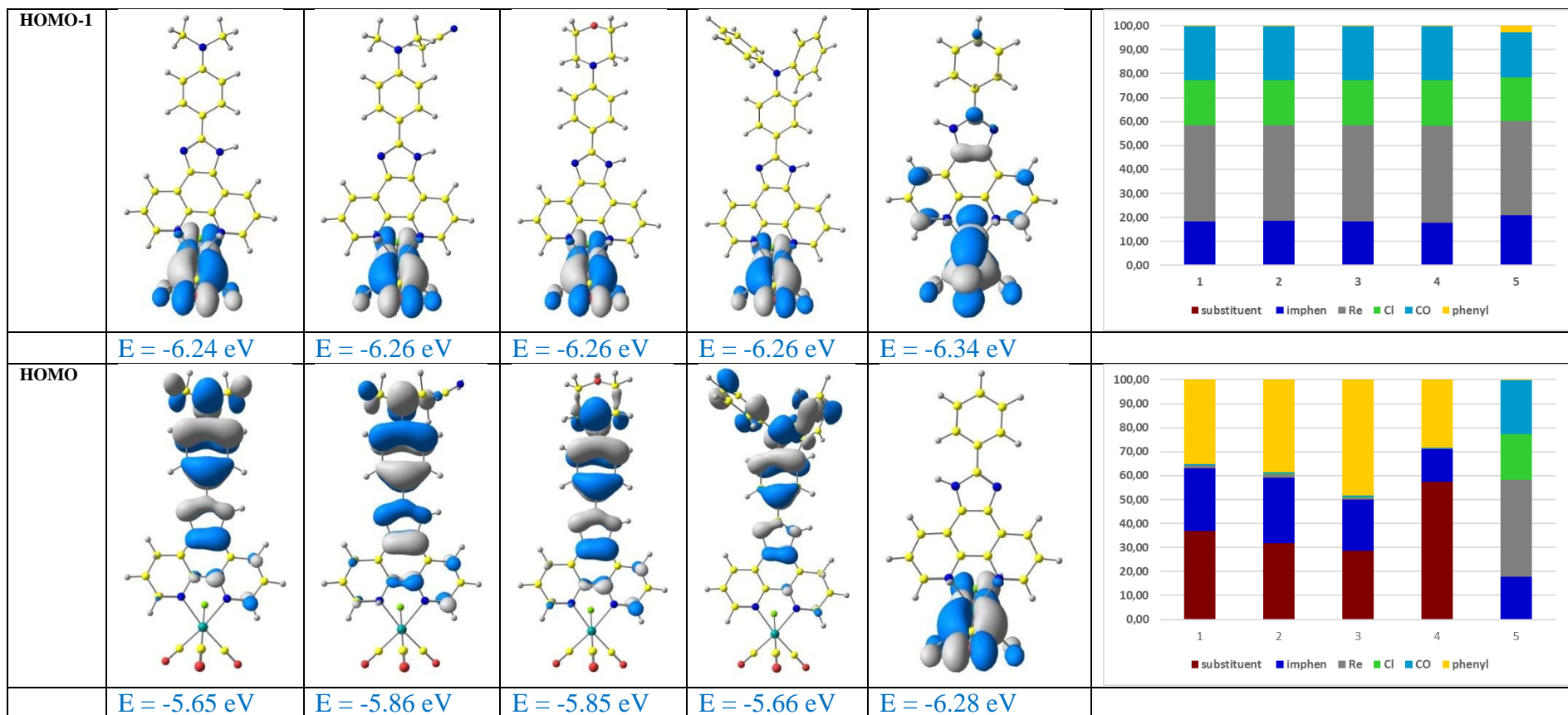
Compound	1	2	3	4	5	4 X-Ray	XUMGAQ
Bond lengths							
Re(1)–C(1)	1.91730	1.91727	1.91737	1.91713	1.91748	1.906(7)	1.907(5)
Re(1)–C(2)	1.91714	1.91722	1.91723	1.91732	1.91731	1.901(7)	1.917(6)
Re(1)–C(3)	1.90412	1.90432	1.90424	1.90439	1.90452	1.893(7)	1.971(5)
Re(1)–N(1)	2.19387	2.19410	2.19382	2.19405	2.19392	2.163(5)	2.180(4)
Re(1)–N(2)	2.19231	2.19240	2.19247	2.19216	2.19242	2.166(5)	2.163(5)
Re(1)–Cl(1)	2.48568	2.48512	2.48570	2.48495	2.48479	2.4859(17)	2.490(1)
C(1)–O(1)	1.15045	1.15036	1.15038	1.15034	1.15022	1.153(8)	1.173(6)
C(2)–O(2)	1.15064	1.15056	1.15056	1.15052	1.15043	1.170(8)	1.167(8)
C(3)–O(3)	1.15490	1.15484	1.15486	1.15481	1.15473	1.156(8)	1.076(6)
Bond angles							
C(1)–Re(1)–N(1)	173.046	172.953	173.041	172.995	173.019	170.3(3)	171.1(2)
C(1)–Re(1)–N(2)	98.652	98.607	98.662	98.615	98.668	95.5(3)	95.9(2)
C(2)–Re(1)–N(1)	98.574	98.649	98.582	98.630	98.595	99.0(2)	99.9(2)
C(2)–Re(1)–N(2)	172.982	173.056	172.977	173.016	172.963	174.6(3)	175.2(2)
C(3)–Re(1)–N(1)	93.818	93.909	93.828	93.825	93.857	95.7(2)	92.3(2)
C(3)–Re(1)–N(2)	93.779	93.772	93.791	93.816	93.814	95.6(2)	93.7(2)
C(1)–Re(1)–C(2)	87.834	87.801	87.827	87.816	87.824	89.4(3)	88.7(2)
C(2)–Re(1)–C(3)	88.990	88.986	88.986	88.994	88.991	86.7(3)	87.8(2)
C(1)–Re(1)–C(3)	88.967	89.018	88.968	89.004	88.970	89.6(3)	90.6(2)
N(1)–Re(1)–N(2)	74.826	74.824	74.814	74.822	74.795	75.94(18)	75.5(2)
C(1)–Re(1)–Cl(1)	93.219	93.190	93.240	93.146	93.247	91.1(2)	94.5(2)
C(2)–Re(1)–Cl(1)	93.077	93.080	93.098	93.117	93.104	95.2(2)	95.1(2)
C(3)–Re(1)–Cl(1)	177.045	177.031	177.018	177.041	177.003	177.96(19)	174.2(2)
N(1)–Re(1)–Cl(1)	83.791	83.676	83.756	83.813	83.716	83.27(14)	82.2(1)
N(2)–Re(1)–Cl(1)	83.931	83.940	83.900	83.857	83.864	82.43(14)	83.1(1)

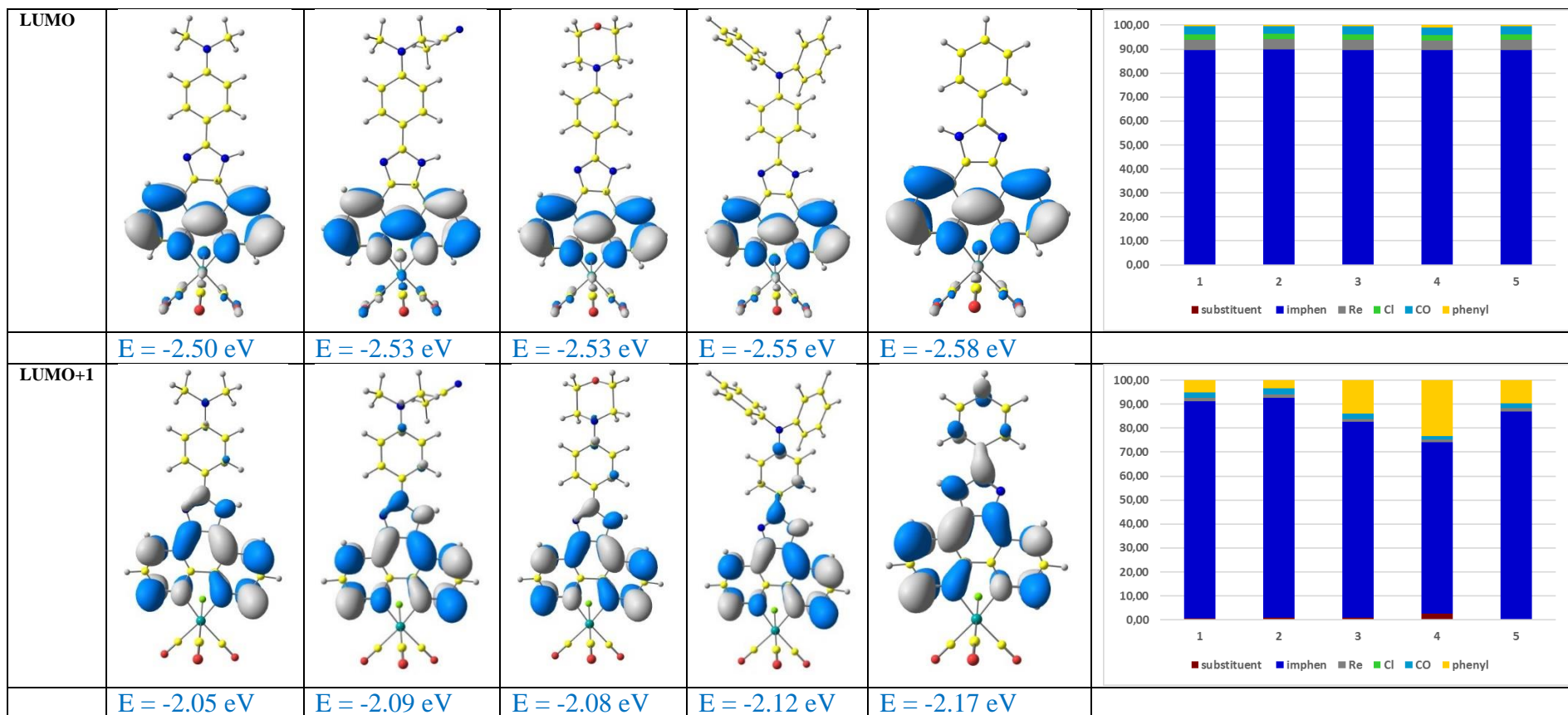
Ref. [1]: The Cambridge Structural Database. C. R. Groom, I. J. Bruno, M. P. Lightfoot and S. C. Ward, *Acta Cryst.* (2016). B72, 171-179.

Figure S31. Selected molecular orbitals of **1–5** and their percentage composition in chloroform. The calculations were performed at DFT/PBE0/def2-TZVPD/def2-TZVP level with the use of the PCM model at polarities corresponding to CHCl₃.









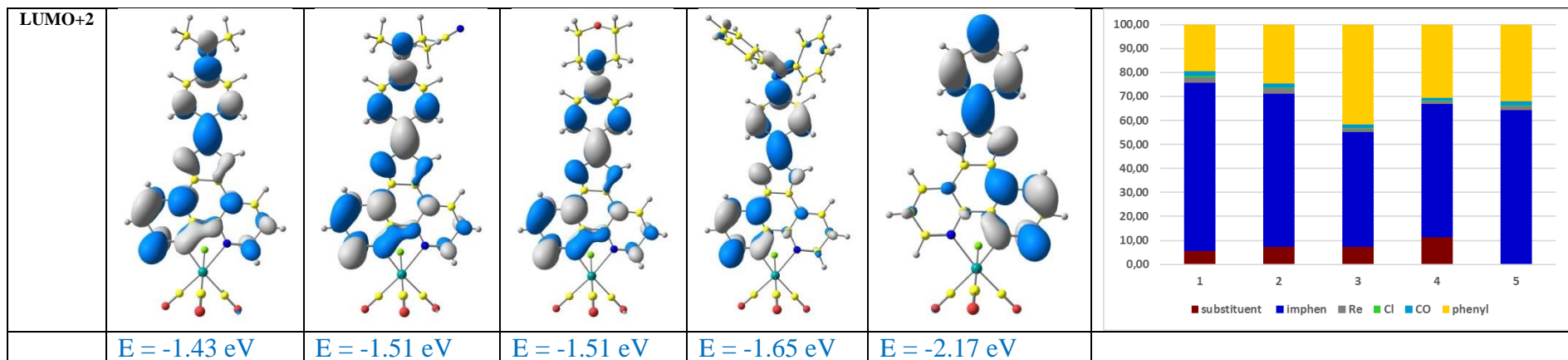
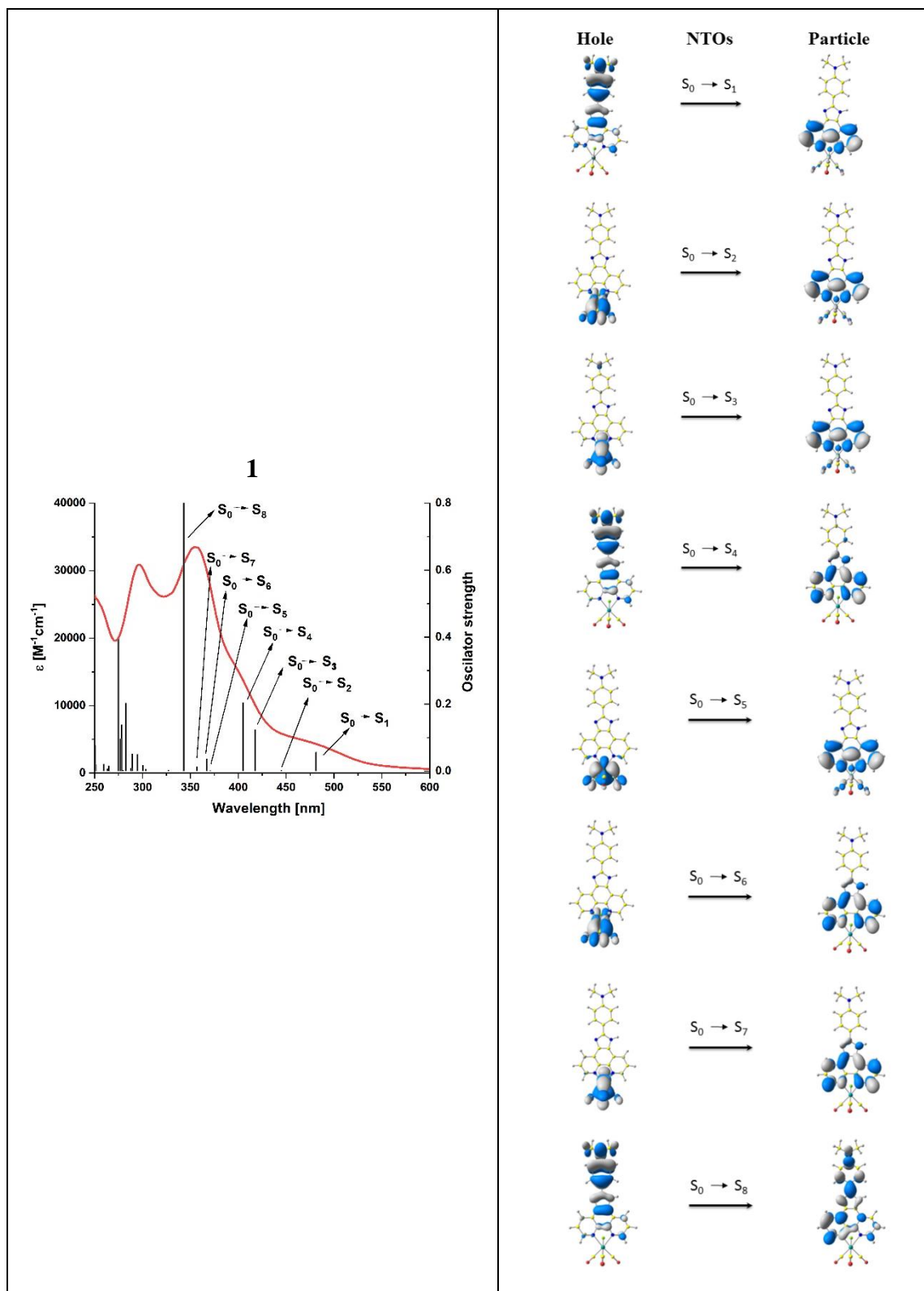
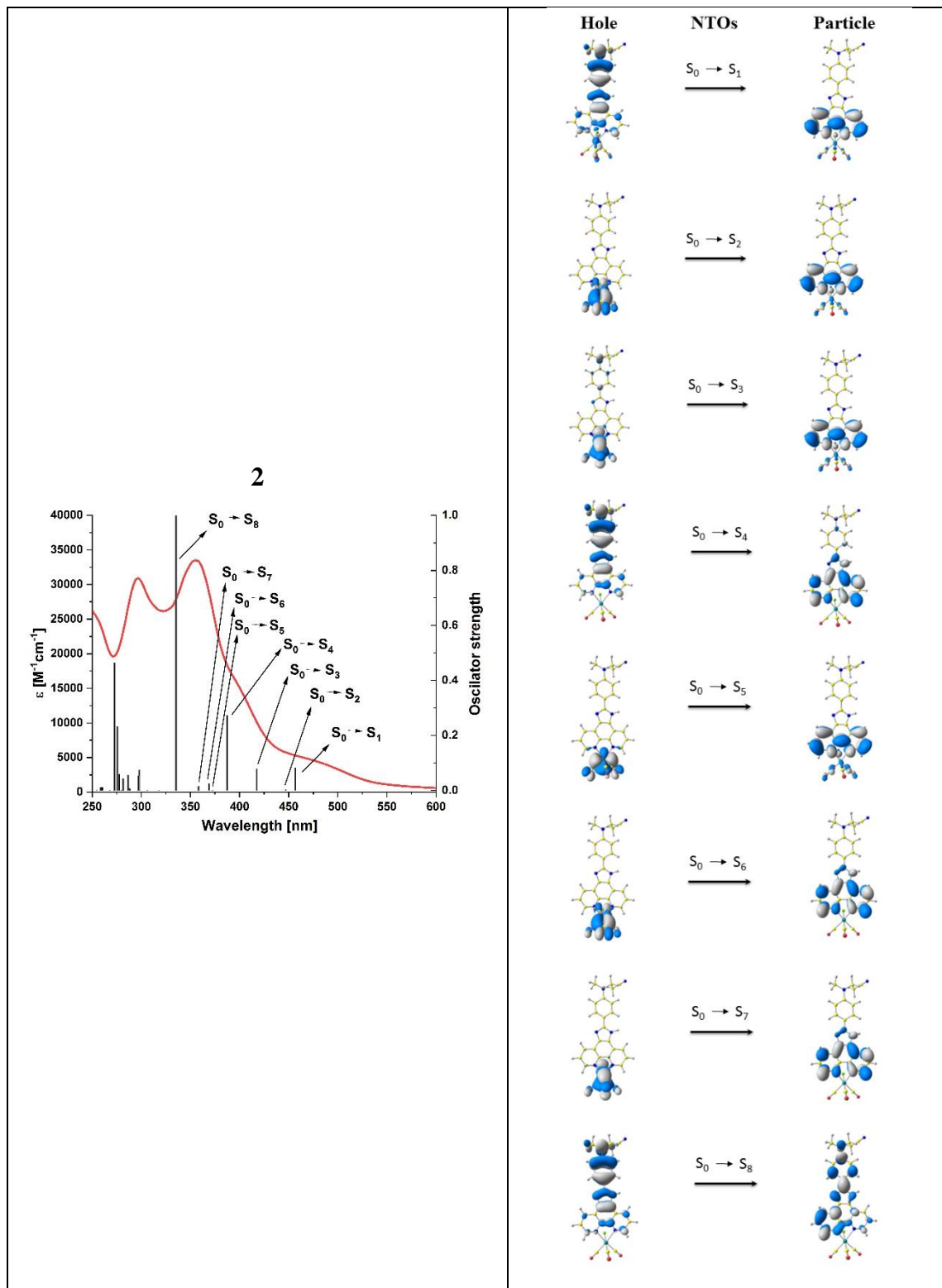


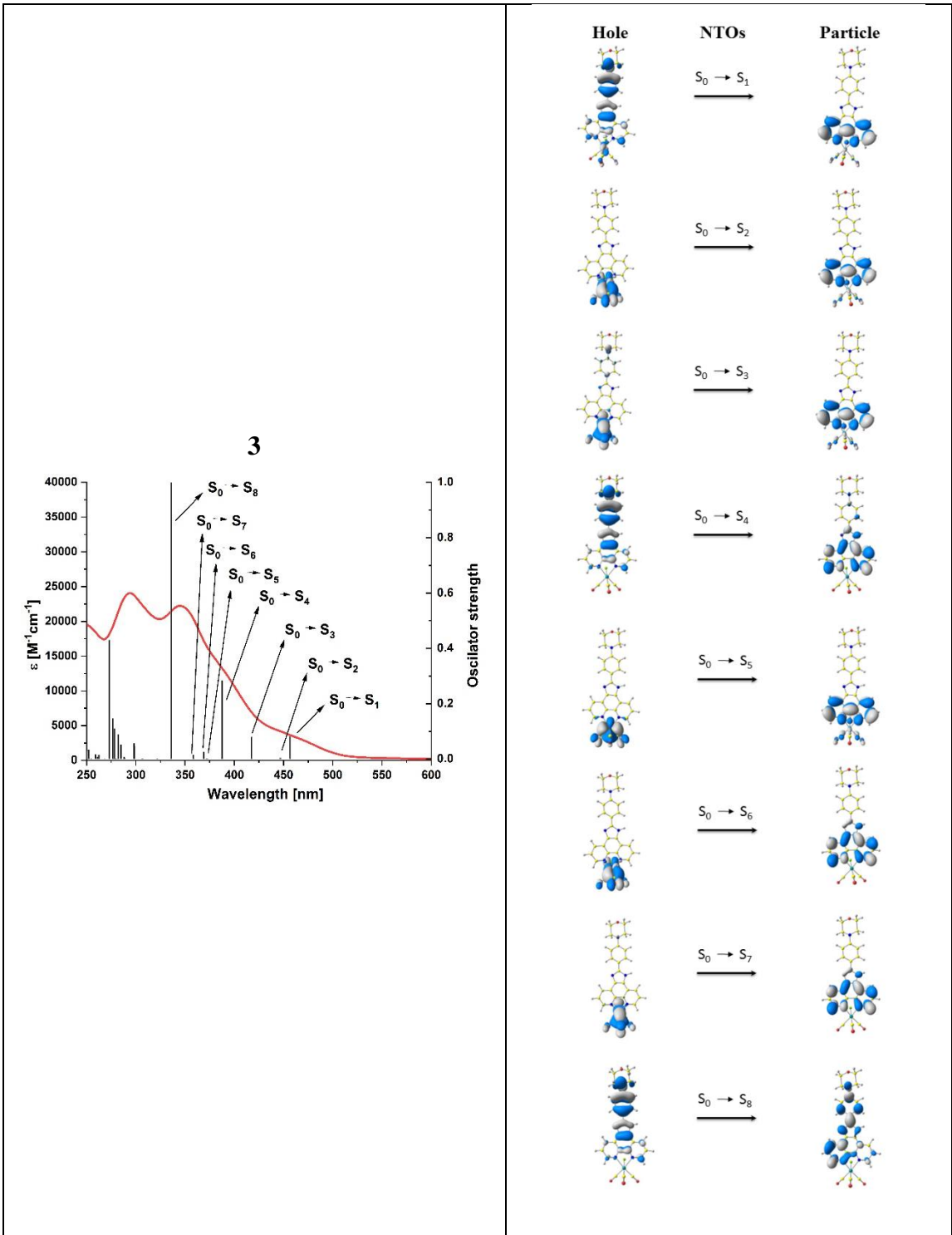
Table S9. Calculated ionization potentials and electron affinities (vertical and adiabatic), energy gap, as well as hole and electrons reorganization energies and extraction potentials for **1–5**. The calculations were performed at DFT/PBE0/def2-TZVPD/def2-TZVP level with the use of the PCM model at polarities corresponding to CHCl_3

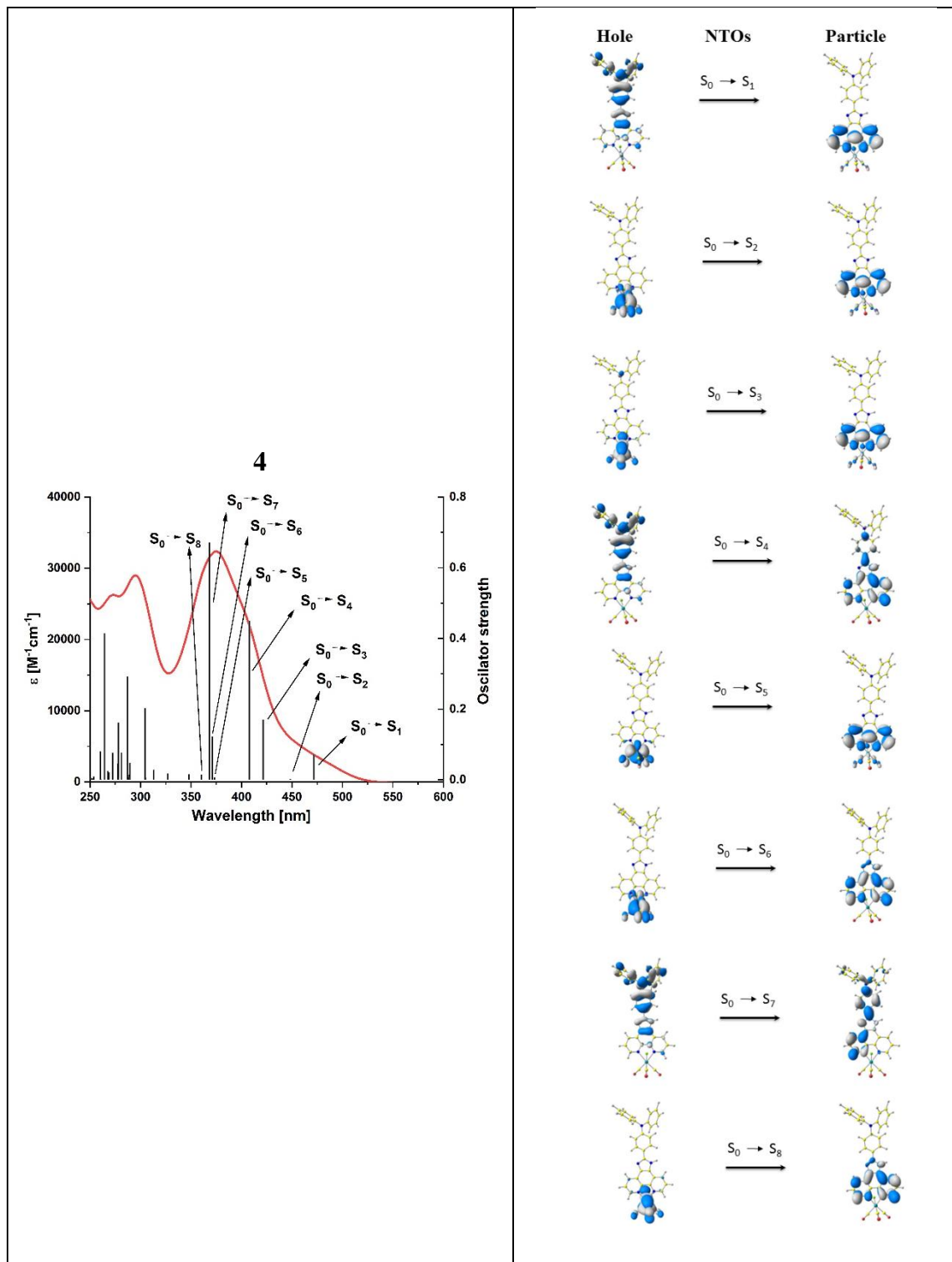
Complex	IP(v) [eV]	IP(a) [eV]	EA(v) [eV]	EA(a) [eV]	λ_{hole} [eV]	$\lambda_{\text{electron}}$ [eV]	HEP [eV]	EEP [eV]	energy gap(a) [eV]
1	5.66	5.58	2.50	2.66	0.16	0.32	5.50	2.82	3.15
2	5.87	5.75	2.54	2.69	0.23	0.31	5.64	2.85	3.32
3	5.86	5.62	2.53	2.69	0.39	0.32	5.47	2.85	3.32
4	5.63	5.57	2.55	2.71	0.12	0.32	5.51	2.87	3.11
5	6.34	6.01	2.58	2.73	0.67	0.31	5.67	2.89	3.69

$EEP = E^0(M^-) - E^-(M^-)$; $HEP = E^+(M^+) - E^0(M^+)$; $\lambda_{\text{electron}} = EEP - EA_v$; $\lambda_{\text{hole}} = IP_v - HEP$









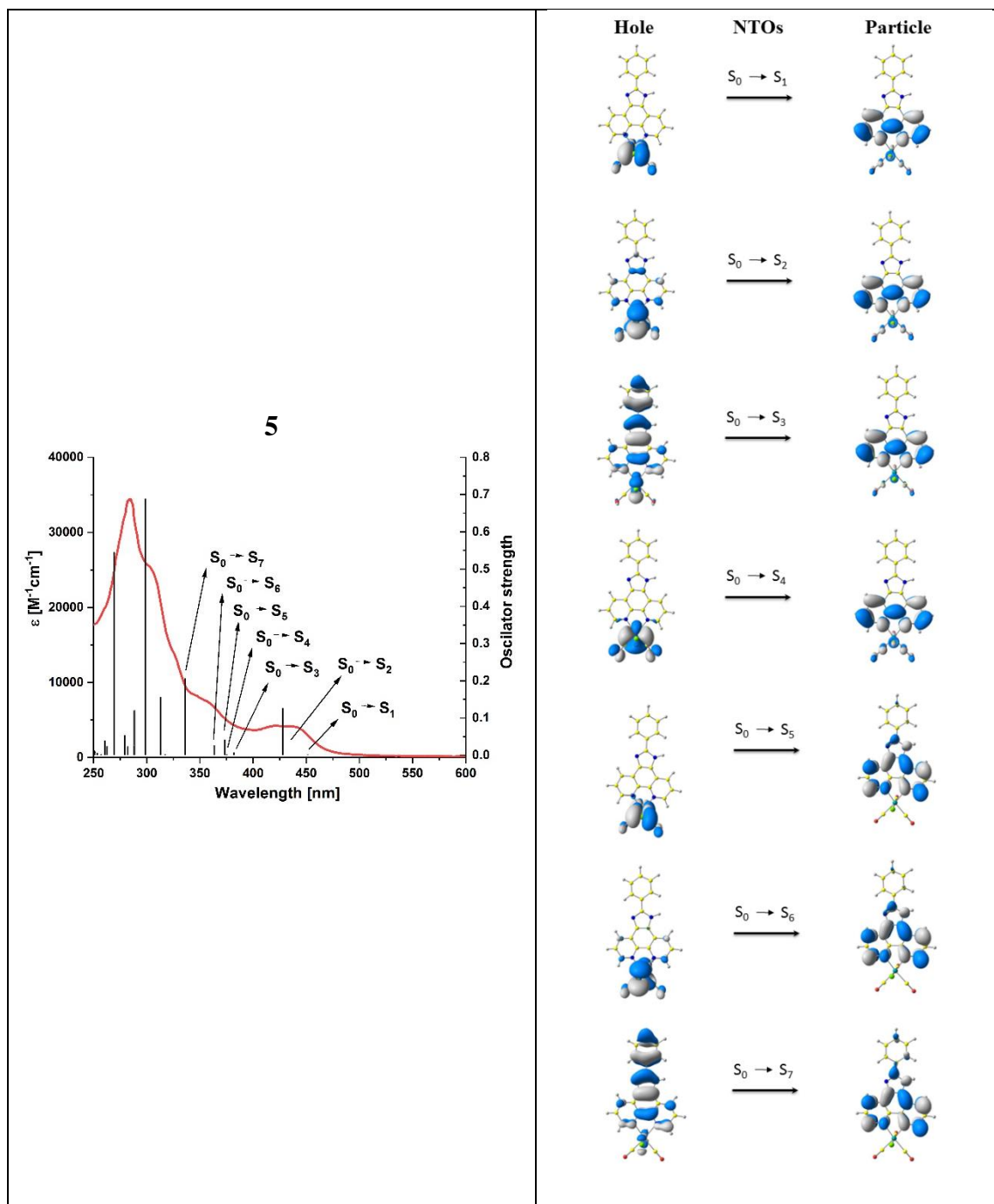
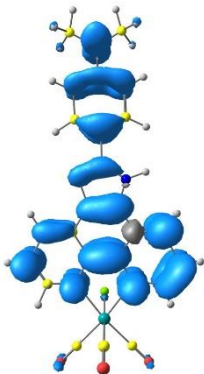
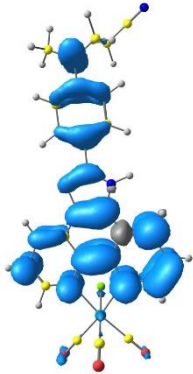
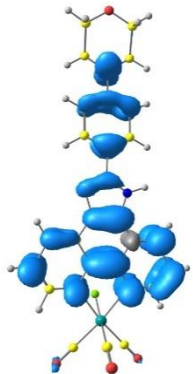
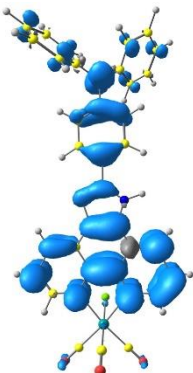


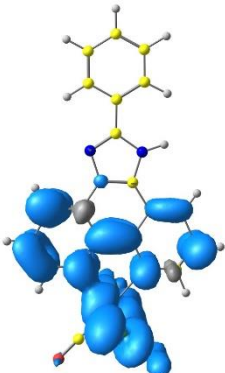
Figure S32. Experimental (red line) absorption spectra of **1–5** in CHCl_3 alongside with national transition orbitals calculated for vertical excitations, which were assigned to the lowest-energy absorption band. The calculations were performed at TD-DFT/PCM/PBE1PBE/def2-TZVPD/def2-TZVP level with the use of the PCM model at polarities corresponding to CHCl_3 .

Table S10. The energies and characters of the spin-allowed electronic transitions assigned to the lowest wavelength absorption bands of **1–5** computed at TD-DFT/PBE0/def2-TZVPD/def2-TZVP level with the use of the PCM model at polarities corresponding to CHCl_3 .

Experimental absorption λ [nm] (ϵ [$\text{M}^{-1}\text{cm}^{-1}$])	Calculated transitions				
	Major contribution (%)	Character	E[eV]	λ [nm]	Oscillator strength
1					
473 (4885)	$\text{S}_0 \rightarrow \text{S}_1$	ILCT	2.57	481.2	0.0565
	$\text{S}_0 \rightarrow \text{S}_2$	MLCT	2.78	444.9	0.0021
2					
461 (3795)	$\text{S}_0 \rightarrow \text{S}_1$	ILCT	2.71	456.9	0.0822
	$\text{S}_0 \rightarrow \text{S}_2$	MLCT	2.77	446.9	0.0041
3					
455 (3685)	$\text{S}_0 \rightarrow \text{S}_1$	ILCT	2.71	456.5	0.0820
	$\text{S}_0 \rightarrow \text{S}_2$	MLCT	2.77	446.8	0.0038
4					
468 (4015)	$\text{S}_0 \rightarrow \text{S}_1$	ILCT	2.62	471.6	0.0719
	$\text{S}_0 \rightarrow \text{S}_2$	MLCT	2.76	448.5	0.0025
5					
433 (4120)	$\text{S}_0 \rightarrow \text{S}_1$	MLCT	2.74	451.4	0.0019
	$\text{S}_0 \rightarrow \text{S}_2$	MLCT/IL	2.89	428.0	0.1269

Table S11. The energies of theoretical phosphorescence emissions, calculated from the difference between the ground singlet and the triplet state $\Delta E_{T_1-S_0}$, along with the experimental values and the spin density surface plots for **1–5**. Blue and grey colours show regions of excess α spin density and excess β spin density values, respectively.

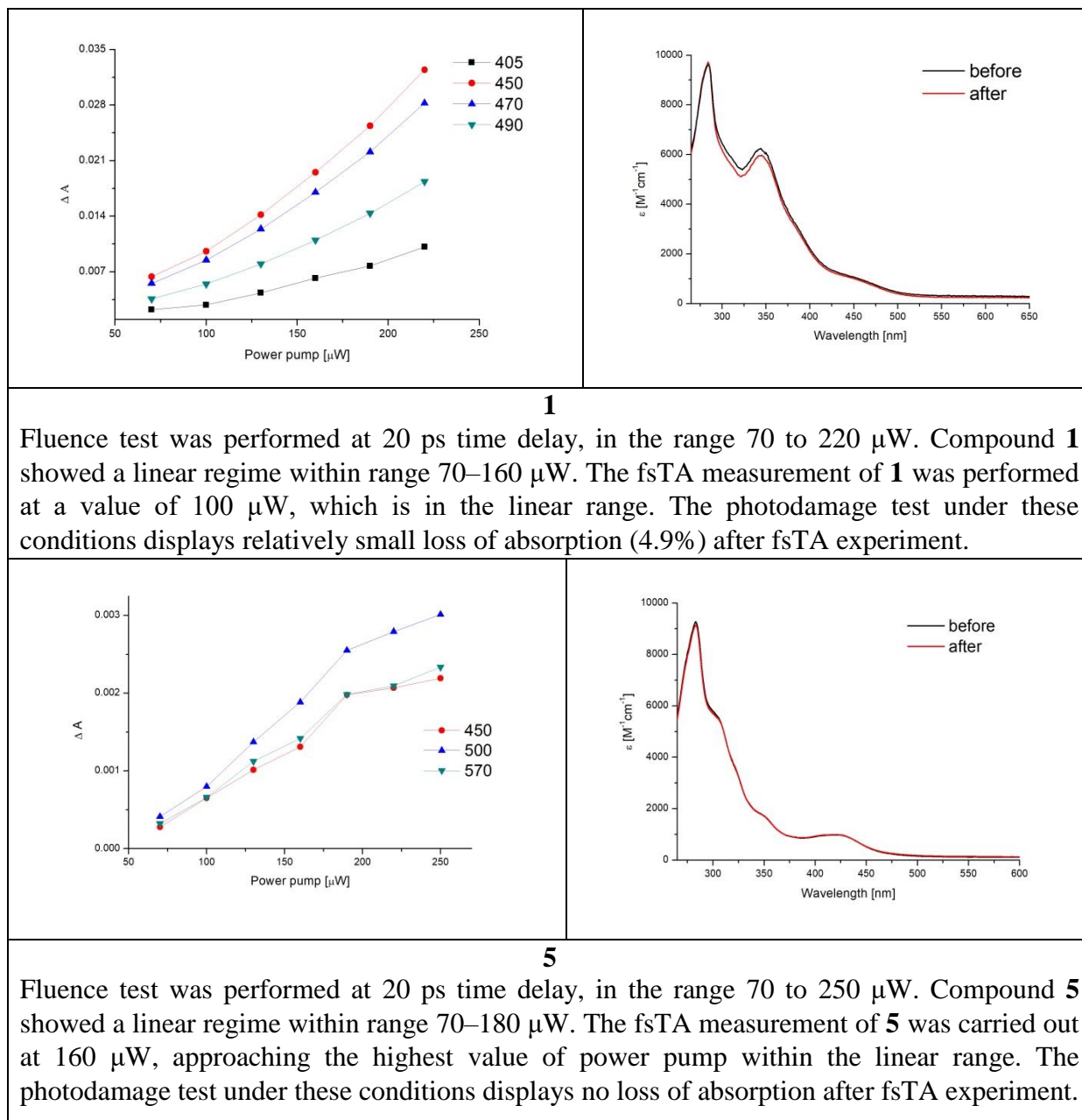
Code	Experimental emission maximum	Calculated emission maximum	Spin density surface plots
1	623 nm (1.99 eV)	639 nm (1.94 eV)	
2	592 nm (2.09 eV)	613 nm (2.02 eV)	
3	610 nm (2.03 eV)	645 nm (1.92 eV)	
4	600 nm (2.06 eV)	616 nm (2.01 eV)	

5	587 nm (2.11 eV)	668 nm (1.85 eV)	
---	---------------------	---------------------	---

FEMTOSECOND TRANSIENT ABSORPTION SPECTROSCOPY

Photodamage test and fluence analysis of solution samples for TA studies

Before starting the femtosecond experiments, fluence dependence and photodamage tests carried out in order to determine appropriate experiment conditions. The results of fluence dependence and photodamage tests of sample **1** and **5** are given below:



The fsTA spectra were measured using a pump–probe transient absorption spectroscopy system (Ultrafast Systems, Helios). A regenerative amplified femtosecond Ti:sapphire laser system (Astrella, Coherent) delivered pulses under 100 fs duration with 5mJ pulse with repetition rate of 1kHz and a central wavelength of 800 nm. The excitation pulses of 355 nm

sourced from an optical parametric amplifier (Light Conversion, TOPAS prime). A white light continuum pulse, which arise by focusing the residual of the fundamental light at CaF₂ crystal, was used as a probe beam. The pump pulse was chopped by a mechanical chopper synchronised to one-half of the laser repetition rate (1kHz), resulting in a pair of spectra with and without the pump, from which absorption changes induced by the pump pulse were estimated. Pump beam was depolarised to mimic dynamical changes of the orientation of the molecules. The delay time between pump and probe pulses was controlled by a moveable delay line in a time scale up to 7.5 ns. For the detection of the transient absorption signals, the white light continuum after passing through the sample was sent to CCD detector .

Transient absorption data were prepared using the Surface Explorer (Ultrafast Systems) software and then analysed with use of OptimusTM software¹. Correction of background, scattered light subtraction, solvent signal contribution subtraction as well as removing of spikes were performed routinely prior to the analysis. Moreover, coherent artefact analysis provided necessary information about IRF (IRF FWHM was estimated as about 150 fs (for **1**) and 210 fs (for **5**)) and allowed to the corrections of the probe chirp. The transient spectra consist of positive and negative bands, in which the former are due to excited-state absorption (ESA), whereas the latter are ground state bleaching (GSB). The analysis implemented in OptimusTM software¹ allowed to make the deconvolution of the transient spectra into species-associated spectra (SAS) and provides the decay-associated spectra (DAS) as a linear combination of the SAS of the compartments.

1. Slavov C, Hartmann H, Wachtveitl J, Implementation and evaluation of data analysis strategies for time-resolved optical spectroscopy. *Anal. Chem.* **2015**, 87, 2328–2336.

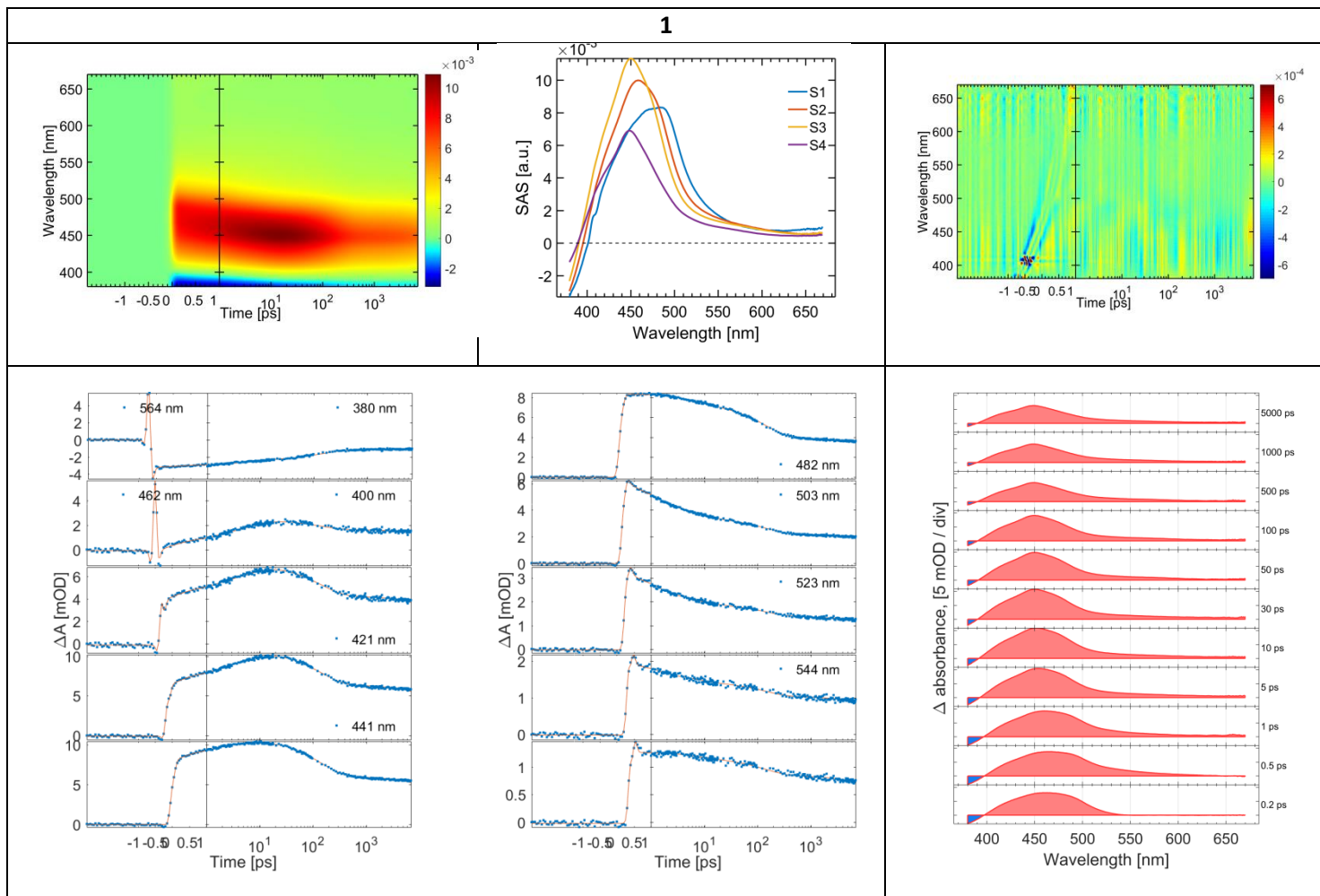
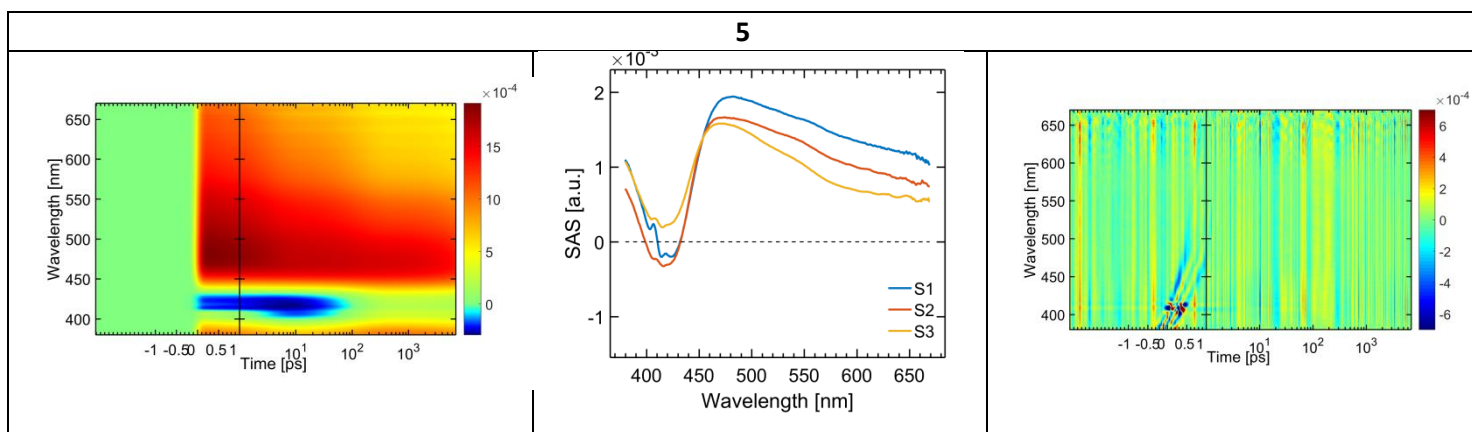


Figure S33. Summary of the global lifetime analysis of **1** (pump wavelength 355 nm; pump power 0.2 μj per pulse) containing 3d fsTA map, evolution associated spectra, residual map, time traces at several wavelength and transient spectra.



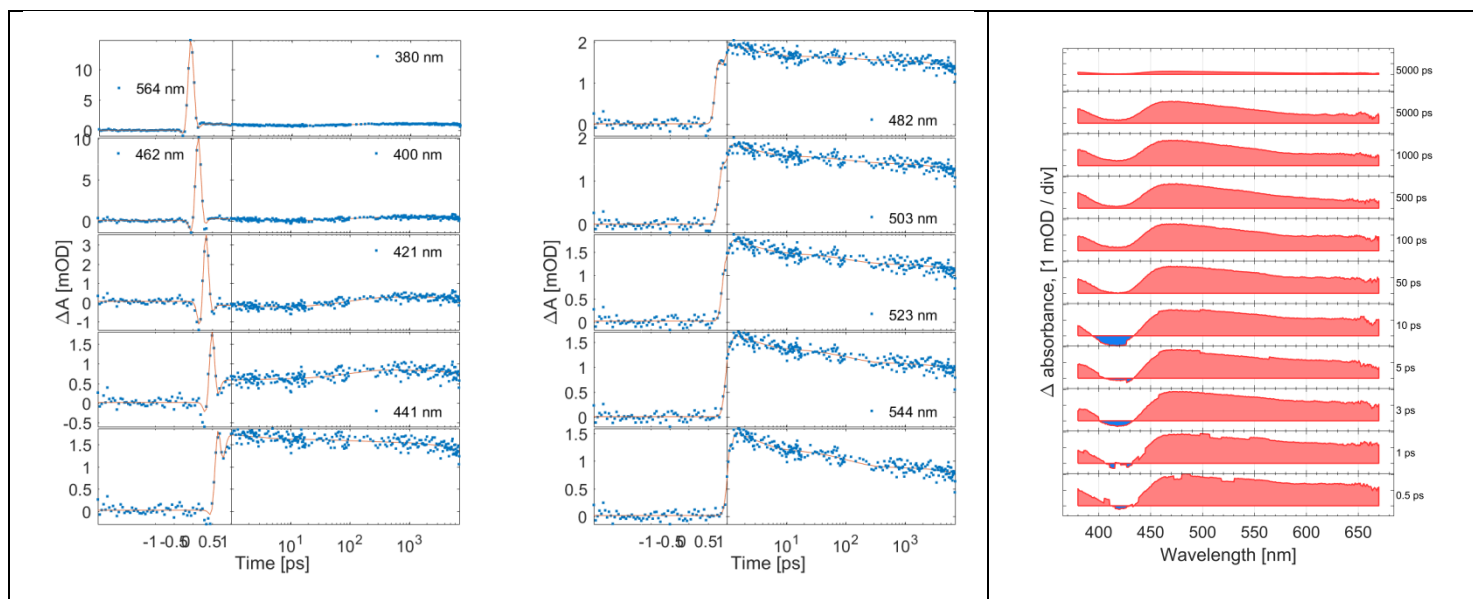


Figure S34. Summary of the global lifetime analysis of **5** (pump wavelength 355 nm; pump power 0.26 μ j per pulse) containing 3d fsTA map, evolution associated spectra, residual map, time traces at several wavelength and transient spectra.